

博士論文

Development of phenylboronate ester cross-linked polyplex micelles
for spatiotemporal control of nucleic acid delivery systems through
intracellular pH- and ATP-responsivity

(細胞内 pH および ATP 応答性による核酸送達システムの時空間制御に
向けたフェニルボロン酸架橋ポリプレックスミセルの開発)

吉永 直人

博士論文

Development of phenylboronate ester cross-linked polyplex micelles
for spatiotemporal control of nucleic acid delivery systems through
intracellular pH- and ATP-responsivity

(細胞内 pH および ATP 応答性による核酸送達システムの時空間制御に
向けたフェニルボロン酸架橋ポリプレックスミセルの開発)

Doctoral Dissertation
Department of Bioengineering
Graduate School of Engineering
The University of Tokyo
2019

吉永 直人 Naoto Yoshinaga

Preface

This dissertation presents results from three years of my research on the development of multi-functionalized polyplex micelles by introducing phenylboronate ester linkage as a smart cross-linking unit in Prof. Horacio Cabral laboratory from 2016 to 2019.

I believe that this work contributed to the understanding and exploitation of the utility of stimuli-responsive polyplex micelles for constructing progressive nucleic acids-based therapeutics system. I would like to appreciate supervisors and many colleagues for their kindly helps and valuable suggestions.

Naoto Yoshinaga

Department of Bioengineering, Graduate School of Engineering

The University of Tokyo

March 2019

Acknowledgement

This dissertation was financially supported by Specially Promoted Research Program of the Japan Society for the Promotion of Science (JSPS), Research on the Innovative Development and the Practical Application of New Drugs for Hepatitis B from Japan Agency for Medical Research and Development (AMED), and Center of Innovation (COI) program from Japan Science and Technology Corporation (JST).

I would like to show my greatest appreciation to Prof. Kazunori Kataoka and Prof. Horacio Cabral for providing me with the great opportunities and effective advices in my doctoral dissertation. I also appreciate all of the professors and senior postdoctoral researchers in Prof. Kataoka and Prof. Cabral laboratories, especially, Assistant Prof. Satoshi Uchida, Dr. Kensuke Osada, Dr. Takehiko Ishii and Dr. Mitsuru Naito. I am deeply grateful to Ms. Hiroko Koyama for her secretarial support and kindness for daily laboratory life and office work. Also, I would like to offer my special thanks to all of the members in Prof. Kataoka and Prof. Cabral laboratories for fruitful discussion and kind experimental help. Finally, I sincerely appreciate my family for their support and encouragement.

Contents

Chapter 1. General Introduction

1.1. Gene therapy	2
1.2. Non-viral gene delivery	4
1.3. 1.3. Stabilization and functionalization of polyplex micelles	6
1.4. Phenylboronic acid as an environmentally responsive motif for biomaterials	8
1.5. Purpose and strategy of this dissertation	11
1.6. Overview of this dissertation	13
1.7. References	15

Chapter 2. Development of pDNA-loaded polyplex micelles with pH- and ATP-dual responsive phenylboronate ester cross-linking

2.1. Introduction	29
2.2. Materials and methods	31
2.3. Results and discussion	41
2.3.1 Synthesis of PEG-PAsp(DET-FPBA) and PEG-PAsp(DET-GlcAm)	41
2.3.2 Preparation of PMs and optimization of introduction ratio of cross-linking agents	42
2.3.3 Stimuli-responsiveness of PMs against ATP and pH	46
2.3.4 Effect of FPBA/GlcAm cross-linking on cellular uptake and transfection	51
2.3.5 Effect of FPBA/GlcAm cross-linking on endosomal escape and ATP-responsive release of loaded pDNA	53
2.3.6 Stabilization effect of FPBA/GlcAm cross-linking in mouse blood	56
2.4. Conclusion	57

2.5. Appendix	57
2.5. References	60

Chapter 3. Improvement of Core condensation status by introducing cholesterol moieties into polyplex micelle core possessing FPBA/GlcAm cross-linking

3.1. Introduction	66
3.2. Materials and methods	67
3.3. Results and discussion	74
3.3.1 Synthesis of a series of block copolymers	74
3.3.2 Preparation and characterization of PMs	75
3.3.3 Optimization cationic segment and introduction ratio of FPBA and GlcAm	76
3.3.4 Characterization of PMs prepared from PEG-PAsp(DET-FPBA)-Chol and PEG-PAsp(DET-GlcAm)-Chol	79
3.4. Conclusion	81
3.5. Appendix	85
3.6. References	90

Chapter 4. Development of mRNA/polymer direct cross-linked polyplex micelles through phenylboronate ester linkage

4.1. Introduction	93
4.2. Materials and methods	94
4.3. Results and discussion	101
4.3.1 Optimization of the length of OligoRNA	101

4.3.2 Preparation of PMs loaded with mRNA hybridized with GlcAm-OligoRNA	104
4.3.3 Characterization of PMs loaded with hybridized mRNA	106
4.3.4. pH- and ATP-responsiveness of mRNA/polymer cross-linked PMs	111
4.3.5 Effect of mRNA/polymer cross-linking on mRNA expression and intracellular stability	113
4.4. Conclusion	115
4.5. Appendix	115
4.6. References	124

Chapter 5. Promotion of mRNA condensation in polyplex micelle core through hybridization of cholesteryl RNA oligonucleotides to get synergetic effect with phenylboronate ester cross-linking

5.1. Introduction	129
5.2. Materials and methods	130
5.3. Results and discussion	136
5.3.1 Preparation and characterization of polyplex micelles loaded with Chol-OligoRNA hybridized mRNA	136
5.3.2 Effect of cholesterol modification to mRNA in transfection efficiency of PMs	141
5.3.3 <i>In vivo</i> intratracheal administration into a mouse lung	142
5.3.4 Combination of Chol-OligoRNA system and phenylboronate ester cross-linking - Characterization and tolerability test of PMs-	144
5.3.5 Effect of combination strategy of phenylboronate ester cross-linking and Chol-OligoRNA on transfection efficiency	147

5.3.6 Stabilization effect of pheyboronate ester cross-linking and cholesterol installation on blood circulation	149
5.4 Conclusion	151
5.5 Appendix	151
5.6 References	155
Chapter 6. Summary and perspectives	
6.1. Summary	159
6.2. Future perspectives	162
List of publications	165

Chapter 1

Introduction

1.1. Gene therapy and nucleic acid delivery

Gene therapy has been gathering much attention as increasing the knowledge about nucleic acid biology, such as human genome sequences and central dogma.¹⁻⁴ Especially, the knowledge about the behavior of natural nucleic acids in diseases has opened up the opportunity to use nucleic acids as drug for curing diseases at gene level. Designed nucleic acid expressing therapeutic proteins in disease site, specifically longer nucleic acids such as plasmid DNA (pDNA) and messenger RNA (mRNA), can treat diseases or at least reduce disease progression (**Figure 1-1**). Actually, nucleic acid for some specific disease were showed fruitful therapeutic effect and now became commercially available.¹ Behind the successful achievement of the nucleic acid drugs, there was development of delivery carriers. Loading therapeutic nucleic acid in delivery carriers overcomes two major problems for gene therapy; avoiding enzymatic degradation of nucleic acid during delivery process,⁵⁻⁶ and enabling negatively-charged nucleic acid to enter target cells.⁵ Nucleic acid can be easily degraded by nucleases in living body. The half-life time of naked exogenous DNA in rat plasm and blood was known to be approximately 1 and 0.15 min, respectively,⁷⁻⁸ so that it is difficult to obtain therapeutic effect from nucleic acids in naked state. Even though nucleic acids coincidentally

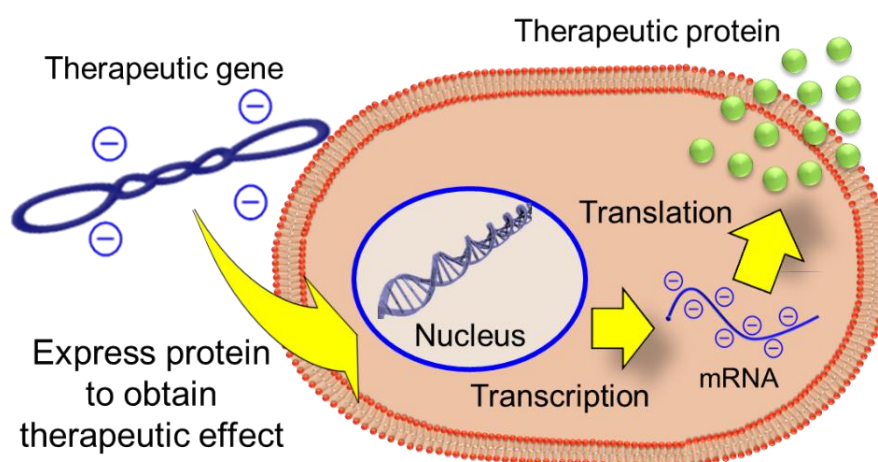


Figure 1-1. Schematic illustration of gene therapy using pDNA.

avoid nuclease attacks, nucleic acid cannot pass through cell membrane because of electrostatic repulsion between nucleic acids and anionic biomacromolecules on cell membrane, such as glycosaminoglycans. Therefore, there is no doubt that delivery carriers are required to get therapeutic effect, and actually many efforts have been devoted to effective gene therapy.

The first nucleic acid drug, Gendicine, was approved in Chinese commission in 2003. Gendicine based on an adenovirus (AV) vectors encoding wildtype-p53 gene.⁹⁻¹⁰ Starting with that, various AV and adeno-associated viral (AAV) vectors achieved therapeutic effect and got marketing authorization (**Table 1-1**).^{1, 11} Retroviral vectors also used as delivery vehicle to cure several diseases, such as X-linked severe combined immunodeficiency and X-linked chronic granulomatous disease.¹²⁻¹³ Viral vectors are, actually, most efficient delivery carriers for the nucleic acid transfection in possible carriers, and almost clinical trials are based on viral vectors.¹ While viral vectors achieved great therapeutic effect by such a high transfection efficiency, viral vectors possess severe problems; immunogenicity, limitation of cargo gene length, and difficulty in mass production.^{3, 14}

Table 1-1. List of Approved gene medicine using viral vectors

Commercial Name	Date of approval	Approving agency	Target disease
Gendicine	Oct. 2013	State Food and Drug Administration of China	Head and neck squamous cell carcinoma
Oncorine H101	Nov. 2006	State Food and Drug Administration of China	Head and neck cancer
Glybera	Nov. 2012	European Marketing Authorization (EMA)	Lipoprotein lipase deficiency
IMLYGIC	Dec. 2015	EMA	melanoma
Strimvelis	May. 2016	EMA	Adenosine deaminase deficiency
Kymriah	Aug. 2017	Food and Drug Administration (FDA)	Acute lymphoblastic leukaemia
Yescarta	Oct. 2017	FDA	B-cell lymphoma
Luxturna	Dec. 2017	FDA	Retinal dystrophy

1.2. Non-viral gene delivery

In order to overcome the problems on viral vectors, a lot of non-viral delivery carriers have been developed.^{4,16-19} Non-viral carriers can be mainly categorized into two types; lipid-based carriers and polymeric carriers. Lipid-based delivery carriers are well studied,²⁰⁻²² and lots of studies reached to clinical trials.^{1, 23-24} Lipid-based carriers are basically prepared from cationic lipids and nucleic acids, which form lipoplexes by electrostatic interaction. The charge neutralization by lipoplex formation allows complexed nucleic acids to interact with cellular membrane, and eventually to enter into the cells.²¹ The high affinity to cellular membrane is one of the great advantages of lipoplexes. However, such a strong affinity can sometimes cause unexpectedly cytotoxicity.²⁵ Thus, chemical structure of lipid composition was fine-tuned to control the interaction between lipoplexes and cellular membrane.²⁶⁻²⁷ As an *in vivo* application, lipid carriers often accumulate in liver and spleen after intravenous injection through the recognition by immune cells such as macrophages, which exist in liver and spleen a lot.²⁸⁻³⁰ The accumulation property of lipid carriers is an advantage to target liver or spleen diseases,^{22-23,31} while it behaves as disadvantage to target other organs. Size control is also a problem on lipid carriers for *in vivo* application. The size of lipid carriers prepared by common method, *i.e.* extruder method, becomes ~100 nm, sometimes showing disadvantage to target a specific disease.³²

Polymeric carriers are prepared from nucleic acids via electrostatic interaction between polycation and nucleic acids.³³⁻³⁷ Comparing to lipoplexes, polyplexes can easily prepared by simple mixing polycation and nucleic acid in aqueous solution. However, there is a barrier on uptake process of polymeric carriers. Polymeric carriers are known to be taken up

by micropinocytosis and/or endocytosis pathway depending on these sizes^{33,38} because size limit of macropinocytosis and endocytosis can be larger than polymeric carriers.³⁹⁻⁴³ As particles captured by macropino/endocytosis can be degraded enzymatically in lysosomes, polymeric carriers should escape from endosomes to cytoplasm before degradation in lysosomes. The demand of polymeric carriers for efficient delivery have provided motivation with researchers to design chemical structure of polymers sophisticatedly.⁴⁴⁻⁵³ For *in vivo* application, polyplex micelles (PMs) is one of the promising methods as non-viral polymeric carriers for efficient gene therapy.^{33-37,44,46,51,53-56} PMs are prepared from negatively-charged nucleic acid and block copolymers composed of amphiphilic or hydrophilic segment, such as poly(ethylene glycol) (PEG), and cationic segment through electrostatic interaction. Finally, PM forms a unique core-shell structure (**Figure 1-2**), which reduces unspecific absorption to biomacromolecules during delivery process and protect loaded nucleic acid in harsh physiological condition. Furthermore, PMs can be easily functionalized by engineering block copolymers comparing to lipid molecules, and such functionalization of block copolymers can lead enhanced transfection efficiency.

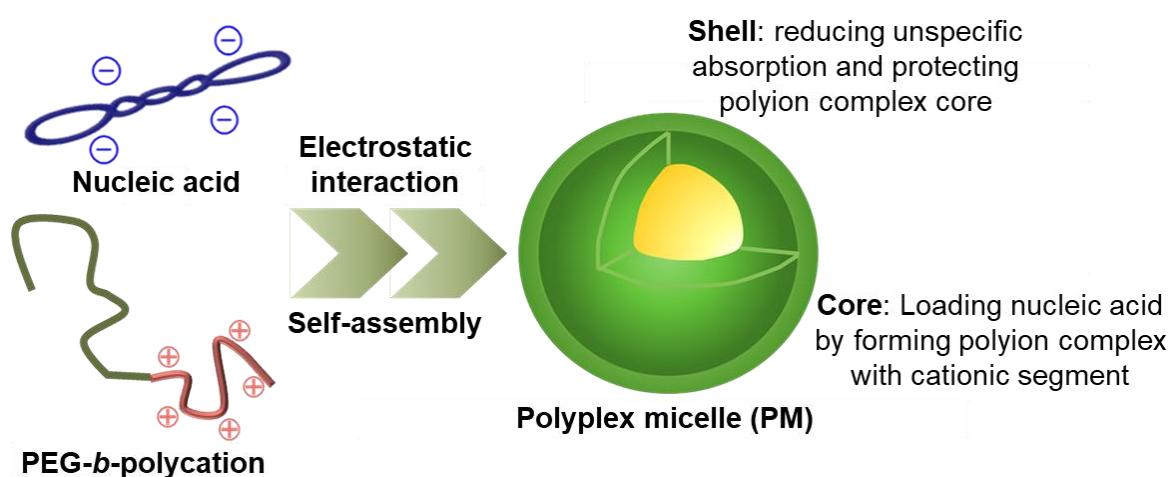


Figure 1-2. Schematic illustration of polyplex micelles prepared from negatively-charged nucleic acid and block copolymers having cationic segment.

1.3. Stabilization and functionalization of polyplex micelles

For efficient delivery using PMs, following functions are mainly required; (i) protecting encapsulated nucleic acids from enzymatic degradation during delivery process to target sites, (ii) facilitating endosomal escape of PMs to avoid degradation in lysosomes, and (iii) inducing rapid PM dissociation in cytoplasm for efficient transition to transcription/translation process. Recently, many studies devoted to developing and optimizing each function. For function (i), hydrophobic moieties, such as cholesterol group,⁵⁷⁻⁶⁰ and chemical cross-linking was introduced into PM core to form robust structure.⁶¹⁻⁶³ For instance, PMs prepared from PEG-poly(lysine) (PLys) with cross-linkable thiol groups in the PLys side chain stabilized PM structure by forming disulfide cross-linking in PM core, which can be cleaved in reductive environment, such as cytoplasm, and did not disturb encapsulated gene transcription in the cells. Eventually, disulfide cross-linked PMs achieved efficient gene transfection *in vitro* and *in vivo* condition.⁶³ For function (ii), pH-responsive chemical motifs were manipulated in block copolymers.^{44-53,64} Polycation and hydrophobic moieties usually help carriers to escape from endosome to cytosol by membrane disruptive ability. However, such membrane disruptive motifs sometimes result in undesirable cytotoxicity. Therefore, endosome/lysosome-specific membrane disruptive ability is required for satisfying both efficient endosomal escape and safety issue. To tackle this issue, pH drop in endosomal compartment to acidic pH (~5.5) is used to perform endosomal/lysosomal membrane disruptive ability.^{44,59,64} pH-responsive PEG detachable PM system is an effective strategy for endosomal escape.⁵³ In this strategy, after detachment of PEG segments from PMs in late endosomes/lysosomes responding to pH drop, uncovered polyplex core, whose surface

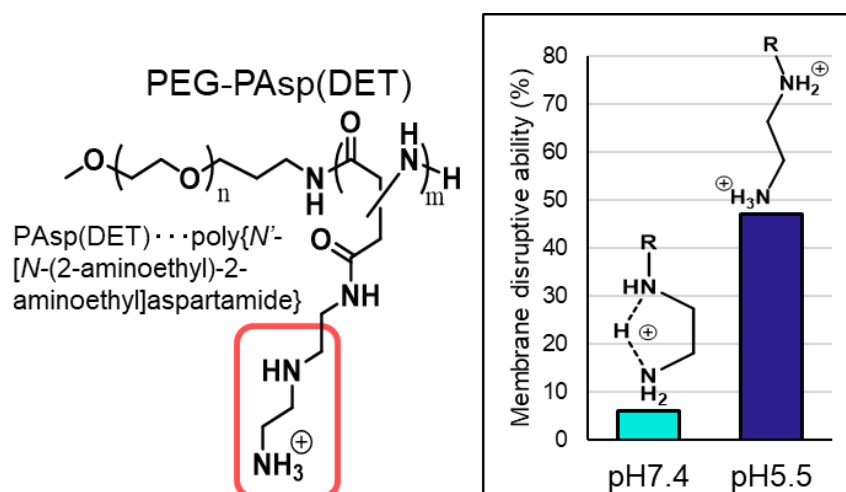


Figure 1-3. Chemical structure of PEG-PAsp(DET) block copolymer and its pH-responsive membrane disruptive ability by changing protonation degree of the side chain.⁴⁴

possessed cationic charge, associated with endosomal/lysosomal membrane via electrostatic interaction. Eventually, the carrier achieved efficient endosomal escape and brought high gene transfection. Fine-tuning of acid dissociation constant (pK_a) value of amine groups on polycation is another attractive strategy for endosomal escape. Poly[N' -[N -(2-aminoethyl)-2-aminoethyl]aspartamide] (PAsp(DET)) is a polycation changing protonation degree between physiological pH and endosomal pH (**Figure 1-3**).⁴⁴ PAsp(DET) has two major advantages; (1) diaminoethane units in the side chain change from mono-protonated form into the di-protonated form at acidic pH of the endosome, facilitating smooth endosomal escape of PMs after endocytosis, and (2) sustained degradation of the main chain occurs through self-catalytic mechanism, circumventing cumulative toxicity of PMs.^{44,65} For function (iii), cytoplasmic stimuli-responsive chemical moieties to trigger PM dissociation are commonly integrated into block copolymers not to disturb gene transfection.⁶¹⁻⁶³ As described above, introduction of disulfide cross-linking is one of the promising strategies for efficient gene transfection. Each function has been well studied, but multi-functionalization of PMs is still a difficult problem.

1.4. Phenylboronic acid as an environmentally responsive motif for biomaterials

Phenylboronic acid (PBA) is an attractive small molecule to overcome three functions described above. PBA derivatives switch its chemical structure in aqueous condition from hydrophilic tetrahedral form to hydrophobic trigonal form depending on pH and its pK_a value (**Figure 1-4**).⁶⁶⁻⁷⁰ In 1959, J. P. Lorand and J. O. Edwards first reported that PBA can form reversible boronate ester linkage with diol compound in hydrophilic tetrahedral structure.⁶⁶ In 1970s, the unique character of PBA derivatives has been widely used as a ligand of affinity chromatography to purify polyol moieties, including ribonucleic acids.⁷²⁻⁷³ Then, T. D. James and S. Shinkai focused on measuring glucose concentration by using PBA modified applications in 1990s,⁷⁴⁻⁷⁶ which accelerated biological use of PBA derivatives. Actually, PBA derivatives are known to associate with polyol carbohydrates on biological membranes.⁷⁷⁻⁸⁰ It is worth noting that the formation of phenylboronate ester linkage is facilitated by increasing both diol compounds concentration and environmental pH because these affect the degree of acid dissociation of PBA derivatives^{81,82}. The pK_a value of PBA derivatives is determined by substituents on phenyl ring (**Figure 1-5**).⁸³ Previous studies reported that electron-withdrawing substituent decreased the pK_a value of PBA while electron-donating one increased. Although the pK_a value can be controlled to some extent, decreasing pK_a value is limited at physiological

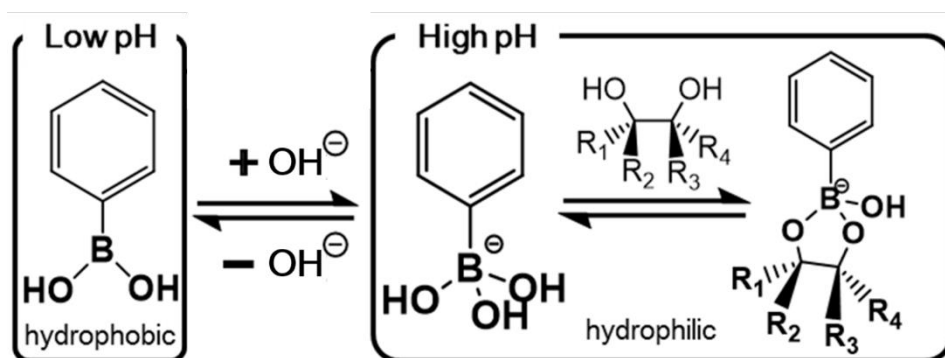


Figure 1-4. Equilibrium of phenylboronic acid in aqueous solution with diol compound.

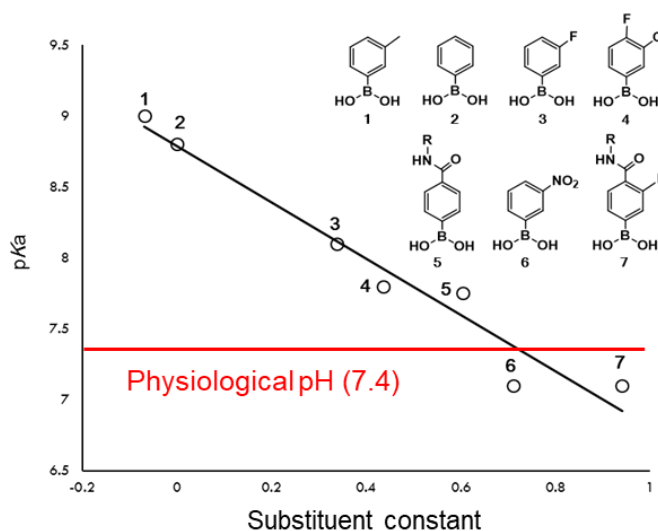


Figure 1-5. Relationship between acid dissociation constant of PBA and substituent constant on phenyl ring.

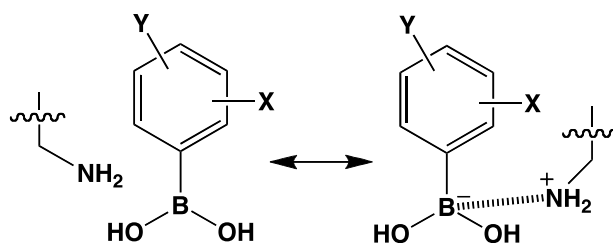


Figure 1-6. Boron-nitrogen interaction between boronic acid and amine group.

pH (pH 7.4) by fine-tuning of substituent. Amine groups neighboring to boronic acid can solve the problem. The boron atom on hydrophobic trigonal PBA moiety takes an sp^2 hybrid orbital, meaning that empty orbit exists on the boron atom. An unshared electron pair of nitrogen atom on an amine group can coordinates to the empty orbit on the boron atom, and PBA formed ionized hydrophilic structure (**Figure 1-6**).⁸⁴⁻⁸⁹ Eventually, amine groups accelerate phenylboronate ester formation. Binding affinity of diol compounds to PBA is also strongly depended on the chemical structure of diol compounds (**Table 1-2**).⁷¹ For instance, catechol derivatives, where hydroxy groups exist on the same plane, show high affinity to PBA derivatives. Also, straight-chain polyol moiety, such as sorbitol, form phenylboronate ester efficiently due to the large number of hydroxy groups and less steric repulsion. The difference of affinity to PBA derivatives allows exchange reaction between one diol (polyol) compound

Table 1-2. Binding affinity of each diol (polyol) compound to PBA in aqueous solution.⁷¹

Diol compound	Binding affinity (/glucose)	Diol compound	Binding affinity (/glucose)
Alizarin Red S	283	Sialic acid	4.6
Catechol	180	Gluconic acid	3.4
D-Sorbitol	80	D-Galactose	3.3
D-Fructose	35	D-Xylose	3.0
D-Tagatose	32.5	D-Mannose	2.8
D-Mannitol	26	D-Glucose	1
L-Arabinose	5.4	Maltose	0.54
D-Ribose	5.2	Saccharose	0.14

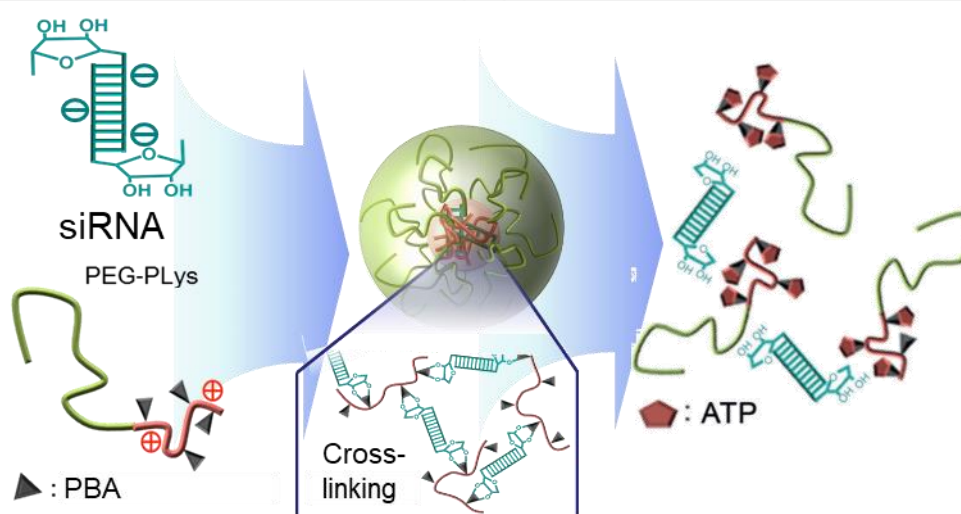


Figure 1-7. Schematic illustration of PBA/siRNA cross-linked polyion complex micelles. The formation of cross-linking at the both ends of siRNA stabilized micelle structure. Also, intracellular highly concentrated ATP triggered micelle dissociation by exchanging reaction with siRNA.⁹⁰

and competitive another one.

Phenylboronate ester linkage was recently used as a smart cross-linker of polymeric carrier for small interfering RNA (siRNA) delivery (**Figure 1-7**).⁹⁰ PBA moieties on block copolymers can bind to ribose rings at the end of siRNA and stabilize carrier structure. After entering target cells, the polymeric carrier can be dissociated in response to highly concentrated cytosolic adenosine triphosphate (ATP), thereby allowing loaded siRNA to perform RNA interfering inside the cells.

1.5. Purpose and strategy of this dissertation

Although a lot of efforts have been devoted to developing delivery carriers to satisfy each function, such as stability, endosomal escapability and active release of loaded nucleic acids, few studies achieved to integrate all three functions in one carrier probably because each function conflicts with one another. Thus, in this dissertation, I attempted to develop a novel smart nucleic acid delivery carrier based on PMs introducing PBA to block copolymers as a cross-linker in PM core without complicated preparation.

Hydrophobicity of trigonal PBA moieties and negative charge on tetrahedral PBA should be considered in introducing PBA moieties to cationic side chain because these characters may prevent efficient PM formation. The pK_a value of PBA derivatives is, as described in above section, determined by the substituents on phenyl ring, but it takes around 7 even though strong electron-withdrawing groups are introduced (**Figure 1-5**). It means that some of PBA moieties on block copolymers form hydrophobic trigonal structure and other PBA moieties form negatively-charged hydrophilic structure. The hydrophobicity of PBA can decrease solubility of block copolymers in aqueous solution at physiological pH, and limit introduction of many PBA groups into block copolymers. Actually, PEG-PLys with highly introduced 3-fluoro substituted PBA moieties in PLys segment did not dissolve in aqueous solution at physiological pH (pH 7.4).⁹⁰ Negatively-charged PBA groups on cationic segment also disturb efficient PM formation because it decreases charge density of cationic segment, leading weak electrostatic interaction between nucleic acid and block copolymers. Thus, to guarantee the solubility of block copolymers after PBA modification, PAsp(DET), which possesses cationic charge after PBA introduction, was selected as cationic segment (**Figure 1-**

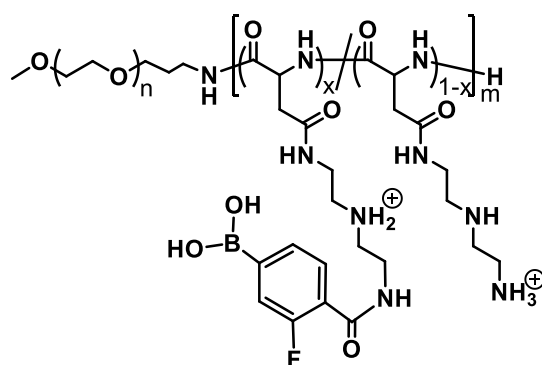


Figure 1-8. Chemical structure of PEG-PAsp(DET) modified with PBA in the PAsp(DET) side chain.

8).

The utility of integrating phenylboronate ester cross-linking in PM core was firstly attempted to be proved. To apply PBA-based cross-linked PMs to various type of nucleic acids, a couple of block copolymers was designed; one was PBA modified and the other was diol compound modified. Using two type of block copolymers allowed efficient cross-linking in PM core because it can avoid cross coupling before PM formation due to electrostatic repulsion between block copolymers. Moreover, in this strategy, intramolecular cross-linking, which may not stabilize PM structure, can be avoided. As an encapsulated nucleic acid, pDNA was chosen for the first study to prove phenylboronate ester cross-linking because pDNA is relatively stable against nuclease attacks in nucleic acids. Then, I tried to apply the phenylboronate ester cross-linking system to messenger RNA (mRNA) delivery. mRNA has gathered much attention due to its potency as a nucleic acid drug.⁹¹⁻⁹² To get expression of therapeutic protein, pDNA has mainly been used for the purpose, but mRNA possesses more advantages than pDNA; (1) mRNA can express protein in non-dividing cells because mRNA need not to enter cell nuclei to express protein, (2) protein expression of mRNA is faster than that of pDNA, and (3) mRNA can avoid genome insertion, which may happen in transfection of pDNA (**Figure 1-9**). There attractive advantages accelerate mRNA therapy research in recent years.⁹³⁻⁹⁹

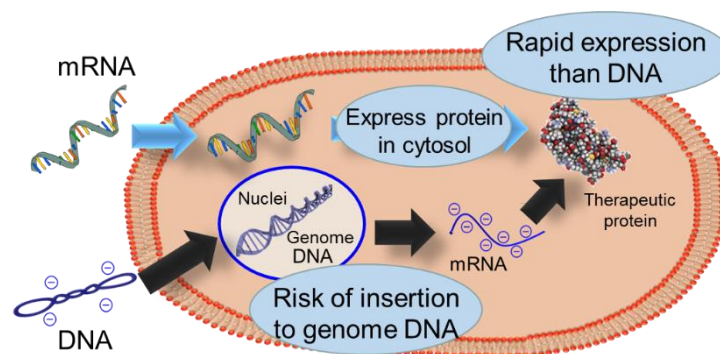


Figure 1-9. Schematic illustration of benefits of mRNA therapeutics.

1.6 Overview of this dissertation

The dissertation focused on development of phenylboronate ester cross-linked PMs satisfying required three demands; stability en route to target cells, effective endosomal escape, and release property allowing efficient protein expression.

In Chapter 2, I designed the phenylboronate ester cross-linked PMs prepared from a couple of block copolymers. As a cationic segment of block copolymer PAsp(DET) was chosen, and then 3-fluoro substituted PBA, whose pK_a is estimated to be 7.2 after introduction into PAsp(DET) side chain,¹⁰⁰ and polyol compound (*N*-gluconamide (GlcAm)) were introduced to PAsp(DET) side chain, respectively (**Figure 1-10**). In PM formation, both PBA and GlcAm moieties are highly concentrated in PM core, and then form cross-linking efficiently, which stabilized PM structure. Noteworthy, the phenylboronate ester cross-linking can automatically

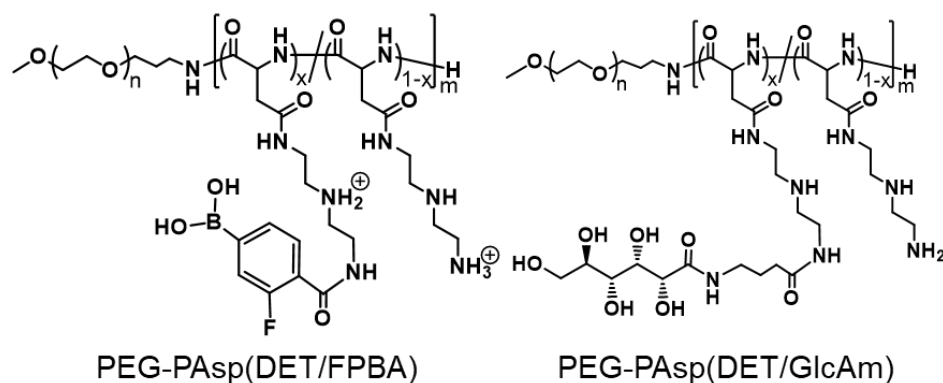


Figure 1-10. Chemical structure of PEG-PAsp(DET) modified with FPBA or GlcAm moiety.

form in PM core by simple mixing of block copolymers and nucleic acid, which is a great advantage of multi-functional nucleic acid delivery carriers. After cellular uptake through endocytosis, equilibrium shift of PBA from hydrophilic to hydrophobic structure can accelerate endosomal escape due to the hydrophobicity of PBA moieties. In cytoplasm, highly concentrated ATP is replaced with GlcAm moieties on block copolymers, and trigger PM dissociation, which leads efficient transcription/translation. The phenylboronate ester cross-linked PMs showed 20-fold higher protein expression in cultured cell condition comparing to non-cross-linked PMs.

After proving the utility of phenylboronate ester cross-linking for effective pDNA delivery, I tried to apply the system to mRNA delivery in Chapter 3. As described in the previous section, mRNA has various advantage to achieve therapeutic effect comparing to pDNA. However, much robust delivery carriers are required to get sufficient protein expression because mRNA is quite biologically-fragile in physiological condition. Thus, cationic segment of block copolymers was first optimized for efficient mRNA delivery in Chapter 3. In addition, cholesterol (Chol) moiety was introduced to ω end of block copolymers for enhancing PM core condensation, which is known as a critical factor to improve nuclease resistance.¹⁰¹ Functionalization of mRNA itself is another attractive method for efficient mRNA delivery. In Chapter 4, complementary short RNA oligonucleotide (OligoRNA) with functional group at the 5' end was designed and hybridized with mRNA to introduce functional groups to mRNA without inhibiting translational activity (**Figure 1-11**). In this Chapter, 5' end GlcAm-modified OligoRNA (GlcAm-OligoRNA) was introduced to mRNA for direct formation of phenylboronate ester linkage with PBA-modified block copolymers. The direct linkage between block copolymers and mRNA except electrostatic interaction actually provided PMs

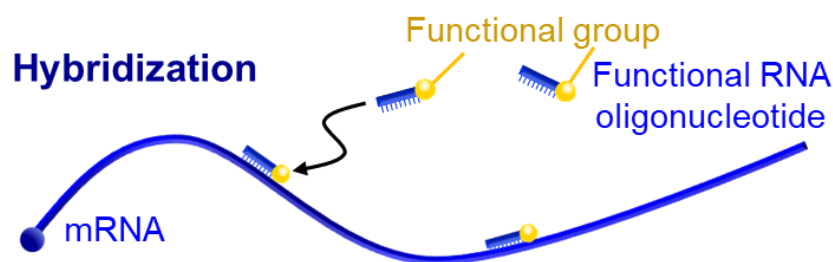


Figure 1-11. Schematic illustration of mRNA modification by hybridizing short RNA oligonucleotide having functional group at the end.

with high nuclease resistance. Finally, all my techniques were combined into one PMs in Chapter 5. Based on the polymer design in Chapter 3, mRNA hybridized with cholesterol modified OligoRNA (Chol-OligoRNA) was encapsulated in PM. In this PMs, it was expected to synergetic stabilization effect by phenylboronate ester cross-linking and additional interaction between mRNA and block copolymers through hydrophobic interaction of Chol moieties. The mRNA loading PMs showed enhanced protein expression efficiency, further confirming the essential role of phenylboronate ester linkage and integration of additional interaction between mRNA and block copolymers.

1.6. References

1. Ginn, S. L.; Amaya, A. K.; Alexander, I. E.; Edelstein, M.; Abedi, M. R., Gene therapy clinical trials worldwide to 2017: An update, *J. Gene Med.* **2018**, 20, e3015.
2. Wirth, T.; Parker, N.; Ylä-Herttua, S., History of gene therapy, *Gene* **2013**, 525, 162-169.
3. Thomas, C. E.; Ehrhardt, A.; Kay, M. A., Progress and problems with the use of viral vectors for gene therapy, *Nat. Rev. Genet.* **2003**, 4, 346-358.
4. Yin, H.; Kanasty, R. L.; Eltoukhy, A. A.; Vegas, A. J.; Dorkin, J. R.; Anderson, D. G., Non-viral vectors for gene-based therapy, *Nat. Rev. Genet.* **2014**, 15, 541-555.

5. Gosse, C.; Le Pecq, J. B.; Defrance, P.; Paoletti, C., Initial Degradation of Deoxyribonucleic Acid after Injection in Mammals, *Cancer Res.* **1965**, 25, 877-883.
6. Kawabata, K.; Takakura, Y.; Hashida, M., The Fate of Plasmid DNA After Intravenous Injection in Mice: Involvement of Scavenger Receptors in Its Hepatic Uptake, *Pharm. Res.* **1995**, 12, 825-830.
7. Houk, B. E.; Hochhaus, G.; Hughes, J. A., Kinetic Modeling of Plasm DNA Degradation in Rat Plasma, *AAPS Pharm. Sci.* **1999**, 1, E9.
8. Houk, B. E.; Martin, R.; Hochhaus, G.; Hughes, J. A., Pharmacokinetics of Plasmid DNA in the Rat, *Pharm. Res.* **2001**, 18, 67-74.
9. Pearson, S.; Jia, H.; Kandachi, K., China approves first gene therapy. *Nat. Biotechnol.* **2004**, 22, 3-4.
10. Frew, S. E.; Sammut, S. M.; Shore, A. F.; Ramjist, J. K.; Al-Bader, S.; Rezaie, R.; Daar, A. S.; Singer, P. A., Chinese health biotech and the billion-patient market, *Nat. Biotechnol.* **2008**, 26, 37-53.
11. Mingozzi, F.; High, K. A., Therapeutic in vivo gene transfer for genetic disease using AAV: progress and challenges, *Nat. Rev. Genet.* **2011**, 12, 341-355.
12. Hacein-Bey-Abina, S.; Von Kalle, C.; Schmidt, M.; McCormack, M. P.; Wulffraat, N.; Leboulch, P.; Lim, A.; Osborne, C. S.; Pawliuk, R.; Morillon, E.; Sorensen, R.; Forster, A.; Fraser, P.; Cohen, J. I.; de Saint Basile, G.; Alexander, I.; Wintergerst, U.; Frebourg, T.; Aurias, A.; Stoppa-Lyonnet, D.; Romana, S.; Radford-Weiss, I.; Gross, F.; Valensi, F.; Delabesse, E.; Macintyre, E.; Sigaux, F.; Soulier, J.; Leiva, L. E.; Wissler, M.; Prinz, C.; Rabbitts, T. H.; Le Deist, F.; Fischer, A.; Cavazzana-Calvo, M., LMO2-associated clonal T cell proliferation in two patients after gene therapy for SCID-X1, *Science* **2003**, 302, 415-419.

13. Kang, E. M.; Choi, U.; Theobald, N.; Linton, G.; Long Priel, D. A.; Kuhns, D.; Malech, H. L., Retrovirus gene therapy for X-linked chronic granulomatous disease can achieve stable long-term correction of oxidase activity in peripheral blood neutrophils. *Blood* **2010**, 115, 783-791.
14. Phillips, A. J., The challenge of gene therapy and DNA delivery, *J. Pharm. Pharmacol.* **2001**, 53, 1169-1174.
15. Luo, D.; Saltzman, W. M., Synthetic DNA delivery systems, *Nat. Biotechnol.* **2000**, 18, 33-37.
16. Glover, D. J.; Lipps, H. J.; Jans, D. A., Towards safe, non-viral therapeutic gene expression in humans, *Nat. Rev. Genet.* **2005**, 6, 299-310.
17. Pack, D. W.; Hoffman, A. S.; Pun, S.; Stayton, P. S., Design and development of polymers for gene delivery, *Nat. Rev. Drug Discov.* **2005**, 4, 581-593.
18. Li, S.-D.; Huang, L., Gene therapy progress and prospects: non-viral gene therapy by systemic delivery, *Gene Ther.* **2006**, 13, 1313-1319.
19. Nguyen, J.; Szoka, F. C., Nucleic Acid Delivery: The Missing Pieces of the Puzzle?, *Acc. Chem. Res.* **2012**, 45, 1153-1162.
20. Harashima, H.; Ishida, T.; Kamiya, H.; Kiwada, H., Pharmacokinetics of targeting with liposomes, *Crit. Rev. Ther. Drug Carrier Syst.* **2002**, 19, 235-275.
21. Khalil, I. A.; Kogure, K.; Akita, H.; Harashima, H., Uptake pathways and subsequent intracellular trafficking in nonviral gene delivery, *Pharmacol Rev* **2006**, 58, 32-45.
22. Pattni, B. S.; Chupin, V. V.; Torchilin, V. P., New Developments in Liposomal Drug Delivery, *Chem. Rev.* **2015**, 115, 10938-10966.
23. Allen, T. M.; Cullis, P. R., Liposomal drug delivery systems: From concept to clinical

applications, *Adv. Drug Deliv. Rev.* **2013**, 65, 36-48.

24. Bobo, D.; Robinson, K. J.; Islam, J.; Thurecht, K. J.; Corrie, S. R., Nanoparticle-Based Medicines: A Review of FDA-Approved Materials and Clinical Trials to Date, *Pharm. Res.* **2016**, 33, 2373-2387.

25. Dokka, S.; Toledo, D.; Shi, X.; Castranova, V.; Rojanasakul, Y., Oxygen radical-mediated pulmonary toxicity induced by some cationic liposomes, *Pharm. Res.* **2000**, 17, 521-525.

26. Smistad, G.; Jacobsen, J.; Sande, S. A., Multivariate toxicity screening of liposomal formulations on a human buccal cell line *Int. J. Pharm.* **2007**, 330, 14-22.

27. Alhajlan, M.; Alhariri, M.; Omri, A., Efficacy and safety of liposomal clarithromycin and its effect on *Pseudomonas aeruginosa* virulence factors *Antimicrob. Agents Chemother.* **2013**, 57, 2694-2704.

28. Immordino, M. L.; Dosio, F.; Cattel, L., Stealth liposomes: review of the basic science, rationale, and clinical applications, existing and potential, *Int. J. Nanomed.* **2006**, 1, 297-315.

29. Woodle, M.; Engbers, C.; Zalipsky, S., New amphipatic polymer-lipid conjugates forming long-circulating reticuloendothelial system-evading liposomes, *Bioconjug. Chem.* **1994**, 5, 493-496.

30. Maruyama, K.; Okuizumi, S.; Ishida, O.; Yamauchi, H.; Kikuchi, H.; Iwatsuru, M., Phosphatidyl polyglycerols prolong liposome circulation in vivo, *Int. J. Pharm.* **1994**, 111, 103-107.

31. Morille, M.; Passirani, C.; Letrou-Bonneval, E.; Benoit, J.-P.; Pitard, B., Galactosylated DNA lipid nanocapsules for efficient hepatocyte targeting, *Int. J. Pharm.* **2009**, 379, 293-300.

32. Cabral, H.; Matsumoto, Y.; Mizuno, K.; Chen, Q.; Murakami, M.; Kimura, M.; Terada, Y.; Kano, M. R.; Miyazono, K.; Uesaka, M.; Nishiyama, N.; Kataoka, K., Accumulation of sub-

100 nm polymeric micelles in poorly permeable tumors depends on size, *Nat. Nanotechnol.* **2011**, 6, 815-823.

33. Cabral, H.; Miyata, K.; Osada, K.; Kataoka, K., Block copolymer micelles in nanomedicine applications, *Chem. Rev.* **2018**, 118, 6844-6892.

34. Lin, G.; Zhang, H.; Huang, L., Smart Polymeric Nanoparticles for Cancer Gene Delivery, *Mol. Pharmaceutics* **2015**, 12, 314-321.

35. Pack, D. W.; Hoffman, A. S.; Pun, S.; Stayton, P. S., Design and development of polymers for gene delivery, *Nat. Rev. Drug Discov.* **2005**, 4, 581-593.

36. Kataoka, K.; Harada, A.; Nagasaki, Y., Block copolymer micelles for drug delivery: Design, characterization and biological significance, *Adv. Drug Deliv. Rev.* **2001**, 47, 113-131.

37. Lachelt, U.; Wagner, E., Nucleic Acid Therapeutics Using Polyplexes: A Journey of 50 Years (and Beyond), *Chem. Rev.* **2015**, 115, 11043-11078.

38. Wattiaux, R.; Laurent, N.; Coninck, S. W.; Jadot, M., Endosomes, lysosomes: their implication in gene transfer, *Adv. Drug Deliv. Rev.* **2000**, 41, 201-208.

39. Lim, J. P.; Gleeson, P. A., Macropinocytosis: An Endocytic Pathway for Internalising Large Gulp, *Immunol. Cell Biol.* **2011**, 89, 836-843.

40. McMahon, H. T.; Boucrot, E., Molecular Mechanism and Physiological Functions of Clathrin-Mediated Endocytosis, *Nat. Rev. Mol. Cell Biol.* **2011**, 12, 517-533.

41. Rejman, J.; Oberle, V.; Zuhorn, I. S.; Hoekstra, D., Size-Dependent Internalization of Particles via the Pathways of Clathrin- and Caveolae-Mediated Endocytosis, *Biochem. J.* **2004**, 377, 159-169.

42. Pelkmans, L.; Helenius, A., Endocytosis via Caveolae, *Traffic* **2002**, 3, 311-320.

43. Conner, S. D.; Schmid, S. L., Regulated Portals of Entry into the Cell, *Nature* **2003**, 422,

37-44.

44. Miyata, K.; Oba, M.; Nakanishi, M.; Fukushima, S.; Yamasaki, Y.; Koyama, H.; Nishiyama, N.; Kataoka, K., Polyplexes From Poly(Aspartamide) Bearing 1,2-Diaminoethane Side Chains Induce pH-Selective, Endosomal Membrane Destabilization with Amplified Transfection and Negligible Cytotoxicity, *J. Am. Chem. Soc.* **2008**, 130, 16287-16294.

45. Luo, D.; Haverstick, K.; Belcheva, N.; Han, E.; Saltzman, W. M., Poly(Ethylene Glycol)-Conjugated PAMAM Dendrimer for Biocompatible, High-Efficiency DNA Delivery. *Macromolecules* **2002**, 35, 3456-3462.

46. Ogris, M.; Brunner, S.; Schüller, S.; Kircheis, R.; Wagner, E., PEGylated DNA/transferrin-PEI Complexes: Reduced Interaction with Blood Components, Extended Circulation in Blood and Potential for Systemic Gene Delivery, *Gene Ther.* **1999**, 6, 595-605.

47. Yang, S.; May, S., Release of Cationic Polymer-DNA Complexes from the Endosome: A Theoretical Investigation of the Proton Sponge Hypothesis, *J. Chem. Phys.* **2008**, 129, 1-9.

48. Midoux, P.; Monsigny, M., Efficient Gene Transfer by Histidylated Polylysine/pDNA Complexes, *Bioconjugate Chem.* **1999**, 10, 406-411.

49. Hwang, H. S.; Hu, J.; Na, K.; Bae, Y. H., Role of Polymeric Endosomolytic Agents in Gene Transfection: A Comparative Study of Poly(L-lysine) Grafted with Monomeric L-Histidine Analogue and Poly(L-histidine). *Biomacromolecules* **2014**, 15, 3577-3586.

50. Leng, Q.; Mixson, A. J., Modified Branched Peptides with a Histidine-Rich Tail Enhance in vitro Gene Transfection, *Nucleic Acids Res.* **2005**, 33, 1-9.

51. Yu, H.; Nie, Y.; Dohmen, C.; Li, Y.; Wagner, E., Epidermal Growth Factor-PEG Functionalized PAMAM-Pentaethylenehexamine Dendron for Targeted Gene Delivery Produced by Click Chemistry, *Biomacromolecules* **2011**, 12, 2039-2047.

52. Uchida, H.; Miyata, K.; Oba, M.; Ishii, T.; Suma, T.; Itaka, L.; Nishiyama, N.; Kataoka, K., Odd-Even Effect of Repeating Aminoethylene Units in the Side Chain Of N-Substituted Polyaspartamides on Gene Transfection Profiles, *J. Am. Chem. Soc.* **2011**, 133, 15524-15532.
53. Walker, G. F.; Fella, C.; Pelisek, J.; Fahrmeir, J.; Boeckie, S.; Ogris, M.; Wagner, E., Toward synthetic viruses: endosomal pH-triggered deshielding of targeted polyplexes greatly enhances gene transfer in vitro and in vivo, *Mol. Ther.* **2005**, 11, 418-425.
54. Kabanov, A. V.; Kabanov, V. A., Interpolyelectrolyte and block ionomer complexes for gene delivery: physico-chemical aspects, *Adv. Drug Delivery Rev.* **1998**, 30, 49-60.
55. Lee, M.; Kim, S. W., Polyethylene glycol-conjugated copolymers for plasmid DNA delivery, *Pharm. Res.* **2005**, 22, 1-10.
56. Park, T. G.; Jeong, J. H.; Kim, S. W., Current status of polymeric gene delivery systems, *Adv. Drug Delivery Rev.* **2006**, 58, 467-486.
57. Wang, D. A.; Narang, A. S.; Kotb, M.; Gaber, A. O.; Kim, S. W.; Mahato, R. I., Novel branched poly(ethylenimine)-cholesterol water-soluble lipopolymers for gene delivery, *Biomacromolecules* **2002**, 3, 1197-1207.
58. Anwer, K.; Barnes, M. N.; Fewell, J.; Lewis, D. H.; Alvarez, R. D., Phase-I clinical trial of IL-12 plasmid/lipopolymer complexes for the treatment of recurrent ovarian cancer, *Gene Ther.* **2010**, 17, 360-369.
59. Oba, M.; Miyata, K.; Osada, K.; Christie, R. J.; Sanjoh, M.; Li, W. D.; Fukushima, S.; Ishii, T.; Kano, M. R.; Nishiyama, N.; Koyama, H.; Kataoka, K., Polyplex micelles prepared from ω -cholesteryl PEG-polycation block copolymers for systemic gene delivery, *Biomaterials* **2011**, 32, 652-663.
60. Chen, Q.; Osada, K.; Ge, Z. S.; Uchida, S.; Tockary, T. A.; Dirisala, A.; Matsui, A.; Toh,

K.; Takeda, K. M.; Liu, X. Y.; Nomoto, T.; Ishii, T.; Oba, M.; Matsumoto, Y.; Kataoka, K., Polyplex micelle installing intracellular self-processing functionalities without free cationomers for safe and efficient systemic gene therapy through tumor vasculature targeting, *Biomaterials* **2017**, 113, 253-265.

61. Kakizawa, Y.; Harada, A.; Kataoka, K., Environment-Sensitive Stabilization of Core–Shell Structured Polyion Complex Micelle by Reversible Cross-Linking of the Core through Disulfide Bond, *J. Am. Chem. Soc.* **1999**, 121, 11247-11248.

62. Park, Y.; Kwok, K. Y.; Boukarim, C.; Rice, K. G., Synthesis of sulfhydryl cross-linking poly(ethylene glycol)-peptides and glycopeptides as carriers for gene delivery, *Bioconjugate Chem.* **2002**, 13, 232-239.

63. Miyata, K.; Kakizawa, Y.; Nishiyama, N.; Yamasaki, Y.; Watanabe, T.; Kohara, M.; Kataoka, K., Freeze-dried formulations for in vivo gene delivery of PEGylated polyplex micelles with disulfide crosslinked cores to the liver, *J. Control. Release* **2005**, 109, 15-23.

64. Yessine, M. A.; Leroux, J. C., Membrane-destabilizing polyanions: interaction with lipid bilayers and endosomal escape of biomacromolecules, *Adv. Drug Delivery Rev.* **2004**, 56, 999-1021.

65. Itaka, K.; Ishii, T.; Hasegawa, Y.; Kataoka, K., Biodegradable polyamino acid-based polycations as safe and effective gene carrier minimizing cumulative toxicity, *Biomaterials* **2010**, 31, 3707-3714.

66. Lorand, J. P.; Edwards, J. O., Polyol Complexes and Structure of the Benzenboronate Ion, *J. Org. Chem.* **1959**, 24, 769-774.

67. Kitano, S.; Kataoka, K.; Koyama, Y.; Okano, T.; Sakurai, Y., Glucose-responsive complex formation between poly(vinyl alcohol) and poly(*N*-vinyl-2-pyrrolidone) with pendent

phenylboronic acid moieties, *Makromol. Chem., Rapid Commun.* **1991**, 12, 227-233.

68. Kataoka, K.; Miyazaki, H.; Bunya, M.; Okano, T.; Sakurai, Y., Sensitive Glucose-Induced Change of the Lower Critical Solution Temperature of Poly[*N,N*-(dimethylacrylamide)-co-3-(acrylamido)-phenylboronic acid] in Physiological Saline, *J. Am. Chem. Soc.* **1998**, 120, 12694-12695.

69. Singh, N.; Willson, R. C., Boronate affinity of RNA: possible role of conformational changes, *J. Chromato. A* **1999**, 840, 205-213.

70. Springsteen, G.; Wang, B. H., A detailed examination of boronic acid–diol complexation, *Tetrahedron* **2002**, 58, 5291-5300.

71. Yan, J.; Springsteen, G.; Deeter, S.; Wang, B., The relationship among pK_a, pH, and binding constants in the interactions between boronic acids and diols—it is not as simple as it appears, *Tetrahedron* **2004**, 60, 11205-11209.

72. Rosenberg, M.; Wiebers, J. L.; Gilham, P. T., Interactions of nucleotides, polynucleotides, and nucleic acids with dihydroxyboryl-substituted celluloses, *Biochemistry* **1972**, 11, 3623-3628.

73. Gehrke, C. W.; Kuo, K. C.; Davis, G. E.; Suits, R. D.; Waalkes, T. P.; Borek, E., Chromatography and modifications of nucleosides, *J. Chromatogr.* **1978**, 150, 455-476.

74. James, T. D.; Sandanayake, K. R. A. S.; Shinkai, S., Chiral discrimination of monosaccharides using a fluorescent molecular sensor, *Nature* **1994**, 374, 345-347.

75. James, T. D.; Sandanayake, K. R. A. S.; Iguchi, R.; Shinkai, S., Novel saccharidephotoinduced electron transfer sensors based on the interaction of boronic acid and Amine, *J. Am. Chem. Soc.* **1995**, 117, 8982-8987.

76. James, T. D.; Sandanayake, K. R. A. S.; Shinkai, S., Saccharide sensing with molecular

receptors based on boronic acid, *Angew. Chem. Int. Ed. Engl.* **1996**, 35, 1910-1922.

77. Uchimura, E.; Otsuka, H.; Okano, T.; Sakurai, Y.; Kataoka, K., Totally synthetic polymer with lectin-like function: induction of killer cells by the copolymer of 3-acrylamidophenylboronic acid with N, N-dimethylacrylamide, *Biotechnol. Bioeng.* **2001**, 72, 307-314.

78. Chen, X.; Scgauter, S.; Potier, N.; Dorsselaer, A. V.; Pelczer, I.; Bassler, B. L.; Hughson, F. M., Structural identification of a bacterial quorum-sensing signal containing boron, *Nature* **2002**, 415, 545-549.

79. Pasparakis, G.; Cockayne, A.; Alexander, C., Control of bacterial aggregation by thermoresponsive glycopolymers. *J. Am. Chem. Soc.* **2007**, 129, 11014-11015.

80. Peng, Q.; Chen, F.; Zhong, Z.; Zhuo, R., Enhanced gene transfection capability of polyethylenimine by incorporating boronic acid groups, *Chem. Commun.* **2010**, 46, 5888-5890.

81. Hartley, J. H.; Phillips, M. D.; James, T. D., Saccharide-accelerated hydrolysis of boronic acid imines, *New J. Chem.* **2002**, 26, 1228-1237.

82. Brooks, W. L. A.; Sumerlin, B. S., Synthesis and Applications of Boronic Acid-Containing Polymers: From Materials to Medicine, *Chem. Rev.* **2016**, 116, 1375-1397.

83. Singhal, R. P.; Ramamurthy, B.; Govindraj, N.; Sarwar, Y., New ligands for boronate affinity chromatography synthesis and properties, *J. Chromatogr.* **1991**, 543, 17-38.

84. Wulff, G., Selective Binding to Polymers via Covalent Bonds. The Construction of Chiral Cavities as Specific Receptor Sites, *Pure Appl. Chem.* **1982**, 54, 2093-2102.

85. Shiino, D.; Kubo, A.; Murata, Y.; Koyama, Y.; Kataoka, K.; Kikuchi, A.; Sakurai Y.; Okano, T., Amine effect on phenylboronic acid complex with glucose under physiological pH in aqueous solution, *J. Biomaterials Sci. Polymer* **1996**, 7, 697-705.

86. Höpfl, H., The tetrahedral character of the boron atom newly defined—a useful tool to evaluate the N→B bond, *J. Organomet. Chem.* **1999**, 581, 129-149.
87. Wiskur, S. L.; Lavigne, J. J.; Ait-Haddou, H.; Lynch, V.; Hung Chiu, Y.; Canary, J. W.; Anslyn, E. V., pK_a Values and Geometries of Secondary and Tertiary Amines Complexed to Boronic Acids—Implications for Sensor Design, *Org. Lett.* **2001**, 3, 1311-1314.
88. Franzen, S.; Ni, W.; Wang, B., Study of the Mechanism of Electron-Transfer Quenching by Boron-Nitrogen Adducts in Fluorescent Sensors, *J. Phys. Chem. B* **2003**, 107, 12942-12948.
89. Bosch, L. I.; Fyles, T. M.; James, T. D., Binary and ternary phenylboronic acid complexes with saccharides and Lewis bases, *Tetrahedron* **2004**, 60, 11175-11190.
90. Naito, M.; Ishii, T.; Matsumoto, A.; Miyata, K.; Miyahara, Y.; Kataoka, K., A phenylboronate-functionalized polyion complex micelle for ATP-triggered release of siRNA, *Angew. Chem. Int. Ed.* **2012**, 51, 10751.
91. Sahin, U.; Kariko, K.; Tureci, O., mRNA-based therapeutics—developing a new class of drugs, *Nat. Rev. Drug Discov.* **2014**, 13, 759-780.
92. Sullenger, B. A.; Nair, S., From the RNA world to the clinic, *Science* **2016**, 352, 1417-1420.
93. Mays, L. E.; Ammon-Treiber, S.; Mothes, B.; Alkhaled, M.; Rottenberger, J.; Muller-Hermelink, E. S.; Grimm, M.; Mezger, M.; Beer-Hammer, S.; von Stebut, E.; Rieber, N.; Nurnberg, B.; Schwab, M.; Handgretinger, R.; Idzko, M.; Hartl, D.; Kormann, M. S., Modified Foxp3 mRNA protects against asthma through an IL-10-dependent mechanism, *J. Clin. Invest.* **2013**, 123, 1216-1228.
94. Zangi, L.; Lui, K. O.; von Gise, A.; Ma, Q.; Ebina, W.; Ptaszek, L. M.; Spater, D.; Xu, H.; Tabebordbar, M.; Gorbakov, R.; Sena, B.; Nahrendorf, M.; Briscoe, D. M.; Li, R. A.; Wagers, A. J.; Rossi, D. J.; Pu, W. T.; Chien, K. R., Modified mRNA directs the fate of heart progenitor

cells and induces vascular regeneration after myocardial infarction, *Nat. Biotechnol.* **2013**, 31, 898-907.

95. Matsui, A.; Uchida, S.; Ishii, T.; Itaka, K.; Kataoka, K., Messenger RNA-based therapeutics for the treatment of apoptosis-associated diseases, *Scientific reports* **2015**, 5, 15810.

96. Kaczmarek, J. C.; Patel, A. K.; Kauffman, K. J.; Fenton, O. S.; Webber, M. J.; Heartlein, M. W.; DeRosa, F.; Anderson, D. G., Polymer-Lipid Nanoparticles for Systemic Delivery of mRNA to the Lungs, *Angew. Chem. Int. Ed. Engl.* **2016**, 55, 13808-13812.

97. Perche, F.; Uchida, S.; Akiba, H.; Lin, C. Y.; Ikegami, M.; Dirisala, A.; Nakashima, T.; Itaka, K.; Tsumoto, K.; Kataoka, K., Improved Brain Expression of Anti-Amyloid β scFv by Complexation of mRNA Including a Secretion Sequence with PEG-based Block cationomer, *Current Alzheimer research* **2017**, 14, 295-302.

98. Stadler, C. R.; Bahr-Mahmud, H.; Celik, L.; Hebich, B.; Roth, A. S.; Roth, R. P.; Kariko, K.; Tureci, O.; Sahin, U., Elimination of large tumors in mice by mRNA-encoded bispecific antibodies, *Nat. Med.* **2017**, 23, 815-817.

99. Sahin, U.; Derhovanessian, E.; Miller, M.; Kloke, B. P.; Simon, P.; Lower, M.; Bukur, V.; Tadmor, A. D.; Luxemburger, U.; Schrors, B.; Omokoko, T.; Vormehr, M.; Albrecht, C.; Paruzynski, A.; Kuhn, A. N.; Buck, J.; Heesch, S.; Schreeb, K. H.; Muller, F.; Ortseifer, I.; Vogler, I.; Godehardt, E.; Attig, S.; Rae, R.; Breitkreuz, A.; Tolliver, C.; Suchan, M.; Martic, G.; Hohberger, A.; Sorn, P.; Diekmann, J.; Ciesla, J.; Waksman, O.; Bruck, A. K.; Witt, M.; Zillgen, M.; Rothermel, A.; Kasemann, B.; Langer, D.; Bolte, S.; Diken, M.; Kreiter, S.; Nemecek, R.; Gebhardt, C.; Grabbe, S.; Holler, C.; Utikal, J.; Huber, C.; Loquai, C.; Tureci, O., Personalized RNA mutanome vaccines mobilize poly-specific therapeutic immunity against cancer, *Nature* **2017**, 547, 222-226.

100. Matsumoto, A.; Ishii, T.; Nishida, J.; Matsumoto, H.; Kataoka, K.; Miyahara, Y., A synthesis approach toward a self-regulated insulin delivery system, *Angew. Chem., Int. Ed.* **2012**, 51, 2124-2128.
101. Uchida, S.; Kinoh, H.; Ishii, T.; Matsui, A.; Tockary, T. A.; Takeda, K. M.; Uchida, H.; Osada, K.; Itaka, K.; Kataoka, K., Systemic delivery of messenger RNA for the treatment of pancreatic cancer using polyplex nanomicelles with a cholesterol moiety, *Biomaterials* **2016**, 82, 221-228.

Chapter 2

Development of pDNA-loaded polyplex micelles with pH- and ATP-
dual responsive phenylboronate ester cross-linking

2.1. Introduction

I focused on a phenylboronic acid (PBA) moiety in order to provide PMs with three functions as described in Chapter 1. PBA is known to be in equilibrium between a hydrophobic trigonal form and a hydrophilic tetrahedral form, and hydrophilic tetrahedral PBAs can form reversible ester linkage with diol compounds in aqueous solution (**Figure 2-1**).¹⁻⁶ This dual responsiveness enables PMs to achieve stabilization effect, endosomal escapability, and loaded nucleic acid release in response to cytosolic-specific stimulus for efficient gene delivery. Actually, introducing 3-fluoro-substituted PBA (FPBA) moieties to block copolymers gives adenosine triphosphate (ATP)-responsiveness to delivery carriers, which selectively released encapsulated cargos in response to highly concentrated ATP in cytoplasm because ribose ring on ATP binds to PBA at high affinity.⁷⁻⁸ Note that, FPBA can form phenylboronate ester linkage at physiological pH condition because its acid dissociation constant (pK_a) is estimated to be 7.2 after introduction via amide coupling.⁹ Moreover, hydrophobicity of PBA at lower pH condition can also accelerate gene transfection because hydrophobic moieties are known to enhance endosomal escapability.

In this Chapter, I developed phenylboronate ester cross-linked PMs achieving the stability during delivery process, endosomal escapability and loaded nucleic acid release in response to intracellular ATP concentration. The PMs were prepared from plasmid DNA

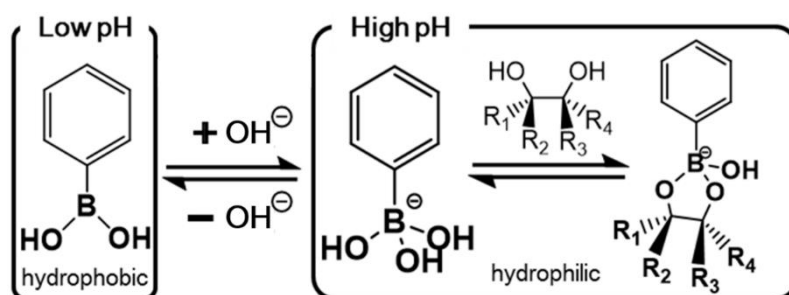


Figure 2-1. Equilibrium of PBA and diol compound in aqueous solution

(pDNA) and two kind of block copolymers; one with FPBA moieties, and the other with D-gluconamide (GlcAm) moieties. As a platform of block copolymer, PEG-*b*-poly{*N*'-[*N*-(2-aminoethyl)-2-aminoethyl]aspartamide} (PEG-PAsp(DET)), which demonstrate efficient endosomal escape due to double protonated property in response to pH decrease in late endosomes (pH 5.5) (**Figure 2-2**),¹⁰⁻¹¹ was used. FPBA/GlcAm cross-linking selectively formed in PM core through self-assembly with pDNA due to highly concentrated cross-linkable agents. The FPBA/GlcAm cross-linking was expected to stabilize PM structure and protect loaded pDNA from nuclease attacks en route to target cells. After cellular uptake by endocytosis, the equilibrium of FPBA shifted to hydrophobic trigonal structure responding endosomal pH drop, which leading the cleavage of FPBA/GlcAm cross-linking. At the same time, the number of protonated amine groups on PAsp(DET) side chain increased at the endosomal pH. These pH-responsive behaviors allowed release of block copolymers from PM in endosomal compartments, and the released block copolymers would facilitate endosomal escape due to membrane disruption by PAsp(DET) and hydrophobic FPBA. Moreover, highly concentrated ATP was replaced with GlcAm in cytosol. The replaced ATP could break charge

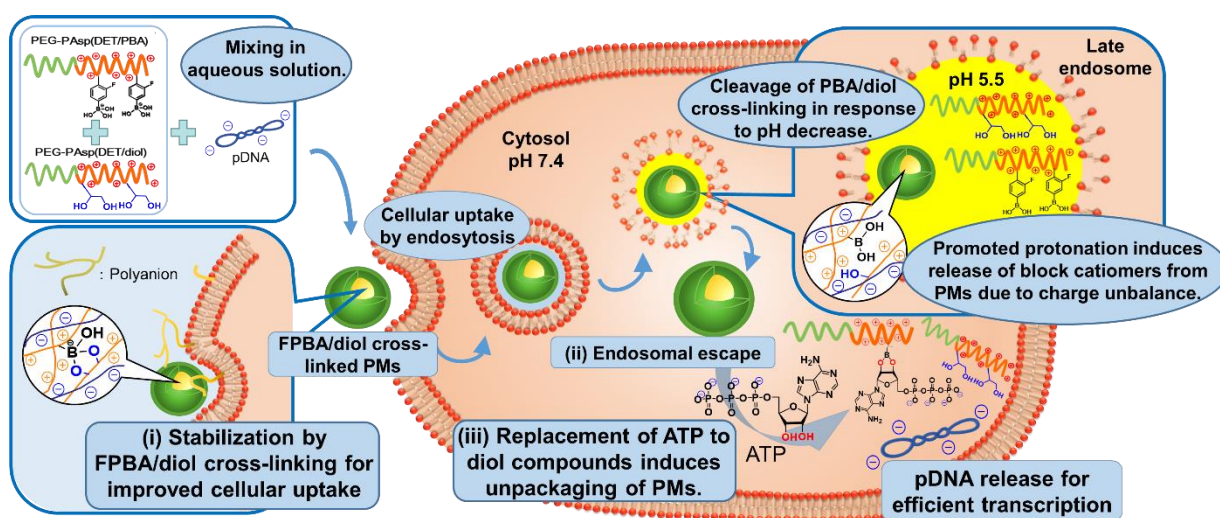


Figure 2-2. Schematic illustration of intracellular behavior of FPBA/GlcAm cross-linked PMs

balance of PM core, and finally induce PM dissociation inside the cells (**Figure 2-2**).

To demonstrate the utility of this strategy, the structure of block copolymers was firstly optimized from stability of PMs and pH-/ATP-responsiveness, followed by *in vitro* experiments were conducted.

2.2 Experimental section

2.2.1 Materials

β -Benzyl-L-aspartate-*N*-carboxy anhydride (BLA-NCA) was purchased from Chuo Kaseihin Co., Inc. (Osaka, Japan). α -Methoxy-PEG-NH₂ (M_w of PEG: 12 kDa) was purchased from NOF CO., Ltd. (Tokyo, Japan). *N, N*-dimethylformamide (DMF), dichloromethane (DCM), benzene, *N*-methylpyrrolidone (NMP), triethylamine (TEA) and diethylene triamine (DET) were purchased from Nakalai Tesque, Inc. (Kyoto, Japan). DMF, DCM, NMP and DET were used after distillation over calcium hydride. Methanol, acetone, 4-carboxy-3-fluorophenylboronic acid, D-sorbitol, D-glucose, L-(+)-ascorbic acid sodium salt, 2-amino-2-hydroxymethyl-1,3-propandiol (Tris), sodium dextran sulfate (M_w: 50,000 g/mol), 4-(4,6-dimethoxy-1,3,5-triazin-2-yl)-4-methylmorpholinium chloride n-hydrate (DMT-MM), D-PBS and Trypsin-EDTA Solution were purchased from Wako Pure Chemical Industries, Ltd. (Osaka, Japan). D-(+)-Glucono-1,5-lactone and 4-aminobutyric acid were purchased from Tokyo Kasei Kogyo Co., Ltd. (Tokyo, Japan). ATP was purchased from Oriental Kobo Co., Ltd. (Osaka, Japan). 2-[4-(2-Hydroxyethyl)-1-piperazinyl]ethanesulfonic acid (HEPES), 2-morpholinoethanesulfonic acid, monohydrate (MES), EDTA·2Na, Hoechst 33342 and Cell Counting Kit-8 (CCK-8) were purchased from Dojindo Laboratories (Kumamoto, Japan). The luciferase-coded pDNA (6.5 kbp) with CAG promoter obtained from RIKEN Gene Bank

(Tsukuba, Japan) was amplified in competent DH5 α *Escherichia coli* and purified using a QIAGEN HiSpeed Plasmid MaxKit (Germantown, MD). Agarose L03 TAKARA and 10 \times loading buffer were purchased from TAKARA Bio Inc. (Shiga, Japan). Ethidium bromide was purchased from NIPPON GENE Co., Ltd. (Tokyo, Japan). Cell culture medium was prepared from 450 mL of Dulbecco's modified Eagle's medium (DMEM) (Sigma-Aldrich Co., Madison, WI), 50 mL of fetal bovine serum (FBS) (Dainippon Sumitomo Pharma Co., Ltd., Osaka, Japan) and 5 mL of Penicillin-Streptomycin Solution Stabilized (Sigma-Aldrich). Human Hepatocarcinoma cells (HuH-7) were obtained from RIKEN Cell Bank (Tsukuba, Japan). Heparanase II was from *Flavobacterium heparinum* were purchased from Sigma-Aldrich Co. (Madison, WI). Cy3- and Cy5-labeled pDNA were prepared using Label IT Tracker Intracellular Nucleic Acid Localization Kit (Mirus Bio Corporation, Madison, WI) according to manufactures' protocol. CF594 succinimidyl ester was purchased from Biotium, Inc. (Fremont, CA). YO-PRO 1 Iodide was purchased from Thermo Fisher Scientific Inc. (Tokyo, Japan). LysoTracker Green was purchased from Molecular Probes (Eugene, OR). Luciferase Assay System Kit and Passive Lysis buffer were purchased from Promega Co. (Madison, WI). Cell culture plates were purchased from Becton Dickinson (Franklin Lakes, NJ, USA).

2.2.2 Synthesis of *N*-substituted-D-gluconamide (GlcAm)

GlcAm was synthesized from D-(+)-Glucono-1,5-lactone and 4-aminobutyric acid as shown in Scheme X. D-(+)-Glucono-1,5-lactone (89 mg, 0.5 mmol) and 4-aminobutyric acid (52 mg, 0.5 mmol) were dissolved in the mixture of methanol and TEA (14 mL and 1.5 mL, respectively). The solution was refluxed overnight at 75 °C. The product (GlcAm) was recrystallized from the mixture of hexane and ethyl acetate (hexane/ethyl acetate = 1/1), and

collected by filtration (yield; 86%, 122 mg). The structure of GlcAm was confirmed by ^1H -NMR spectrum (D_2O at 25 °C) (400 MHz) (JEOL ECS-400, JEOL, Tokyo, Japan).

2.2.3 Synthesis of PEG-PAsp(DET-FPBA) and PEG-PAsp(DET-GlcAm)

First, PEG-PBLA was synthesized by ring-opening reaction of NCA-BLA from PEG-NH₂.¹² MeO-PEG-NH₂ (505 mg) was dissolved in the mixture of DMF/DCM (1/10, 5.1 mL). NCA-BLA (920 mg) was also dissolved 9.2 mL of the same mixture. The NCA-BLA solution was added to PEG solution, and reacted for 72 h at 25 °C. The reacted solution was dropped into the mixture of ethyl acetate and hexane (2/3, 300 mL), and after drying in vacuo PEG-PBLA (1.11 g) was collected as white powder. The degree of polymerization of PBLA and M_w/M_n was analyzed by ^1H -NMR spectra ($\text{DMSO}-d_6$ at 80 °C, $\delta = 3.4 - 3.6$ ppm (4H: $-\text{CH}_2-\text{CH}_2-\text{O}-$), $\delta = 7.9 - 8.1$ ppm (5H: $-\text{C}_6\text{H}_5$)) and gel permeable chromatography (GPC) chart (TOSOH HLC- 8220GPC, column: TSK gel column, carrier: NMP containing 50 mM LiBr, flow rate: 0.3 ml/min, Temperature: 40 °C), respectively.

Then, PEG-PAsp(DET) was synthesized by ester/amide exchange reaction between DET and PBLA.¹³ PEG-PBLA (600 mg) was dissolved in 30 mL of dry NMP containing 0.5 M thiourea. Dry DET (9 mL; 50 eq. to PBLA unit) was diluted with 9 mL of dry NMP containing 0.5 M thiourea. PEG-PBLA solution was slowly dropped into DET solution at 10 °C, reacted for 1 h. The reacted solution was immediately neutralized with 5 M HCl_{aq} at 5 °C or less. After neutralization, the solution was dialyzed using Spectra/Por 4 Membrane (MWCO: 12-14 kDa) (Funakoshi Co., Ltd, Tokyo, Japan) against 0.01 N HCl at 4 °C for 1 day, and against deionized water at 4 °C for one more day. After freeze-drying, PEG-PAsp(DET) was collected as a white powder. The degree of polymerization of PAsp(DET) was analyzed by ^1H -

NMR spectra (D_2O at 80 °C, $\delta = 3.4 - 3.6$ ppm (4H: $-CH_2-CH_2-O-$), $\delta = 4.6 - 4.9$ ppm (1H: $-CO-CH-NH-$)).

PEG-PAsp(DET-FPBA) and PEG-PAsp(DET-GlcAm) were respectively prepared through dehydration condensation reaction using amide coupling agent (DMT-MM). PEG-PAsp(DET-FPBA) was synthesized as follows; PEG-PAsp(DET) (40 mg; 0.10 mmol as residual primary amino group on PAsp(DET) side chain), 155 mg of DMT-MM, and 92 mg of D-sorbitol (0.50 mmol: 5 eq. to residual primary amino group on PAsp(DET) side chain) were dissolved in 3 mL of 40 mM $NaHCO_3$ aqueous solution. FPBA (4.1, 6.2, 12.3, or 18.7 mg; 0.022, 0.033, 0.063, or 0.10 mmol, respectively) was dissolved in 9 mL of methanol, and then added to polymer solution. The mixture was reacted for 6 h at 4 °C with adding additional 155 mg of DMT-MM every 2 h. The reacted solution was immediately dialyzed using Spectra/Por 4 Membrane (MWCO: 12-14 kDa) against 0.01 N HCl at 4 °C for 1 day, and against deionized water at 4 °C for one more day. After freeze-drying, PEG-PAsp(DET-FPBA) was collected as a white powder, and introduction ratio of FPBA was determined by 1H -NMR spectra (D_2O at 80 °C, $\delta = 4.6 - 4.9$ ppm (1H: $-CO-CH-NH-$), $\delta = 7.2 - 7.6$ ppm (3H: $-C_6H_3FB(OH)_2$)). Similarly, PEG-PAsp(DET-GlcAm) was synthesized as follows; PEG-PAsp(DET) (40 mg; 0.10 mmol as residual primary amino group on PAsp(DET) side chain), 155 mg of DMT-MM, and GlcAm (6.0, 9.0, 12.1, or 18.1 mg; 0.020, 0.030, 0.040, or 0.060 mmol, respectively) was dissolved in 12 mL of the mixture of 40 mM $NaHCO_3$ aqueous solution and methanol ($NaHCO_{3aq}/methanol = 1/3$). The mixture was reacted for 6 h at 4 °C with adding additional 155 mg of DMT-MM every 2 h. The reacted solution was immediately dialyzed using Spectra/Por 4 Membrane (MWCO: 12-14 kDa) against 0.01 N HCl at 4 °C for 1 day, and against deionized water at 4 °C for one more day. After freeze-drying, PEG-PAsp(DET-GlcAm) was collected as a white

powder, and introduction ratio of FPBA was determined by ^1H -NMR spectra (D_2O at $80\text{ }^\circ\text{C}$, $\delta = 4.6 - 4.9\text{ ppm}$ (1H: $-\text{CO}-\text{CH}-\text{NH}-$), $\delta = 1.9$ and 2.3 ppm (4H: $-\text{CH}_2-\text{NHCO}-\text{CH}_2\text{CH}_2\text{CH}_2\text{NHCO}-$).

2.2.4 Preparation of PMs

Synthesized block copolymers were dissolved in 10 mM HEPES buffer ($\text{pH } 7.4$), respectively. The concentration of block copolymers was determined by the residual molar ratio of protonated amino groups and negatively-charged tetrahedral FPBA groups as follows: $[\text{N}^+]_{\text{PEG-PAsp}(\text{DET})}$ = (residual molar ratio of protonated amino group on PAsp(DET) side chain), $[\text{N}^+-\text{B}^-]_{\text{PEG-PAsp}(\text{DET-FPBA})}$ = {(residual molar ratio of protonated amino group on PAsp(DET) side chain) – (residual molar ratio of negatively-charged tetrahedral FPBA groups)}, and $[\text{N}^+]_{\text{PEG-PAsp}(\text{DET-GlcAm})}$ = (residual molar ratio of protonated amino group on PAsp(DET) side chain). For this calculation, 53% of residual amino groups in unmodified PAsp(DET) side chain form the protonated state at $\text{pH } 7.4$.¹⁰ In addition, all residual amino groups on PAsp(DET) segment modified with FPBA or GlcAm are also estimated to form the protonated state at $\text{pH } 7.4$. As for FPBA, 61% of FPBA residues were estimated to form negatively-charged tetrahedral structure from the pK_a of 7.2 .²⁸ Similarly, the concentration of pDNA solution was determined by the residual molar ratio of phosphate groups on pDNA ($[\text{P}^-]_{\text{pDNA}}$). To prepare cross-linked PMs, PEG-PAsp(DET-FPBA) and PEG-PAsp(DET-GlcAm) solution was mixed at the same $[\text{N}^+-\text{B}^-]_{\text{PEG-PAsp}(\text{DET-FPBA})}$ and $[\text{N}^+]_{\text{PEG-PAsp}(\text{DET-GlcAm})}$ (0.225 mM), followed by adding to pDNA solution ($[\text{P}^-]_{\text{pDNA}} = 0.15\text{ mM}$) under vortex mixing in residual charge ratio of 1.5 ($r = ([\text{N}^+-\text{B}^-]_{\text{PEG-PAsp}(\text{DET-FPBA})} + [\text{N}^+]_{\text{PEG-PAsp}(\text{DET-GlcAm})}) / [\text{P}^-]_{\text{pDNA}}$). Thus, the PM solution was incubated overnight at $4\text{ }^\circ\text{C}$.

2.2.5 Dynamic light scattering (DLS) measurement

DLS measurement was conducted using Zetasizer Nano (Ar laser: 532 nm, Scattering angle: 173°) (Marvern Instruments, Worcestershire, U. K.) at room temperature to determine the hydrodynamic diameter and polydispersity index (PDI) of PMs with cumulant method.

2.2.6 Tolerability test against polyion exchange reaction (sodium dextran sulfate)

PMs (final pDNA conc.: 25 µg/mL) were incubated with various concentration of sodium dextran sulfate (DS) solution in 10 mM HEPES containing 150 mM NaCl at 37 °C for 1 h. The residual charge ratio of sulfate group on DS per phosphate group on pDNA (A/P ratio) was set to be 8 or 9. After incubation, the mixture with 10×loading buffer was loaded onto a 0.9wt% agarose gel. Gel electrophoresis was conducted at 100 V for 60 min. The migration of pDNA in the agarose gel was visualized by EtBr staining. Images were captured using PharosFX™ System (Bio-rad Laboratories, Inc., CA).

2.2.7 ATP-responsiveness of PMs

PMs (final pDNA conc.: 25 µg/mL) were incubated with various concentration of ATP in 10 mM HEPES containing 150 mM NaCl at 37 °C for 2 h. The final ATP concentration was adjusted to 0.1, 0.5, 1.0, 3.0, or 5.0 mM. After incubation, migration of pDNA was observed through gel electrophoresis using the same method described in the preceding section.

2.2.8 Quantification of binding block copolymers to pDNA in PMs

Block copolymers were labeled with CF594 succinimidyl ester according to the

manufactures' procedure. Two kind of PMs were prepared with the same protocol described in "*Preparation of PM*" section; one with CF594-labeled PEG-PAsp(DET-FPBA) and non-labeled PEG-PAsp(DET-GlcAm), and the other with non-labeled PEG-PAsp(DET-FPBA) and CF594-PEG-PAsp(DET-GlcAm). PMs were incubated at 37 °C for 6 h, and then ultracentrifuged for 1.5 h at 63,000 g using thick-wall polycarbonate tube (Beckman Coulter, Inc., CA) and Beckman XL-1 ultracentrifuge (Beckman Coulter, Inc., CA) equipped with TLA-120.1 rotor. After ultracentrifugation, the fluorescence intensity of free block copolymers in the supernatant was measured using NanoDrop ND-3300 (Wilmington, NC) at a wavelength of 614 nm. The concentration of free block copolymers was determined from the calibration curve of CF594-labeled block copolymer solution. Also, the same experiment was conducted at pH 5.5 using acetate buffer.

2.2.9 Cell culturing

Cells were cultured in DMEM containing 10% FBS and 1% penicillin/streptomycin in a humidified atmosphere with 5% CO₂ at 37 °C.

2.2.10 Evaluation of cellular uptake efficiency of PMs

HuH-7 cells (5,000 cells/well) were seeded on 96-well plate in 100 µL of culture medium. After 24 h incubation, the culture medium was replaced with 100 µL of the fresh one, and 7.5 µL of PM solution containing 250 ng of Cy5-labeled pDNA was added. After 24 h post-incubation, the cells were washed three times by cold D-PBS buffer, and then lysed by 50 µL of Passive Lysis Buffer (Promega Co., Madison, WI). The fluorescence intensity of each cell lysate was measured using Microplate Reader Infinite M1000 Pro (Tecan Japan Co., Ltd.,

Kanagawa, Japan) with an excitation wavelength at 633 nm and an emission wavelength at 672 nm.

To get more insight about the stabilization effect of PMs on cellular uptake, Heparanase II-treated cells were prepared to evaluate the effect of anionic macromolecules on cellular membrane on cell entry of PMs.¹⁴ HuH-7 cells (5,000 cells/well) were seeded on 96-well plate in 100 μ L of culture medium. After 24 h incubation, the culture medium was replaced with Opti-MEM (Thermo Fisher Scientific Inc., Tokyo, Japan) containing Heparanase II (5 units/mL) and incubated more 30 min. Then, the cells were washed twice by cold D-PBS, followed by adding 100 μ L of culture medium and 7.5 μ L of PM solution containing 250 ng of Cy5-labeled pDNA. After 24 h post-incubation, the cells were washed three times by cold D-PBS, and then lysed by 50 μ L of Passive Lysis Buffer. The fluorescence intensity of cell lysate was measured by the same method described the preceding section.

2.2.11 Transfection of PMs to cultured cells

HuH-7 cells (20,000 cells/well) were seeded onto 24-well plate in 400 μ L of culture medium. After 24 h incubation, the culture medium was replaced with the fresh one, followed by adding 30 μ L of PM solution containing 1 μ g of pDNA. The cells were incubated for 48 h with replacing culture medium with fresh one at 24 h time point. Then, the cells were washed three times by cold D-PBS, and lysed by 200 μ L of Passive Lysis buffer. Luciferase activity of 20 μ L of cell lysate was evaluated using Luciferase assay kit and Luminometer Glomax 96 (Promega Co., Madison, WI).

2.2.12 Membrane disruptive ability of block copolymers

The membrane disruptive ability was evaluated by measuring the fluorescence of membrane-impermeable dye, YO-PRO 1, in HuH-7 cells after treatment of block copolymers at pH 7.4 and 5.5.¹⁵⁻¹⁶ HuH-7 cells (20,000 cells/well) were seeded on 48-well plate in 200 μ L of culture medium. After 24 h incubation, the culture medium was replaced with 75 μ L of block copolymer solution in D-PBS (pH 7.4) or 20 mM MES (pH 5.5) containing 150 mM NaCl. The concentration of block copolymers was determined from the residual molar concentration of protonated amino groups ($[N^+]_{\text{PEG-}b\text{-PAsp(DET)}}$, $[N^+]_{\text{PEG-}b\text{-PAsp(DET-GlcAm)}}$, and $[N^+-B^-]_{\text{PEG-}b\text{-PAsp(DET-FPBA)}}$) at pH 7.4 and adjusted to be 6.0 mM, respectively. After 20 min incubation with block copolymers, 2.5 μ M Hoechst 33342 and 1 μ M YO-PRO 1 were added to each well. The fluorescence intensity of YO-PRO 1 was measured using IN Cell Analyzer 1000 with image-analysis software (GE Healthcare UK Ltd., Buckinghamshire, England).

2.2.13 Observation of endosomal escape of PMs

HuH-7 cells (50,000 cells/dish) were seeded onto 35-mm glass-based dishes in 2 mL of culture medium. After 24 h incubation, the culture medium was replaced with 350 μ L of the fresh one, followed by 150 μ L of PM solution containing 5 μ g of Cy3-labeled pDNA. Cells were washed twice by D-PBS to remove extracellular PMs completely after 6h of transfection. The intracellular distribution of Cy3-labeled pDNA was observed using confocal laser scanning microscopy (CLSM) with staining late endosomes/lysosomes by LysoTracker Green and cell nuclei by Hoechst 33342. CLSM images were captured by LSM 520 (Carl Zeiss, Oberkochen, Germany) with a $\times 40$ objective lens, C-Apochromat (Carl Zeiss), at excitation wavelength of 488 nm for LysoTracker Green, 532 nm for Cy3, and 710 nm (MaiTai laser for 2-photon imaging) for Hoechst 33342. Colocalization ratio of Cy3-labeled pDNA with late

endosomes/lysosomes was calculated as follows:

$$\text{Colocalization ratio} = (\text{Cy3 pixels with late endosomes/lysosomes pixels}) / (\text{All Cy3 pixels})$$

2.2.14 Förster resonance energy transfer (FRET) measurement of double labeled pDNA

Cy3/Cy5 double-labeled pDNA was prepared using both label IT Cy3 and Cy5 labeling kit following the manufactures' protocol with slight modification.¹⁷⁻¹⁸ Then, PMs encapsulated with Cy3/Cy5 double-labeled pDNA were prepared by the same protocol as described in the preceding "*Preparation of PM*" section. PM solutions were mixed with the various concentrated ATP solution (0, 1, or 3 mM) in 10 mM HEPES buffer at pH 7.4 containing 150 mM NaCl, and incubated for 2 h at 37 °C. The fluorescence intensity of each sample was measured using Microplate Reader Infinite M1000 Pro at the excitation wavelength of 488 nm and the emission wavelength of 570 nm for Cy3 and 672 nm for Cy5, respectively. The FRET efficiency was calculated as following equation:

$$\text{FRET efficiency} = (\text{Cy5 fluorescence intensity (672 nm)}) / (\text{Cy5 fluorescence intensity (570 nm)})$$

Intracellular FRET observation was also conducted using flow cytometry. HuH-7 cells (100,000 cells/well) were seeded onto 6-well plate in 2 mL of culture medium. After 24 h incubation, the culture medium was replaced with 350 µL of the fresh one, followed by adding 150 µL of PM solution containing 5 µg of Cy3/Cy5 double labeled pDNA. After 6 h of transfection, the cells were washed three times by cold D-PBS to remove extracellular PMs. The cells were collected by trypsinization after 6 h, 12 h and 24 h incubation of transfection. The fluorescence intensity of the collected cells was measured by BD LSR II instrument (BD Bioscience, Franklin Lakes, NJ) using 488 nm laser for excitation and both 575/26 and 550LP

filters for Cy3 and 660/20 nm for Cy5 emission.

2.2.15 Tolerability of PMs in blood stream

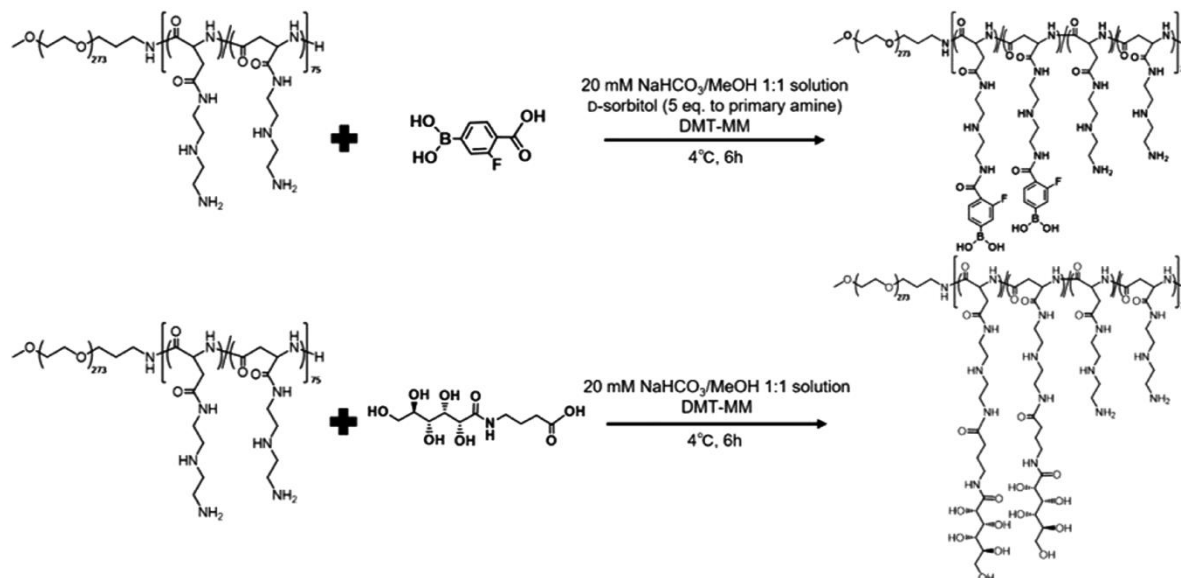
PM solution (200 μ L) in 10 mM HEPES buffer (pH 7.4) with 150 mM NaCl containing 20 μ g of pDNA was administrated to BALB/c mouse (female, 7 weeks old, Charles River Laboratories Japan Inc., Kanagawa, Japan) from tail vein. After 5, 10, 20, 40 min of administration, 2 μ L of blood was collected from tail vein and immediately mixed with 350 μ L of the mixture of PBS/EDTA/Proteinase K. The amount of pDNA in the mixture of 20 μ L of PMs containing 2 μ g of pDNA, 2 μ L of blood and 350 μ L of PBS/EDTA/Proteinase K was regarded as an initial value of pDNA. After adding 10 μ L of 150 mM ATP solution, pDNA was extracted from each blood sample using DNeasy blood & tissue Kit (Qiagen, Hilden, Germany) following the manufactures' protocol. Using these pDNA, qRT-PCR analysis was performed by SYBR green intercalator method using a primer pair for GLuc mRNA (Forward; TGCAAAAGATCCTCAACGTG, and Reverse; AATGGGAAGTCACGAAGGTG) and ABI Prism 7500 Sequence Detector (Applied Biosystems, Foster City, CA). All animal experiments were conducted according to the Guidelines for the Care and Use of Laboratory Animals and the approval of the Animal Committee of the University of Tokyo.

2.3 Results and Discussion

2.3.1 Synthesis of PEG-PAsp(DET-FPBA) and PEG-PAsp(DET-GlcAm)

PEG-PAsp(DET) (M_w of PEG: 12 kDa, Degree of polymerization of PAsp(DET): 75) was synthesized according to the previous report,¹³ and then FPBA and GlcAm moieties were introduced PAsp(DET) side chain, respectively (**Scheme 2-1**). This design can avoid the

Scheme 2-1. Synthetic Schemes of PEG-PAsp(DET-FPBA) and PEG-PAsp(DET-GlcAm) from PEG-PAsp(DET)



intramolecular cross-linking between FPBA and GlcAm which may happen if both FPBA and GlcAm were introduced into the same PAsp(DET) segment. To find the optimum introduction ratio of FPBA and GlcAm moieties in stabilization effect and pH-/ATP-responsiveness, a series of block copolymers with various introduction ratio was prepared. The introduction ratio of FPBA was determined to be 14, 26, 59, and 89%, and that of GlcAm was 9, 14, 27, 54% by ¹H-NMR spectra (**Figure 2-3**). The synthesized block copolymers are referred to as PEG-PAsp(DET-FPBA_X%) and PEG-PAsp(DET-GlcAm_Y%), where X and Y denote the introduction ratio of FPBA or GlcAm units. Note that, PEG-PAsp(DET-FPBA) was dissolved in 10 mM HEPES buffer (pH 7.4) and showed comparable scattering intensity with PEG-PAsp(DET) solution even though 39% of introduced FPBA moieties were estimated to take hydrophobic trigonal structure at pH 7.4, which was estimated from pK_a value of FPBA.⁹

2.3.2 Preparation of PMs and optimization of introduction ratio of cross-linking agents

PEG-PAsp(DET-FPBA_X%) and PEG-PAsp(DET-GlcAm_Y%) were dissolved in 10 mM

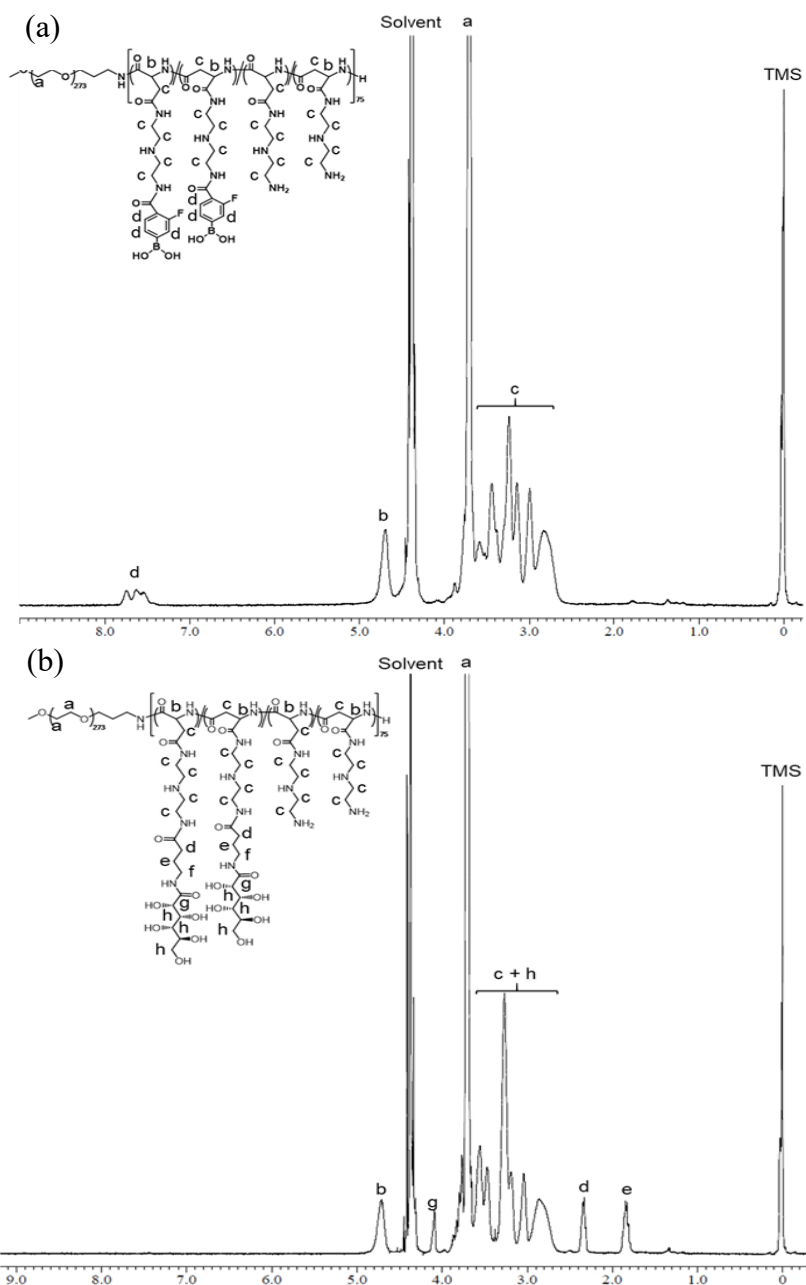


Figure 2-3. Representative ¹H-NMR spectra of (a) PEG-PAsp(DET-FPBA) and (b) PEG-PAsp(DET-GlcAm)

HEPES buffer (pH 7.4), respectively. Then, the library of the mixture of PEG-PAsp(DET-FPBA_{X%}) and PEG-PAsp(DET-GlcAm_{Y%}) was prepared in all combination. All these mixtures showed similar light scattering intensity to PEG-PAsp(DET) solution, indicating that no intermolecular cross-linking between FPBA and GlcAm was formed by mixing block

copolymers. Probably, electrostatic repulsion between block copolymers prevented FPBA and GlcAm moieties approaching to each other to form phenylboronate ester linkage. The polymer mixture was then added to pDNA solution at residual charge ratio of 1.5 (details described in the proceeding section of “*Preparation of polyplex micelles*”). DLS measurement of all prepared samples showed 75 ~ 96 nm cumulant diameter and PDI of 0.15 ~ 0.25, which were comparable with previously reported PMs composed of similar block copolymers (**Table 2-1**)^{13,19} and indicated PM formation of all samples. The PMs prepared from PEG-PAsp(DET-FPBA_{X%}) and PEG-PAsp(DET-GlcAm_{Y%}) are referred to as BX/GY PMs.

The cross-linking efficiency in PM core was evaluated through tolerability test against polyion exchange reaction using sodium dextran sulfate (DS). First, in order to find the optimum combination of PEG-PAsp(DET-FPBA_{X%}) and PEG-PAsp(DET-GlcAm_{Y%}), the tolerability of all PMs against DS was evaluated though agarose gel electrophoresis. Electrophoregram showed the migration of pDNA from PMs after incubation with DS at A/P ratio of 8 (**Figure 2-4 (a)-(d)**). Obviously, there was an optimal combination of FPBA and GlcAm introduction ratio onto PAsp(DET) segment, and B59/G27 PM and B59/G54 PM maintained encapsulated pDNA in the core (**Figure 2-4 (c)**). With increasing DS at A/P ratio

Table 2-1. Cumulant diameter and polydispersity index of PMs evaluated by DLS measurement at 25 °C in 10 mM HEPES buffer (pH 7.4)

GlcAm ratio (%)	<i>d.</i> nm/ PDI				
	FPBA ratio (%)				
	0	14	26	59	89
0	76/ 0.16	—	—	—	—
9	—	75/ 0.20	80/ 0.23	81/ 0.17	88/ 0.16
14	—	80/ 0.20	80/ 0.20	81/ 0.17	91/ 0.17
27	—	88/ 0.19	88/ 0.16	82/ 0.15	96/ 0.15
54	—	92/ 0.25	87/ 0.19	84/ 0.18	87/ 0.25

of 9, while B59/G54 PM released loaded pDNA, B59/G27 PM kept loaded pDNA in the core (**Figure 2-4 (e)**). The optimum introduction ratio of FPBA and GlcAm against polyeion exchange reaction can be explained by the balance between the efficiency of cross-linking and the strength of electrostatic interaction between block copolymers and pDNA. Actually, increasing the introduction ratio of FPBA and GlcAm in PAsp(DET) side chain was preferable to efficient cross-linking in PM core. On the other hand, high modification of FPBA moieties into PAsp(DET) decreased charge density of cationic segment due to negatively-charged

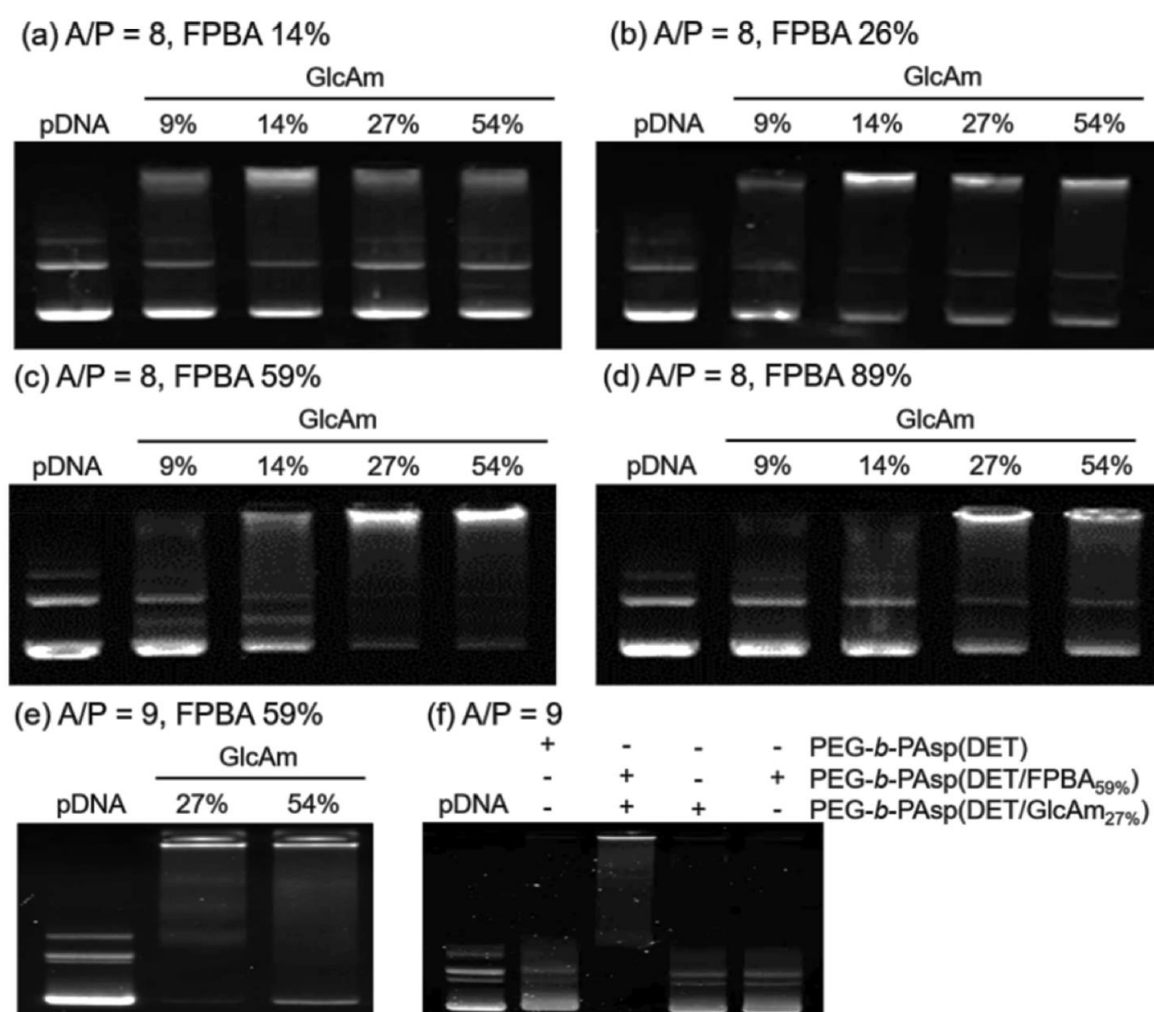


Figure 2-4. Electrophoregrams of PMs incubated with sodium dextran sulfate (DS). (a - d) Electrophoregrams of PMs prepared from PEG-PAsp(DET-FPBA) and PEG-PAsp(DET-GlcAm) in all combination at A/P ratio of 8. (e) Electrophoregram of B59/G27 PMs and B59/G54 PMs at A/P ratio of 9. (f) Electrophoregram of PEG-PAsp(DET) PMs, cross-linked PMs, PEG-PAsp(DET-FPBA) PMs and PEG-PAsp(DET-GlcAm) PMs at A/P ratio of 9.

tetrahedral FPBA moieties, and may prevent stable PM formation. In addition, high modification of GlcAm might also inhibit pDNA condensation due to its hydrophilicity. Therefore, there was an optimal introduction ratio of FPBA and GlcAm to stabilize PM structure. Importantly, as shown in **Figure 2-4 (f)**, stabilization effect against polyion exchange reaction was observed only when PMs were prepared from both PEG-PAsp(DET-FPBA_{59%}) and PEG-PAsp(DET-GlcAm_{27%}), suggesting intermolecular cross-linking between FPBA and GlcAm moieties improved the tolerability of PMs against polyion exchange reaction.

2.3.3 Stimuli-responsiveness of PMs against ATP and pH

pH-responsiveness of cross-linked PMs was evaluated through both quantification of the number of block copolymers binding to pDNA and membrane disruptive ability of block copolymers at pH 7.4 and 5.5, which respectively mimicked physiological pH and late endosomal pH. In previous report, a part of PEG-PAsp(DET) was released from PMs in response to pH change from 7.4 to 5.5 because increase of the protonation degree of PAsp(DET) side chain at acidic pH induced electrostatic repulsion among block copolymers in PM.^{10,15} Thus, if FPBA/GlcAm ester linkage in PM core was cleaved due to the shift of FPBA equilibrium from cross-linkable tetrahedral structure to uncross-linkable trigonal structure responding to pH drop, it was reasonable to expect release of block copolymers from cross-

Table 2-2. The number of block copolymers binding to pDNA at pH 7.4 and 5.5

	pH 7.4	pH 5.5	Difference between pH 7.4 and 5.5
PEG-PAsp(DET/FPBA _{59%})	197	169	28
PEG-PAsp(DET/GlcAm _{27%})	120	106	14

Table 2-3. Cumulant diameter and PDI of PMs incubated in 10 mM HEPES buffer with 150 mM NaCl at pH 7.4 and 5.5 for 6 h

	Cumulant diameter (d. nm)/ PDI	
	pH 7.4	pH 5.5
PEG-PAsp(DET) PMs	80/0.14	82/0.13
B59/G27 PMs	88/0.12	91/0.16

linked PMs. Actually, ultracentrifuge analysis performed the release of both PEG-PAsp(DET-FPBA_{59%}) and PEG-PAsp(DET-GlcAm_{27%}) from PMs by changing pH from 7.4 to 5.5 (**Table 2-2**). Note that, the cumulant diameter and PDI of B59/G27 PMs after incubation at pH 5.5 was comparable with these at pH 7.4 (**Table 2-3**), indicating that PM structure was maintained after release of some block copolymers release. Released block copolymers from PMs were expected to disrupt endosomal membrane and finally to facilitate escape of PMs from endosomes to cytoplasm. To assess membrane disruptive ability of PEG-PAsp(DET-FPBA_{59%}) and PEG-PAsp(DET-GlcAm_{27%}), the cell-membrane permeability of a completely impermeable fluorescence dye, YO-PRO1, to HuH-7 cells was monitored after treatment of block copolymer solution. All of PEG-PAsp(DET), PEG-PAsp(DET-FPBA_{59%}), and PEG-PAsp(DET-GlcAm_{27%}) showed the significant increase of YO-PRO 1 fluorescence intensity in HuH-7 cells with decreasing pH from 7.4 to 5.5 (**Figure 2-5**), indicating that synthesized block copolymers destabilized cellular membrane more efficiently at lower pH, especially late endosomal pH, than at physiological pH. While PEG-PAsp(DET-GlcAm_{27%}) showed lower membrane disruptive ability at pH 5.5 than unmodified PEG-PAsp(DET) probably due to the

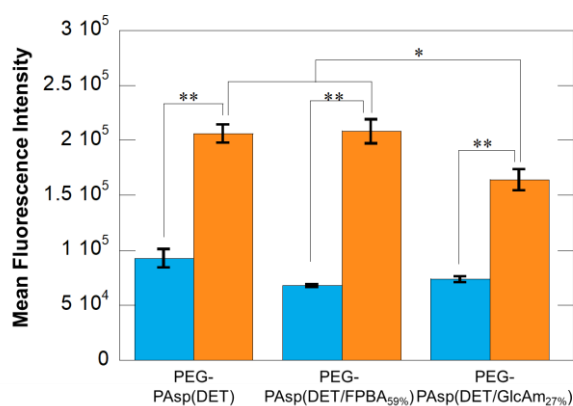


Figure 2-5. Membrane disruptive ability of each block copolymer at pH 7.4 (blue bar) and 5.5 (orange bar). The residual positively-charged amino group concentration was set to be 6.0 mM at pH 7.4. Data were shown as means \pm SEM ($n = 6$). Statistical difference was analyzed by Student's unpaired 2-tailed test. (* $p < 0.05$, ** $p < 0.01$)

decrease of the number of double-protonated PAsp(DET) side chain by GlcAm introduction, PEG-PAsp(DET-FPBA_{59%}) interestingly showed comparable membrane disruptive ability at pH 5.5 with PEG-PAsp(DET) in spite of 59% introduction of FPBA moieties into PAsp(DET) segment. These obvious contradictory results can be explained by the interaction of hydrophobic trigonal FPBA groups on PEG-PAsp(DET-FPBA_{59%}) and cellular membrane at pH 5.5. Noteworthy, 98% of FPBA moieties were estimated to form hydrophobic trigonal structure at pH 5.5 calculated from the pK_a value.⁹ Actually, previous study reported that hydrophobic cholesterol groups facilitated membrane disruptive ability.¹⁵

Next, ATP-responsiveness of PMs was analyzed through gel electrophoresis in the presence of various concentrated ATP. As no DS was added to PM solution in this experiment, PM can keep the loaded pDNA in the core during gel electrophoresis. Actually, no migration of pDNA encapsulated in PEG-PAsp(DET) PM was observed regardless of ATP concentration (**Figure 2-6 (a)**). On the other hand, pDNA was released from B59/G27 PMs in the presence of over 1 mM ATP (**Figure 2-6 (b)**). Also, ATP-responsiveness of B26/G14 PMs, which was expected to show lower ATP-responsiveness than B59/G27 PMs due to small number of FPBA moieties, was evaluated. In fact, pDNA was released from B26/G14 PMs in over 3 mM ATP concentration (**Figure 2-6 (c)**). To get further insights into ATP-responsiveness of cross-linked PMs, DLS measurement was conducted after incubation with various concentration of ATP. While PEG-PAsp(DET) PMs was not affected by ATP at all, the size and PDI of both B59/G27 and B26/G14 PMs increased in response to ATP concentration (**Table 2-4**). pDNA encapsulated in B59/G27 PMs was decondensed under over 1 mM ATP concentration, and similarly pDNA in B26/G14 PMs was under over 3 mM ATP concentration. These DLS results were consistent with the results of gel electrophoresis, and indicated the cleavage of FPBA/GlcAm cross-

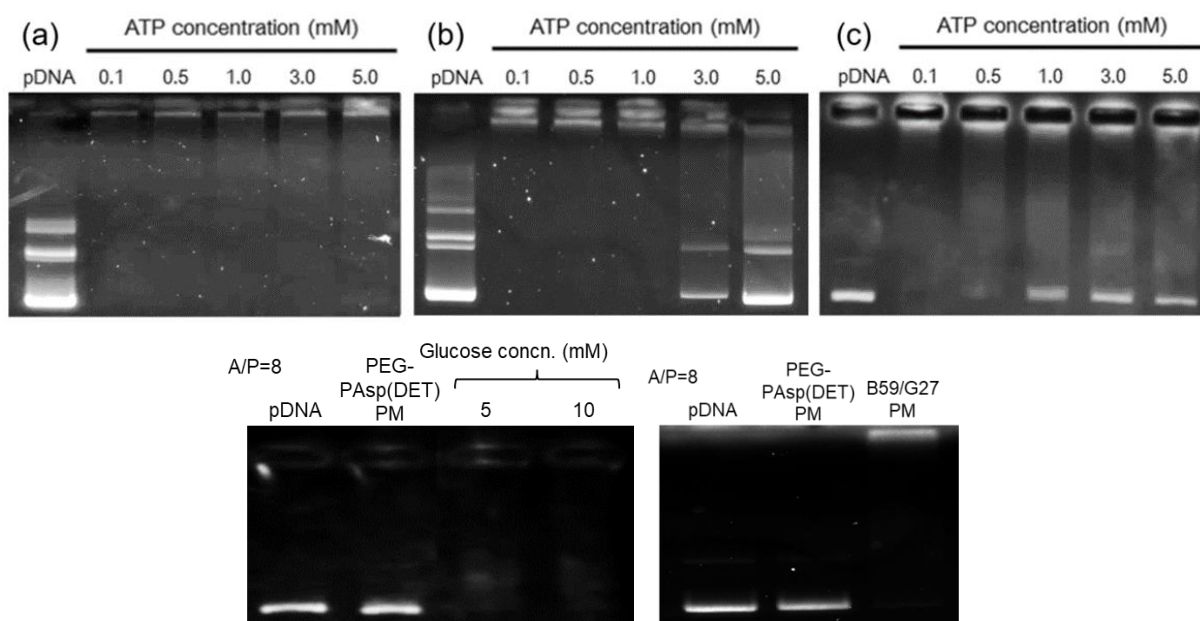


Figure 2-6. Electrophoregram of PMs incubated with several diol compounds. (a-c) Electrophoregram of (a) PEG-PAsp(DET) PMs, (b) B26/G14 PMs, and (c) B59/G27 PMs incubated for 2 h in the presence of various concentrated ATP (0.1, 0.5, 1.0, 3.0, and 5.0 mM). (d) Electrophoregram of PMs incubated with 5 or 10 mM glucose and DS at A/P ratio of 8. (e) Electrophoregram of PMs incubated with 50 μ M ascorbic acid and DS at A/P ratio of 8.

linking in PM core responding to highly concentrated ATP. Moreover, Förster resonance energy transfer (FRET) of Cy3/Cy5 double-labeled pDNA was analyzed. As shown in **Figure 2-7**, loading pDNA into PM core induces the enhancement of FRET signals in double-labeled pDNA due to pDNA condensation in PM core.¹⁷⁻¹⁸ FRET efficiency of B59/G27 and B26/G14 PMs decreased with increasing ATP concentration (**Figure 2-7; orange bar and gray bar**), while such obvious decrease of FRET efficiency in PEG-PAsp(DET) PMs was not observed (**Figure 2-7; blue bar**). These results indicated that pDNA loaded in FPBA/GlcAm cross-linked PMs was decondensed in response to increase of ATP concentration, which was consistent with gel electrophoresis and DLS measurement (**Figure 2-6** and **Table 2-4**). Noteworthy, as is the case of gel electrophoresis, B26/G14 PMs showed lower ATP-responsiveness than B59/G27 PMs. Importantly, because ATP concentration was ~ 0.4 mM in

Table 2-4. Cumulant diameter and PDI of PMs incubated with various concentrated ATP

	Cumulat diameter (nm)/PDI					
	ATP concentration (mM)					
	0	0.1	0.5	1.0	3.0	5.0
PEG- <i>b</i> -PAsp(DET) PM	78/0.14	77/0.10	79/0.10	79/0.10	83/0.10	81/0.14
B26/G14 PM	87/0.10	87/0.10	89/0.10	90/0.10	123/0.27	129/0.27
B59/G27 PM	88/0.12	91/0.13	99/0.20	126/0.25	134/0.27	141/0.27

extracellular condition and ~ 3 mM in cytoplasm, respectively.²⁰⁻²² Therefore, these results strongly suggested that cross-linked PMs can selectively release loaded pDNA inside the cells. Glucose and ascorbic acid (vitamin C) (**Figure 2-6 (d), (e)**) are other considerable diol containing biomolecules existing adequately *in vivo*.^{9,23} These competitive diols with GlcAm moieties may cleave FPBA/GlcAm cross-linking and finally destabilize PM structure during delivery process. Thus, the resistance of cross-linked PMs against glucose and vitamin C was evaluated by incubation in the presence of DS (A/P ratio of 9), and glucose or vitamin C. The concentration of glucose was mimicked that of human diabetic patient's blood (10 mM), and also that of vitamin C was human blood (50 μ M). Electrophoregram showed no migration of pDNA released from B59/G27 PMs even in the presence of glucose or vitamin C, while clear

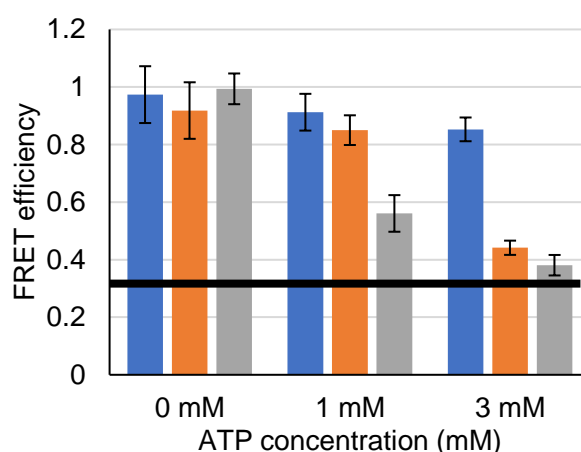


Figure 2-7. FRET efficiency of PEG-PAsp(DET) PMs (blue bar), B26/G14 PMs (orange bar), and B59/G27 PMs (gray bar) incubated for 2 h in the presence of various concentrated ATP (0, 1, 3 mM). FRET efficiency of naked double-labeled pDNA was represented as a solid line. Data were shown as means \pm SEM ($n = 3$).

pDNA migration from PEG-PAsp(DET) PM was observed (**Figure 2-6 (e), (f)**). Probably lower affinity to PBA and uncharged chemical structure of glucose could not trigger exchange reaction with GlcAm, and also low concentration and uncharged structure of vitamin C could not. These results indicated that GlcAm moieties were not replaced with glucose or vitamin C en route to target cells.

2.3.4 Effect of FPBA/GlcAm cross-linking on cellular uptake and transfection

The amount of PMs entering HuH-7 cells were evaluated. B59/G27 PMs showed 10-fold higher cellular uptake efficiency than other non-cross-linked PMs (**Figure 2-8; blue bar**). Anionic glycosaminoglycans (GAGs), such as heparan sulfate and chondroitin sulfate, are believed to destabilize PM structure as shown in the model experiment using DS (**Figure 2-4**).²⁴ Thus, cellular uptake efficiency of PMs after Heparanase II treatment, which reduces the amount of heparan sulfate on cell surface, to HuH-7 cells was evaluated. Heparanase II pre-treatment to HuH-7 cells improved cellular uptake efficiency of non-cross-linked PMs (PEG-

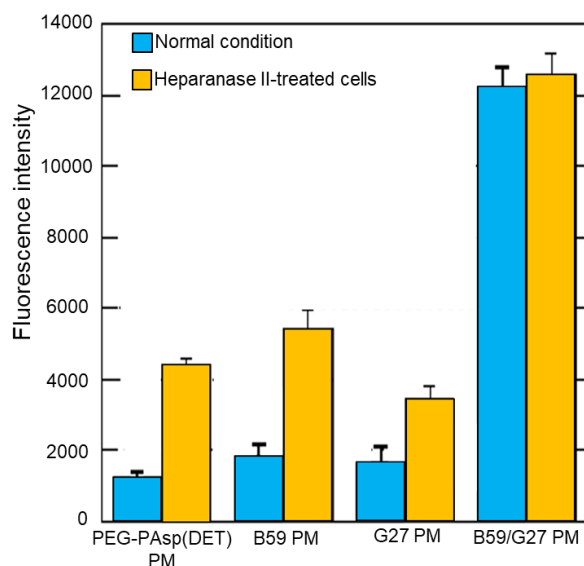


Figure 2-8. Cellular uptake efficiency of PMs in normal cells (blue bar), and Heparanase II pre-treated cells (orange bar) after 24 h of transfection. Data were shown as means \pm SEM ($n = 3$).

PAsp(DET) PMs, PEG-PAsp(DET-FPBA_{59%}) PMs, and PEG-PAsp(DET-GlcAm_{27%}) PMs), but it did not affect that of B59/G27 PMs (**Figure 2-8; orange bar**). From these results, I could conclude that B59/G27 PMs had sufficient stability against polyion exchange reaction with GAGs for cell entry and that the stability derived significantly higher cellular uptake efficiency of cross-linked PMs. B59/G27 PMs also showed approximately 20-fold higher gene transfection efficiency than other non-cross-linked PMs without any cytotoxicity (**Figure 2-9 (a), and Figure 2-13**). To get further insights into enhanced gene transfection efficiency of B59/G27 PM, transfection efficiency of B59/G27 PMs and PEG-PAsp(DET) PMs were compared after setting to the uptake amount in the same level between B59/G27 PMs and PEG-PAsp(DET) PMs by controlling transfection dose of B59/G27 PMs (**Figure 2-9 (b)**). Interestingly, B59/G27 PMs showed still higher gene expression efficiency than PEG-PAsp(DET) PMs in spite of adjusting cellular uptake amount of PMs (**Figure 2-14**), suggesting that other factor except improvement of cellular uptake efficiency facilitated gene expression efficiency in B59/G27 PMs. To clarify the reasons why B59/G27 PMs showed efficient gene

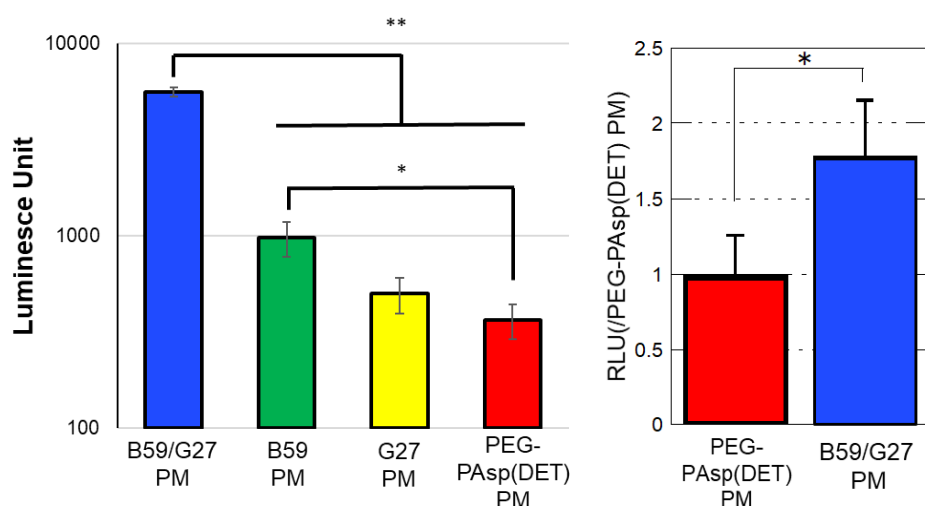


Figure 2-9. Gene expression efficiency of PMs after 48 h of transfection (a) in the same dose of pDNA (1 μ g) and (b) after setting cellular uptake efficiency of PMs to comparable by changing dose of PMs. Data were shown as means \pm SEM ($n = 4$). Statistical difference was analyzed by Student's unpaired 2-tailed test. (* $p < 0.05$, ** $p < 0.01$)

expression, intracellular behavior of PMs was evaluated in the following section.

2.3.5 Effect of FPBA/GlcAm cross-linking on intracellular trafficking of PMs

Endosomal escape is believed as an important factor to enhance gene transfection efficiency. The endosomal escapability of Cy3-labeled pDNA loading PMs was evaluated using confocal laser scanning microscopy (CLSM). In CLSM images, red, green, blue and yellow pixels represented Cy3-labeled pDNA, late endosomes/lysosomes stained by LysoTracker green, cell nuclei stained by Hoechst 33342, and Cy3-labeled pDNA entrapped in late endosomes/lysosomes, respectively (**Figure 2-10 (a)-(d)**). Obviously, clear red spots were

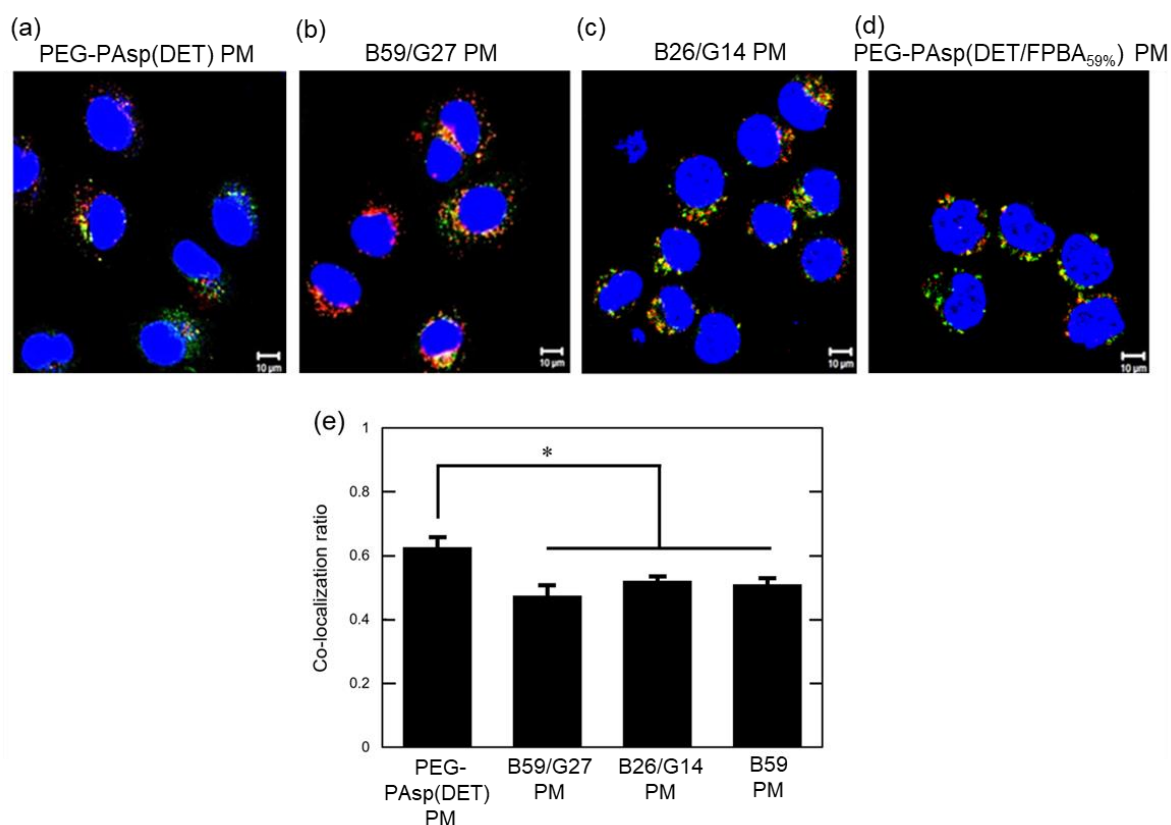


Figure 2-10. Confocal laser scanning microscopy observation of Cy3-labeled pDNA (red) loaded in (a) PEG-PAsp(DET), (b) B59/G27, (c) B26/G14, and (d) PEG-PAsp(DET-*FPBA*_{59%}) PMs (red) after 6h of transfection. (e) Co-localization ratio of PMs with late endosomes/lysosomes calculated for 50 individual cells. Data were shown as means \pm SEM. Statistical difference was analyzed by Dunnett's test. (* $p < 0.05$)

observed in all CLSM images, suggesting that some PMs were translocated from late endosomes/lysosomes to cytoplasm. Interestingly, the quantification of co-localization ratio clarified that even more B59/G27 PMs escaped from late endosomes/lysosomes than PEG-PAsp(DET) PMs (**Figure 2-10 (e)**). As demonstrated in model experiments of block copolymer release from B59/G27 PM in the acidic condition (**Table 2**), the pH decrease in endosomes may facilitate the cleavage of the phenylboronate ester linkage and induce effective destruction of endosomal membranes by released PEG-PAsp(DET-FPBA) with a hydrophobic trivalent FPBA moiety. B26/G14 PMs and PEG-PAsp(DET-FPBA_{59%}) PMs also improved endosomal escapability comparing with PEG-PAsp(DET) PMs, strongly suggested that hydrophobic trigonal FPBA moieties effectively destabilized endosomal/lysosomal membrane for efficient endosomal escape.

The results in **Figure. 2-10** revealed that part of the pDNA was actually transferred from the endo/lysosomal compartment to cytoplasm. Therefore, the next issue was to prove that pDNA loaded in B59/G27 PM was finally released in response to cytoplasmic ATP concentration. As demonstrated in **Figure 2-7**, FRET signal in Cy3/Cy5-double labeled pDNA was one of the indicators to observe pDNA decondensation. Thus, the intracellular FRET signal of B59/G27 and B26/G14 PMs in HuH-7 cells was monitored using flow cytometry analysis (**Figure 2-11(a) and (b)**).²⁵ Because both PMs showed similar cellular uptake efficiency and endosomal escapability to HuH-7 cells (**Figures 2-10(e), 2-15**), it may be safe to directly compare the FRET signals for observation of pDNA decondensation between these cross-linked PMs. After 6 h of transfection, B59/G27 PMs already showed lower FRET efficiency than B26/G14 PM (**Figure 2-11 (c)**). After 12 h later from transfection, a further decrease in FRET efficiency was observed in B59/G27 PMs, but B26/G14 PMs still kept comparable

FRET signal to the observed efficiency in the 6 h incubation. The decrease in FRET efficiency became clearer for B59/G27 PMs with 24 h incubation. These results demonstrated rapid decondensation of pDNA loaded in B59/G27 PMs inside the cells comparing to loaded in B26/G14 PMs. The main mechanism of pDNA decondensation and subsequent release from PMs inside the transfected cells is believed to be an exchange reaction with intracellular anionic biomacromolecules. However, B59/G27 PMs were more stable than B26/G14 PM after experiencing intracellular trafficking process, as is evident from the results of the exchange reaction with DS for PM after incubation at intracellular pH regulation process, *i.e.* PM that

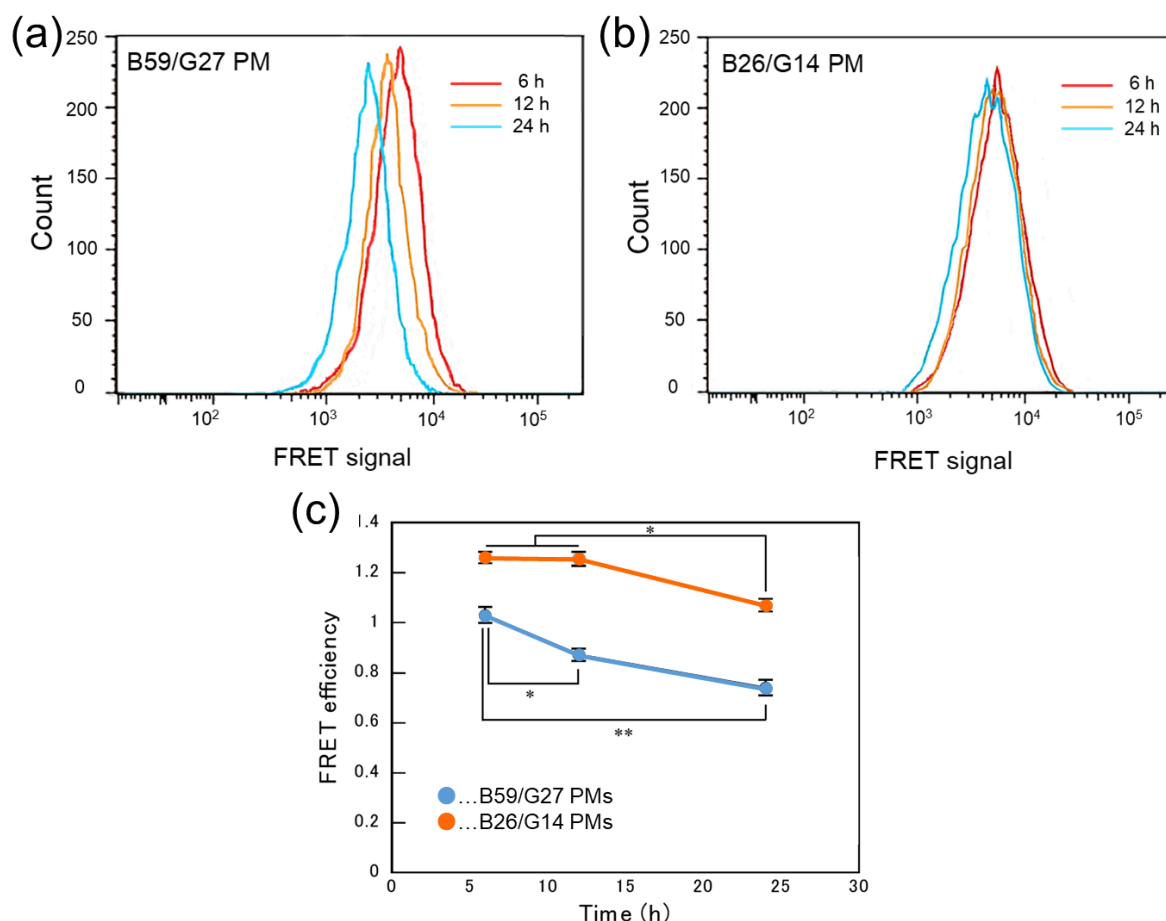


Figure 2-11. Observation of pDNA decondensation loaded in PMs inside the cells using FRET signals measured by flow cytometry. (a, b) Cy5 fluorescence intensity of (a) B59/G27 PMs and (b) B26/G14 PMs excited by 488 nm laser after 6, 12, and 24 h of transfection. (c) FRET efficiency of Cy3/Cy5 double-labeled pDNA loaded in B59/G27 PMs (blue) and B26/G14 PMs (orange). Data were shown as means \pm SEM ($n = 3$). Statistical difference

was first incubated at pH 5.5 mimicking late endosomal pH, and then incubation in the presence of DS (A/P ratio of 9) at cytosolic pH (pH 7.4) (**Figure 2-16**). The results of intracellular FRET measurements are not consistent with this tolerability trend measured with a buffer without ATP, but it supports the mechanism that elevated intracellular ATP concentrations promoted cleavage of FPBA/GlcAm cross-linkings in B59/G27 PMs and were more sensitive to intracellular polyion exchange reaction, as shown in the model experiments shown in **Figures 2-6 and 2-7**.

2.3.6 Stabilization effect of FPBA/GlcAm cross-linking in blood

Long circulation profile in blood allows PMs to be applied to widespread usage for various diseases. The pDNA encapsulated in B59/G27 PMs was remained more than that in PEG-PAsp(DET) PMs (**Figure 2-12**). Especially, after 10 min of administration, 10-fold more pDNA in B59/G27 PMs was still intact in blood stream than that in PEG-PAsp(DET) PMs. These results indicated that FPBA/GlcAm cross-linking stabilized PM structure and protected

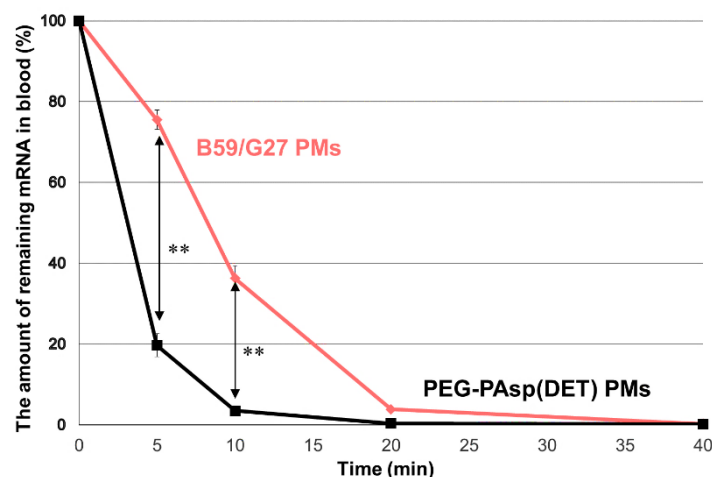


Figure 2-12. Quantification of remaining pDNA loaded in PEG-PAsp(DET) PMs (black line) or B59/G27 PMs (red line) in mouse blood after 5, 10, 20, and 40 min of administration. Data were shown as means \pm SEM ($n = 4$). Statistical difference was analyzed by Student's unpaired 2-tailed test. (** $p < 0.01$)

pDNA from nuclease-based degradation during blood circulation. Noteworthy, because the concentration of glucose in mouse blood is similar to that of human blood,²⁶ B59/G27 PMs is expected to be retained in human blood circulation.

2.4 Conclusion

I developed FPBA/GlcAm cross-linked PMs to overcome major barriers on gene delivery systems, *i.e.*, ensuring efficient delivery and cellular uptake by structurally stabilizing PMs in extracellular environment, improving translocation of pDNA from endocytic compartment to cytoplasm by introducing low pH-specific membrane disruptive chemical structure in block copolymers, and facilitating pDNA decondensation leading smooth gene transcription in response to intracellular stimulus. The optimization of chemical structure of block copolymers brought efficient gene transfection by synergetic effect derived from FPBA/GlcAm cross-linking. Moreover, regulated stabilization effect determined by ATP concentration was monitored inside the cells using FRET efficiency. These observations provided clear insights into the mechanism of PM system spatiotemporally sensing intracellular chemical stimuli, *i.e.*, changing pH and ATP concentration. Finally, these sensitivities demonstrated dramatically higher gene transfection efficiency comparing to non-sensitive PM systems.

2.5 Appendix

2.5.1 Cytotoxicity of PMs to cultured cells

The cytotoxicity of PMs was evaluated using CCK-8 kit. HuH-7 cells (20,000 cells/well) were seeded on 24-well plate in 400 μ L of culture medium and incubated for 24 h.

Culture medium was replaced with the fresh one, and then PMs containing 1 μg of pDNA was transfected to each well. After 48 h, 10 μL of CCK-8 reagent and 100 μL of culture medium was mixed and incubated for 2 h. Then, the absorbance of the culture medium at 450 nm was evaluated using Microplate Reader Infinite M1000 Pro. All PMs showed no specific cytotoxicity to HuH-7 cells.

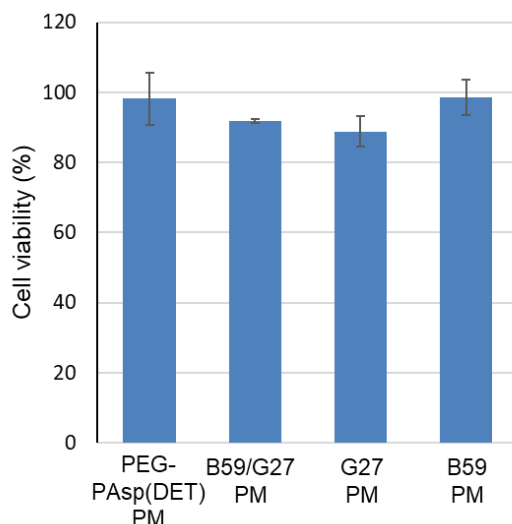


Figure 2-13. Viability of PM transfected cells after 48 of transfection. Data were normalized by untreated cells. Data were shown as means \pm SEM ($n = 4$).

2.5.2 Cellular uptake efficiency at the different dose of PMs

To set the cellular uptake efficiency of B59/G27 PMs comparable to that of PEG-PAsp(DET) PMs, cellular uptake experiment was conducted by changing dose of PMs. B59/G27 PMs containing 5, 0.5, 0.25, and 0.05 μg of Cy5-labeled pDNA were transfected to HuH-7 cells (50,000 cells/well) cultured on 6-well plate. After 24 h of transfection, cells were washed by D-PBS twice and collected by trypsinization. The fluorescence intensity of Cy5 dye in the collected cells was measured by BD LSR II instrument using 633 nm laser for excitation and 660/20 nm filter for emission. As seen in **Figure 2-14**, the cellular uptake efficiency of B59/G27 PMs containing 0.25 μg of pDNA was comparable to that of PEG-PAsp(DET) PMs

containing 5 μg of pDNA.

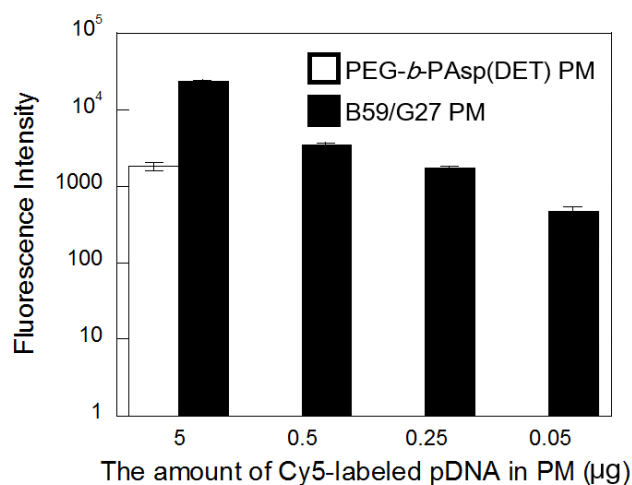


Figure 2-14. Cellular uptake efficiency of PEG-PAsp(DET) PMs (open bar) and B59/G27 PMs (Closed bar) at different dose after 24 h of transfection. Data were shown as means \pm SEM ($n = 4$).

2.5.3 Cellular uptake efficiencies of FPBA/GlcAm cross-linked PMs

Cellular uptake efficiencies of B59/G27 PMs and B26/G14 PMs were analyzed according to the same protocol described in the section of “2.5.2 Cellular uptake efficiency at the different dose of PMs”. The cellular uptake efficiency of B26/G14 PMs was comparable with B59/G27 PMs.

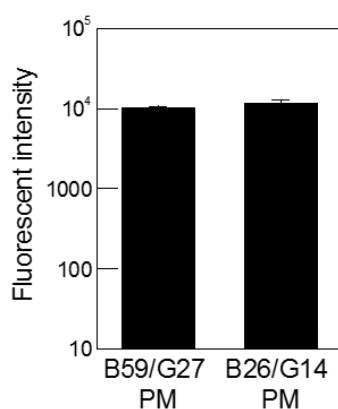


Figure 2-15. Cellular uptake efficiency of Cy5-labeled pDNA loaded in B59/G27 PMs and B26/G14 PMs after 24 h of transfection. Data were shown as means \pm SEM ($n = 3$).

2.5.4 Tolerability of PMs against DS after the incubation at pH 5.5

2.5.4 Tolerability of PMs against polyion exchange reaction after the incubation at acidic pH

PMs were incubated in 10 mM acetate buffer (pH 5.5) containing 150 mM NaCl for 6 h at 37 °C, and then the buffer solution was replaced with 10 mM HEPES buffer (pH 7.4) containing 150 mM NaCl using a 100 kDa MWCO Amicon Ultra-0.5 (Millipore, MA). After the buffer exchange, the PM solutions were incubated with DS at A/P ratio of 9 for 1 h at 37 °C. After incubation, the mixture with 10 × loading buffer was loaded onto a 0.9wt% agarose gel. Gel electrophoresis was conducted at 100 V for 60 min. The migration of loaded pDNA from PMs in the agarose gel was visualized by EtBr staining. Images were captured using PharosFX™ System.

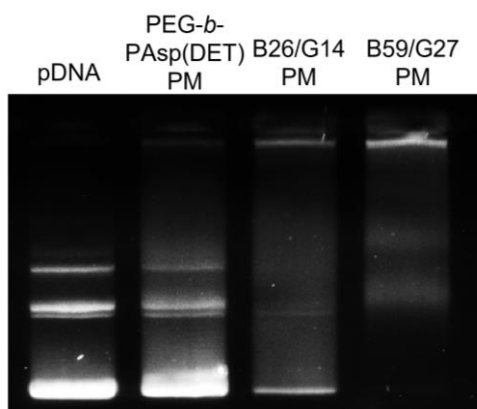


Figure 2-16. Electrophoregrams of PMs of PEG-PAsp(DET) PMs, B26/G14 PMs, and B59/G27 PMs in the presence of dextran sulfate (DS) at A/P ratio of 9. PMs had been incubated at endo/lysosomal pH of 5.5 followed by at cytoplasmic pH of 7.4 to mimic intracellular sequential pH change.

2.6 References

1. Lorand, J. P.; Edwards, J. O., Polyol Complexes and Structure of the Benzenboronate Ion, *J. Org. Chem.* **1959**, 24, 769-774.
2. Kitano, S.; Kataoka, K.; Koyama, Y.; Okano, T.; Sakurai, Y., Glucose-responsive complex

formation between poly(vinyl alcohol) and poly(*N*-vinyl-2-pyrrolidone) with pendent phenylboronic acid moieties, *Makromol. Chem., Rapid Commun.* **1991**, 12, 227-233.

3. Kataoka, K.; Miyazaki, H.; Bunya, M.; Okano, T.; Sakurai, Y., Sensitive Glucose-Induced Change of the Lower Critical Solution Temperature of Poly[*N,N*-(dimethylacrylamide)-co-3-(acrylamido)-phenylboronic acid] in Physiological Saline, *J. Am. Chem. Soc.* **1998**, 120, 12694-12695.

4. Singh, N.; Willson, R. C., Boronate affinity of RNA: possible role of conformational changes, *J. Chromato. A* **1999**, 840, 205-213.

5. Springsteen, G.; Wang, B. H., A detailed examination of boronic acid–diol complexation, *Tetrahedron* **2002**, 58, 5291-5300.

6. Yan, J.; Springsteen, G.; Deeter, S.; Wang, B., The relationship among pKa, pH, and binding constants in the interactions between boronic acids and diols—it is not as simple as it appears, *Tetrahedron* **2004**, 60, 11205-11209.

7. Naito, M.; Ishii, T.; Matsumoto, A.; Miyata, K.; Miyahara, Y.; Kataoka, K., A phenylboronate-functionalized polyion complex micelle for ATP-triggered release of siRNA, *Angew. Chem., Int. Ed.* **2012**, 51, 10751-10755.

8. Kim, J.; Lee, Y. M.; Kim, H.; Park, D.; Kim, W. J., Phenylboronic acid-sugar grafted polymer architecture as a dual stimuli-responsive gene carrier for targeted anti-angiogenic tumor therapy, *Biomaterials* **2016**, 75, 102-111.

9. Matsumoto, A.; Ishii, T.; Nishida, J.; Matsumoto, H.; Kataoka, K.; Miyahara, Y., A synthetic approach toward a self-regulated insulin delivery system, *Angew. Chem. Int. Ed.* **2012**, 51, 2124-2128.

10. Miyata, K.; Oba, M.; Nakanishi, M.; Fukushima, S.; Yamasaki, Y.; Koyama, H.; Nishiyama,

N.; Kataoka, K., Polyplexes from poly(aspartamide) bearing 1,2-diaminoethane side chains induce pH-selective, endosomal membrane destabilization with amplified transfection and negligible cytotoxicity, *J. Am. Chem. Soc.* **2008**, 130, 16287-16294.

11. Kanayama, N.; Fukushima, S.; Nishiyama, N.; Itaka, K.; Jang, W. D.; Miyata, K.; Yamasaki, Y.; Chung, U. I.; Kataoka, K., A PEG-based biocompatible block cationomer with high buffering capacity for the construction of polyplex micelles showing efficient gene transfer toward primary cells, *ChemMedChem* **2006**, 1, 439-444.

12. Harada, A.; Kataoka, K., Formation of Polyion Complex Micelles in an Aqueous Milieu from a Pair of Oppositely-Charged Block Copolymers with Poly(ethylene glycol) Segments, *Macromolecules* **1995**, 28, 5294-5299.

13. Itaka, K.; Ishii, T.; Hasegawa, Y.; Kataoka, K., Biodegradable polyamino acid-based polycations as safe and effective gene carrier minimizing cumulative toxicity, *Biomaterials* **2010**, 31, 3707-3714.

14. Dirisala, A.; Osada, K.; Chen, Q.; Tockary, T. A.; Machitani, K.; Osawa, S.; Liu, X.; Ishii, T.; Miyata, K.; Oba, M.; Uchida, S.; Itaka, K.; Kataoka, K., Optimized rod length of polyplex micelles for maximizing transfection efficiency and their performance in systemic gene therapy against stroma-rich pancreatic tumors, *Biomaterials* **2014**, 35 (20), 5359-5368.

15. Chen, Q.; Osada, K.; Ge, Z. S.; Uchida, S.; Tockary, T. A.; Dirisala, A.; Matsui, A.; Toh, K.; Takeda, K. M.; Liu, X. Y.; Nomoto, T.; Ishii, T.; Oba, M.; Matsumoto, Y.; Kataoka, K., Polyplex micelle installing intracellular self-processing functionalities without free cationomers for safe and efficient systemic gene therapy through tumor vasculature targeting, *Biomaterials* **2017**, 113, 253-265.

16. Uchida, S.; Itaka, K.; Chen, Q. X.; Osada, K.; Miyata, K.; Ishii, T.; Harada-Shiba, M.;

Kataoka, K., Combination of chondroitin sulfate and polyplex micelles from poly(ethylene glycol)-poly{N'-[N-(2-aminoethyl)-2-aminoethyl]aspartamide} block copolymer for prolonged in vivo gene transfection with reduced toxicity, *J. Control. Release* **2011**, 155, 296-302.

17. Matsumoto, Y.; Itaka, K.; Yamasoba, T.; Kataoka, K., Intracellular fluorescence resonance energy transfer analysis of plasmid DNA decondensation from nonviral gene carriers, *J. Gene Med.* **2009**, 11, 615-623.

18. Schneider, S.; Lenz, D.; Holzer, M.; Palme, K.; Suss, R., Intracellular FRET analysis of lipid/DNA complexes using flow cytometry and fluorescence imaging techniques, *J. Controlled Release* **2010**, 145, 289-296.

19. Oba, M.; Miyata, K.; Osada, K.; Christie, R. J.; Sanjoh, M.; Li, W. D.; Fukushima, S.; Ishii, T.; Kano, M. R.; Nishiyama, N.; Koyama, H.; Kataoka, K., Polyplex micelles prepared from ω -cholesteryl PEG-polycation block copolymers for systemic gene delivery, *Biomaterials* **2011**, 32, 652-663.

20. Traut, T. W., Physiological concentrations of purines and pyrimidines, *Mol. Cell. Biochem.* **1994**, 140, 1-22.

21. Leist, M.; Single, B.; Castoldi, A. F.; Kuhnle, S.; Nicotera, P., Intracellular adenosine triphosphate (ATP) concentration: a switch in the decision between apoptosis and necrosis, *J. Exp. Med.* **1997**, 185, 1481-1486.

22. Gorman, M. W.; Feigl, E. O.; Buffington, C. W., Human plasma ATP concentration, *Clin. Chem.* **2007**, 53, 318-325.

23. Padayatty, S. J.; Katz, A.; Wang, Y.; Eck, P.; Kwon, O.; Lee, J.-H.; Chen, S.; Corpe, C.; Dutta, A.; Dutta, S. K.; Levine, M., Vitamin C as an antioxidant: evaluation of its role in disease

prevention, *J. Am. Coll. Nutr.* **2003**, 22, 18-35.

24. Ruponen, M.; Ylä-Herttuala, S.; Urtti, A., Interactions of polymeric and liposomal gene delivery systems with extracellular glycosaminoglycans: physicochemical and transfection studies, *Biochim. Biophys. Acta, Biomembr.* **1999**, 1415, 331-341.

25. Uchida, H.; Itaka, K.; Nomoto, T.; Ishii, T.; Suma, T.; Ikegami, M.; Miyata, K.; Oba, M.; Nishiyama, N.; Kataoka, K., Modulated protonation of side chain aminoethylene repeats in N-substituted polyaspartamides promotes mRNA transfection, *J. Am. Chem. Soc.* **2014**, 136, 12396-12405.

26. Kroon, E.; Martinson, L. A.; Kadoya, K.; Bang, A.G.; Kelly, O.G.; Eliazar, S.; Young, H.; Richardson, M.; Smart, N. G.; Cunningham, J.; Agulnick, A.d.; D'Amour, K. A.; Carpenter M. K.; Baetge, E. E., Pancreatic endoderm derived from human embryonic stem cells generates glucose-responsive insulin-secreting cells in vivo, *Nat. Biotechnol.* **2008**, 26, 443-452.

Chapter 3

Improvement of Core condensation status by introducing cholesterol moieties into polyplex micelle core possessing FPBA/GlcAm cross-linking

3.1 Introduction

As described in Chapter 2, introduction of 3-fluoro-substituted phenylboronic acid (FPBA)/*N*-gluconamide (GlcAm) cross-linking in polyplex micelle (PM) core is a promising method to stabilize PM structure. Then, FPBA/GlcAm cross-linking was introduced into PM prepared from mRNA and a couple of poly(ethylene glycol)-polycation conjugated with FPBA or GlcAm. In applying FPBA/GlcAm cross-linking system to mRNA loading PMs, cationic segments were optimized by changing the number of aminoethylene repeats on *N*-substituted polyaspartamides because it is known that the number of aminoethylene repeats can dramatically change the intracellular behavior of mRNA polyplex; odd-number repeats provided intracellular stability and prolonged protein expression, while even-number repeats showed efficient endosomal escape and rapid protein expression.¹ Thus, PEG-*N*-substituted polyaspartamides with 2 - 4 aminoethylene repeats was conjugated with FPBA and GlcAm at various introduction ratio, respectively, and PMs prepared from synthesized block copolymers were optimized in terms of the tolerability against polyion exchange reaction, ATP-responsiveness and transfection efficiency in cultured cells. After fine-tuning of cationic segment, cholesterol (Chol) moieties was installed to the ω end of block copolymers for further stabilization of PMs due to the enhancement of core condensation status by the hydrophobicity. Integrating both FPBA/GlcAm cross-linking and Chol moieties dramatically improved

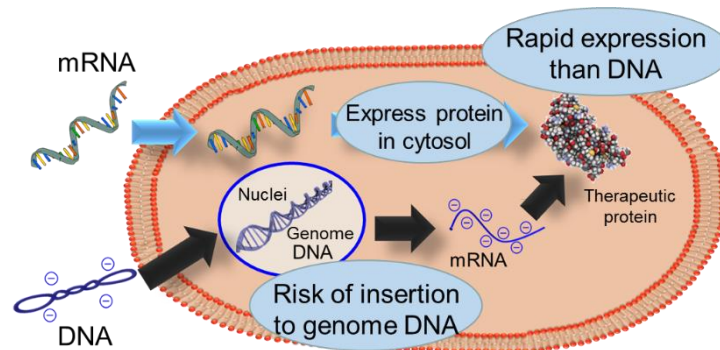


Figure 3-1. Schematic illustration of benefits of mRNA therapeutics.

nuclease resistance of mRNA loaded in PMs and protein expression efficiency of mRNA in cultured cells.

3.2 Materials and Methods

3.2.1 Materials

Dichloromethane (DCM), benzene, *N*-methylpyrrolidone (NMP), triethylamine (TEA), diethylene triamine (DET), triethylene tetramine (TET) and tetraethylene pentaamine (TEP) were purchased from Nakalai Tesque, Inc. (Kyoto, Japan). DCM, NMP, DET, TET, and TEP were used after distillation over calcium hydride. Methanol, 4-carboxy-3-fluorophenylboronic acid, D-sorbitol, 2-amino-2-hydroxymethyl-1,3-propandiol (Tris), sodium dextran sulfate (M_w : 50,000 g/mol), 4-(4,6-dimethoxy-1,3,5-triazin-2-yl)-4-methylmorpholinium chloride n-hydrate (DMT-MM), D-PBS, tris-(hydroxymethyl) aminomethane (Tris), sodium chloride (NaCl), 2-[4-(2-hydroxyethyl)-1-piperazinyl]ethanesulfonic acid (HEPES), hydrochloric acid (HCl), and Trypsin-EDTA Solution were purchased from Wako Pure Chemical Industries, Ltd. (Osaka, Japan). ATP was purchased from Oriental Kobo Co., Ltd. (Osaka, Japan). Cholesterol chloroformate was purchased from Tokyo Kasei Kogyo Co., Ltd. (Tokyo, Japan). Agarose L03 TAKARA was purchased from TAKARA Bio Inc. (Shiga, Japan). Cell culture medium was prepared from the same protocol described in Chapter 2. Human Hepatocarcinoma cells (HuH-7) was obtained from RIKEN Cell Bank (Tsukuba, Japan). Renilla Luciferase Assay System Kit was purchased from Promega Co. (Madison, WI). Cell culture plates were purchased from Becton Dickinson (Franklin Lakes, NJ, USA).

3.2.2 Synthesis of a series of FPBA or GlcAm installed block copolymers

PEG-PBLA was synthesized by the same protocol described in Chapter 2. The DP of PBLA and M_w/M_n of block copolymer was determined to be 78 and 1.05 by $^1\text{H-NMR}$ spectra ($\text{DMSO-}d_6$ at $80\text{ }^\circ\text{C}$, $\delta = 3.4 - 3.6\text{ ppm}$ (4H: $-\text{CH}_2-\text{CH}_2-\text{O}-$), $\delta = 7.9 - 8.1\text{ ppm}$ (5H: $-\text{C}_6\text{H}_5$)) and gel permeable chromatography (GPC) chart (TOSOH HLC- 8220GPC, column: TSK gel column, carrier: NMP containing 50 mM LiBr, flow rate: 0.3 ml/min, Temperature: $40\text{ }^\circ\text{C}$), respectively. PEG-PBLA (300 mg) was dissolved in 30 mL of dry NMP containing 0.5 M thiourea, and then cooled to $10\text{ }^\circ\text{C}$. DET, TET and TEP (4.5 mL, 50 eq. to the PBLA units) were diluted by same volume of dry NMP containing 0.5 M thiourea. The PEG-PBLA solution was added slowly to DET, TET or TEP solution and reacted for 2 h. The reacted solutions were neutralized by 5 N HCl at less than $5\text{ }^\circ\text{C}$ and it was immediately dialyzed (MWCO: 12,000-14,000) at $4\text{ }^\circ\text{C}$ against 0.01 N HCl_{aq} for 1 day, and against deionized water for one more day. The final solution was lyophilized and each block copolymers were collected as a white powder. The degree of polymerization was respectively determined to be 74, 72, 75 for PAsp(DET), PAsp(TET), and PAsp(TEP) by $^1\text{H-NMR}$ spectra (D_2O at $80\text{ }^\circ\text{C}$, $\delta = 3.4 - 3.6\text{ ppm}$ (4H: $-\text{CH}_2-\text{CH}_2-\text{O}-$), $\delta = 4.6 - 4.9\text{ ppm}$ (1H: $-\text{CO}-\text{CH}-\text{NH}-$)).

3-Fluoro-4-carboxypheylboronic acid and GlcAm modified each block cationomers were synthesized by the same protocol described in Chapter 2. For instance, PEG-PAsp(TET-FPBA) was prepared as follows: PEG-PAsp(TET) (30 mg), DMT-MM (97 mg) and D-sorbitol (58 mg: 5 eq. to the primary amine of PAsp(TET)) were dissolved in 3 mL of 50 mM NaHCO_3 aqueous solution. FPBA (3.5, 7.0, 10.5 mg, respectively) was dissolved in 9 mL of methanol. Then, the FPBA solution was dropped to the aqueous solution, and the mixture was reacted for 6 h at $4\text{ }^\circ\text{C}$ with adding additional DMT-MM (97 mg) every 2 h. The reacted solution was

immediately dialyzed (MWCO: 12,000-14,000) at 4 °C against 0.01 N HCl_{aq} for 1 day and then against deionized water for 1 more day. The final solution was lyophilized and PEG-PAsp(TET-FPBA) was obtained as a white powder. The introduction ratios of FPBA to cationic side chain were determined from ¹H-NMR spectra (D₂O at 80 °C, δ = 4.7 – 4.8 ppm (1H, -CO-CH-NH-) and δ = 7.2 – 7.6 ppm (3H, -C₆H₃FB(OH)₂). PEG-PAsp(DET-FPBA) and PEG-PAsp(TEP-FPBA) was synthesized by the same protocol.

Also, PEG-PAsp(TET-GlcAm) was prepared as follows: PEG-PAsp(TET) (30 mg), DMT-MM (97 mg) and GlcAm (5.4, 10.7, 16.1 mg, respectively) were dissolved in the mixture of 50 mM NaHCO₃/MeOH (3 mL/9 mL). The mixture was reacted at 4 °C for 6 h with adding additional DMT-MM (97 mg) every 2 h. The reacted solutions were immediately dialyzed (MWCO: 12,000-14,000) at 4 °C against 0.01 N HCl_{aq} for 1 day and against deionized water for 1 more day. The final solution was lyophilized and PEG-PAsp(TET-GlcAm) was obtained as a white powder. The introduction ratios of GlcAm to cationic side chain was determined from ¹H-NMR spectra (D₂O at 80 °C, δ = 4.7 – 4.8 ppm (1H, -CO-CH-NH-) and δ = 1.9 and 2.3 ppm (4H, -NHCO-CH₂CH₂CH₂-NHCO-). PEG-PAsp(DET-GlcAm) and PEG-PAsp(TEP-GlcAm) was synthesized by the same protocol.

3.2.2 Synthesis of PEG-PAsp(DET-FPBA)-Chol and PEG-PAsp(DET-GlcAm)-Chol

Cholesteryl moiety was introduced into the ω end of PEG-PBLA.² PEG-PBLA (310 mg; 0.011 mmol) was dissolved in 6 mL of DCM, followed by adding 10 v/v% TEA/DCM (300 μ L; 0.22 mmol for TEA, 20 eq. to PEG-PBLA) and cholesterol chloroformate (515 mg; 1.1 mmol) dissolved in 1.5 mL of DCM on ice. The mixture was reacted for 24 h at 25 °C. The reacted solution was dropped into diethyl ether, and after drying in vacuo PEG-PBLA-Chol

(305 mg) was collected as white powder. Cholesterol conjugation efficiency was determined to be 98% by a ^1H -NMR spectrum.

PEG-PBLA-Chol (303 mg) was dissolved in 15 mL of dry NMP containing 0.5 M thiourea. Dry DET (4.5 mL; 50 eq. to PBLA unit) was diluted with 4.5 mL of dry NMP containing 0.5 M thiourea. PEG-PBLA-Chol solution was slowly dropped into DET solution at 10 °C, and reacted for 2 h. The reacted solution was immediately neutralized with 5 M HCl_{aq} at 5 °C or less. After neutralization, the solution was dialyzed using Spectra/Por 4 Membrane (MWCO: 12-14 kDa) (Funakoshi Co., Ltd, Tokyo, Japan) against 0.01 N HCl at 4 °C for 1 day, and against deionized water at 4 °C for one more day. After freeze-drying, PEG-PAsp(DET)-Chol was collected as a white powder. The DP of PAsp(DET) segment was determined to be 63 by a ^1H -NMR spectrum (D_2O at 80 °C, $\delta = 3.4 - 3.6$ ppm (4H: $-\text{CH}_2-\text{CH}_2-\text{O}-$), $\delta = 4.6 - 4.9$ ppm (1H: $-\text{CO}-\text{CH}-\text{NH}-$)). FPBA and GlcAm moieties were introduced into PAsp(DET) segment by the same protocol described in *Chapter 2*.

3.2.3 mRNA preparation

A template pDNA for preparing *Gaussian luciferase (Gluc)* mRNA was made by inserting a *Gluc* sequence (New England BioLabs, Ipswich, MA) having 120 bp poly A/T sequence into a pSP73 vector (Promega, Madison, WI). *In vitro* transcription of the template DNA using mMESSAGE mMACHINE T7 Ultra Kit (Ambion, Carlsbad, CA) provided mRNA encoding *Gluc*. The concentration of mRNA was measured at a wavelength of 260 nm by NanoDrop 1000 spectrophotometer (NanoDrop Technologies Inc., Wilmington, DE). The *Gluc* mRNA sequence was follow:

5'-GGGAGACCGGCCUCGAGCAGCUGAAGCUUGGUACCGAGCUCGGAUCCAGCC

ACCAUGGGAGUCAAAAGUUCUGUUUGCCCUGAUCUGCAUCGCUGUGGCCGAGGC
CAAGCCCACCGAGAACAACGAAGACUUAACAUCGUGGCCGUGGCCAGCAACU
UCGCGACCACGGAUCUCGAUGCUGACCGCGGGAAGUUGCCCGGCAAGAAGCUG
CCGCUGGAGGUGCUCAAAGAGAUGGAAGCCAAUGCCCGGAAAGCUGGCUGCAC
CAGGGGCUGUCUGAUCUGCCUGUCCCACAUCAAGUGCACGCCCAAGAUGAAGA
AGUUCAUCCCAGGACGCUGCCACACCUACGAAGGCGACAAAGAGUCCGCACAG
GGCGGCAUAGGCGAGGCGAUCGUCGACAUUCCUGAGAUUCCUGGGGUUCAAGG
ACUUGGAGCCCAUGGAGCAGUUCAUCGCACAGGUCGAUCUGUGUGUGGACUGC
ACAACUGGCUGCCUCAAGGGGCUUGCCAACGUGCAGUGUUCUGACCUGCUCAA
GAAGUGGCUGCCGCAACGCUGUGCGACCUUUGCCAGCAAGAUCAGGGGCCAGG
UGGACAAGAUCAAGGGGGCCGGUGGUGACUAAGCGGCCGCUCGAGCAUGCAUC
UAGAGGAUCCCCGGGUACCGAGCUCGAAUUCAAAAAAAAAAAAAAAAAAAAAA
AAA
AAA-3'

3.2.4 Preparation and characterization of PMs

Synthesized block copolymers were dissolved in 10 mM HEPES buffer (pH 7.4), respectively. The concentration of block copolymers was determined by the residual charge ratio of protonated amino groups and negatively-charged tetrahedral FPBA groups as described in *Chapter 2* ($[N^+-B^-]_{\text{PEG-PAsp(DET-FPBA)}}$, $[N^+-B^-]_{\text{PEG-PAsp(TET-FPBA)}}$, $[N^+-B^-]_{\text{PEG-PAsp(TEP-FPBA)}}$, $[N^+]_{\text{PEG-PAsp(DET-GlcAm)}}$, $[N^+]_{\text{PEG-PAsp(TET-GlcAm)}}$, $[N^+]_{\text{PEG-PAsp(TEP-GlcAm)}}$). For this calculation, 51%, 56%, and 49% of residual amino group on unmodified PAsp(DET), PAsp(TET), and PAsp(TEP) side chain form protonated state at pH 7.4, respectively.^{1,3} In addition, all residual

amino groups on PAsp(DET), PAsp(TET) or PAsp(TEP) segment modified with FPBA or GlcAm were assumed to behave as PAsp(ethylenediamine) (100% amino group protonation) PAsp(DET) (51% amino group protonation) and PAsp(TET) (56% amino group protonation). To prepare cross-linked PMs, PEG-PAsp(DET-FPBA) and PEG-PAsp(DET-GlcAm) solution was mixed at the same $[N^+-B^-]_{\text{PEG-PAsp(DET-FPBA)}}$ and $[N^+]_{\text{PEG-PAsp(DET-GlcAm)}}$ (0.225 mM). Also, the mixture of PEG-PAsp(TET-FPBA) and PEG-PAsp(TET-GlcAm), or PEG-PAsp(TEP-FPBA) and PEG-PAsp(TEP-GlcAm) was prepared in the same manner. Then, 1-unit volume of these mixtures were added to 2-unit volume of mRNA solution ($[P^-]_{\text{mRNA}} = 0.15 \text{ mM}$) under vortex mixing in residual charge ratio of 1.5 ($r = ([N^+-B^-]_{\text{PEG-PAsp(DET-FPBA)}} + [N^+]_{\text{PEG-PAsp(DET-GlcAm)}})/[P^-]_{\text{mRNA}}$). Thus, the PM solution was incubated overnight at 4 °C.

DLS measurement was conducted using Zetasizer Nano (Ar laser: 532 nm, Scattering angle: 173°) at room temperature to evaluate the hydrodynamic diameter and polydispersity index of PMs with cumulant method.

3.2.5 Stability of PMs against competitive anionic macromolecules

PM solutions containing 500 ng of mRNA (final mRNA conc.: 25 µg/mL) were mixed with DS at residual charge ratio [sulfate groups in DS]/[phosphate groups in mRNA] (A/P ratios) of 1 in the 10 mM HEPES containing 150 mM NaCl at pH 7.4. After 1 h incubation at 37 °C, the PM solution (20 µL) containing 5% glycerol was electrophoresed for 30 min at 100 V in TAE buffer. The migration of mRNA in the agarose gel was observed by 0.5 mg/L of EtBr staining. Images were captured using PharosFX™ System.

3.2.6 ATP-responsiveness of PMs

PMs loaded with Cy3-labeled mRNA (final mRNA conc.: 25 µg/mL) were incubated with various concentration of ATP and non-labeled competitive *Gluc* mRNA (500 µg/mL) in 10 mM HEPES containing 150 mM NaCl for 2 h at 37 °C. The final ATP concentration was adjusted to 0, 0.4, or 3.0 mM. After incubation, migration of mRNA was observed through gel electrophoresis. Fluorescence intensity of Cy3 dye in the gel was measured by PharosFX™ System.

3.2.7 Nuclease resistance of mRNA loaded in PMs

PM solutions containing 100 ng of *Gluc* mRNA (final mRNA concentration: 8.3 µg/mL) were incubated in 10% FBS for 15 min at 37 °C, then PM solution was diluted 3,500-times by 1% 2-mercaptoethanol containing RLT buffer in RNeasy Mini Kit. After 2h incubation at 37 °C, mRNA in 350 µL of diluted solution was purified using RNeasy Mini Kit. After reverse transcription by ReverTra Ace qPCR RT Master Mix kit, qRT-PCR analysis was conducted using a pair of primers for *Gluc* mRNA (Forward sequence; TGAGATTCCTGGGTTCAAGG, and Reverse sequence; GTCAGAACACTGCACGTTGG) and ABI Prism 7500 Sequence Detector (Applied Biosystems, Foster City, CA).

3.2.8 Cell culturing

Cells were cultured in DMEM containing 10% FBS and 1% penicillin/streptomycin in a humidified atmosphere with 5% CO₂ at 37 °C.

3.2.9 Protein expression of mRNA loaded in PMs to the cultured cells

HuH-7 cells (10,000 cells/well) were seeded onto 48-well plates and incubated for 24

h. The culture medium was then replaced with 200 μ L of fresh one, followed by 15 μ L PM solution containing 500 ng of mRNA was added. After 4, 8, 12, 24, 48 and 72 h of transfection, 10 μ L of supernatant of culture medium was evaluated using Renilla Luciferase Assay Kit and Luminometer Glomax 96.

3.2.10 Quantification of the amount of transfected mRNA inside the cells

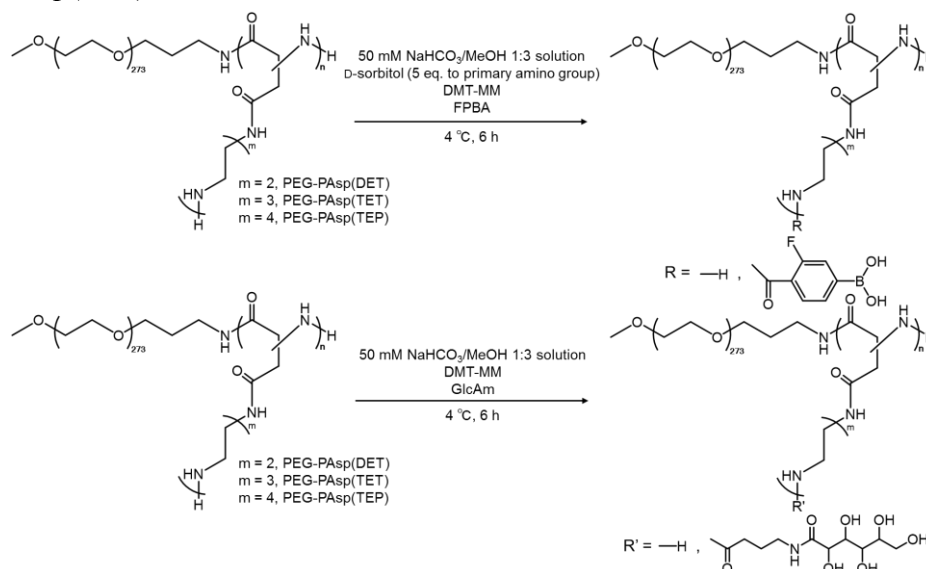
HuH-7 cells (20,000 cells/well) were seeded on 24-well plate, and incubated for 24 h. After removing culture medium, cells were washed by cold D-PBS twice, followed by directly adding PM solution containing 1 μ g of mRNA in 10 mM HEPES with 150 mM NaCl. After 15 min post-incubation, the cells were washed by D-PBS twice to remove PMs completely, followed by adding 400 μ L of fresh culture medium to each well. At the several time points from transfection, cells were lysed by RLT buffer in RNeasy kit (Quiagen) containing 1% 2-mercaptoethanol. The remaining mRNA was extracted and quantified by the same protocol described above. The amount of mRNA after 15 min PM treatment was considered as 100% in each sample.

3.3 Results and discussion

3.3.1 Synthesis of a series of block copolymers

A series of block copolymers with different number of aminoethylene repeats (repeat number: 2 ~ 4) in the cationic side chain were synthesized by aminolysis and dehydration condensation reactions (**Scheme 3-1**).^{1,3} In order to find optimum introduction ratio of FPBA and GlcAm for stabilization of PMs and appropriate ATP-responsiveness, a series of block copolymers with various introduction ratio of FPBA and GlcAm were prepared. The

Scheme 3-1. Synthetic Schemes of block copolymers from PEG-PAsp(DET), PEG-PAsp(TET) and PEG-PAsp(TEP)



introduction ratio of FPBA was 27, 58 and 88% to PAsp(DET) side chain, 21, 64 and 85% to PAsp(TET) side chain, and 29, 56 and 84% to PAsp(TEP) side chain, respectively. Also, that of GlcAm was 31, 54 and 87% to PAsp(DET) side chain, 26, 55 and 88% to PAsp(TET) side chain, and 24, 53 and 89% to PAsp(TEP) side chain, respectively, calculated by ¹H-NMR spectra (**Figure 3-8**). The synthesized block copolymers are referred to as PEG-PAsp(DET-FPBA_{X%}), PEG-PAsp(TET-FPBA_{X%}), PEG-PAsp(TEP-FPBA_{X%}), PEG-PAsp(DET-GlcAm_{Y%}), PEG-PAsp(TET-GlcAm_{Y%}), and PEG-PAsp(TEP-GlcAm_{Y%}), where X and Y denotes the introduction ratio of FPBA or GlcAm moieties. Note that, all synthesized block copolymers were well dissolved in aqueous solution and showed comparable scattering light intensity to PEG-PAsp(DET), PEG-PAsp(TET) and PEG-PAsp(TEP) even though 39% of FPBA can form hydrophobic trigonal structure.

3.3.2 Preparation and characterization of PMs

All synthesized block copolymers were respectively dissolved in 10 mM HEPES

buffer (pH 7.4). The block copolymers mixture with the same aminoethylene repeats on cationic side chain, *i.e.*, PEG-PAsp(DET-FPBA) and PEG-PAsp(DET-GlcAm), was prepared in all combination. All these mixtures showed comparable scattering light intensity to PEG-PAsp(DET), PEG-PAsp(TET) or PEG-PAsp(TEP) solutions. It is safe to consider that no intermolecular cross-linking between FPBA and GlcAm formed by mixing polymer solutions due to electrostatic repulsion between cationic segments. The polymer mixture was mixed with mRNA solution at residual charge ratio of 1.5 (*see materials and methods section*). DLS measurements demonstrated that PEG-PAsp(DET)-based PMs showed wide range of cumulant diameters (47 ~ 92 nm) (**Table 3-1 (a)**) while PEG-PAsp(TET)- and PEG-PAsp(TEP)-based PMs showed around 47 ~ 64 nm of cumulant diameter (**Table 3-1 (b), (c)**). As can be seen in **Table 3-1 (a)**, increase of the introduction ratio of both FPBA and GlcAm moieties tended to make the cumulant diameter of PM larger and, moreover, the introduction ratio of FPBA moieties drastically increased the size increase of PMs. Presumably, the negatively-charged FPBA moieties decreasing charge density of cationic segment prevented efficient mRNA condensation in PM core. Also, hydrophilicity of GlcAm moieties may inhibit mRNA condensation, which can lead size increase of PMs. The PMs prepared from a set of PEG-PAsp(DET-FPBA_{X%}) and PEG-PAsp(DET-GlcAm_{Y%}), PEG-PAsp(TET/FPBA_{X%}) and PEG-PAsp(TET-GlcAm_{Y%}), or PEG-PAsp(TEP-FPBA_{X%}) and PEG-PAsp(TEP-GlcAm_{Y%}) are referred to BX/GY DET PMs, BX/GY TET PMs, BX/GY TEP PMs, respectively.

3.3.3 Optimization cationic segment and introduction ratio of FPBA and GlcAm

First, the effect on tolerability of PMs against polyion exchange reaction was evaluated through gel electrophoresis using sodium dextran sulfate (M_w : 50,000 g/mol).

Electrophoregram showed the migration of mRNA released from PMs after incubation with dextran sulfate at A/P ratio of 1 (**Figure 3-2**). Obviously, there was an optimal the number of aminoethylene repeats and introduction ratio of FPBA and GlcAm. In PEG-PAsp(DET)-based PMs, B58/G54 DET and B58/G87 DET PMs released less mRNA encapsulated in PM core than other PEG-PAsp(DET)-based PMs. Also, in PEG-PAsp(TET)-based PMs, less mRNA was released from B85/G26 TET PMs, B85/G55 TET PMs, and B85/G88 TET PMs than other

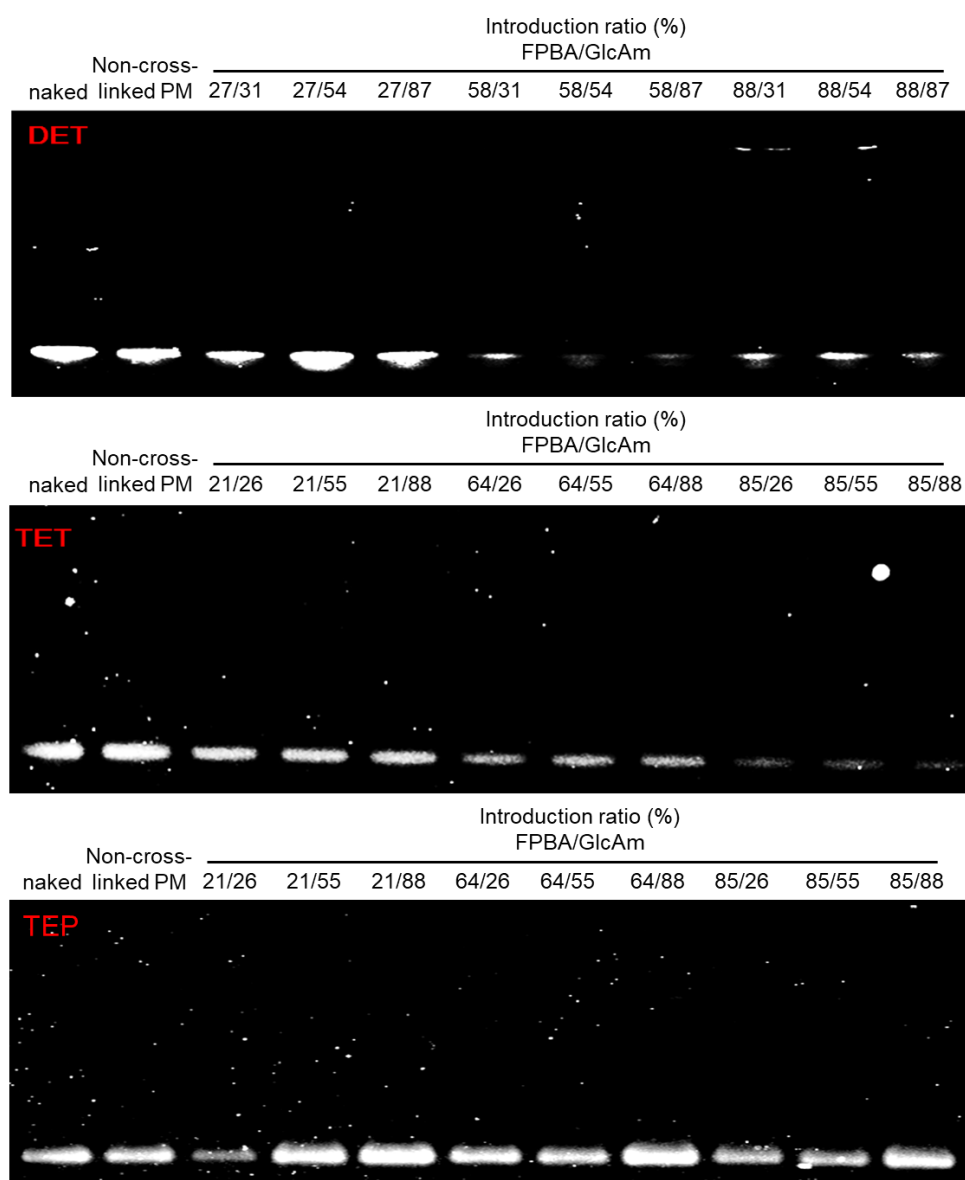


Figure 3-2. Electrophoregrams of (top) PEG-PAsp(DET)-based PMs, (middle) PEG-PAsp(TET)-based PMs, and (bottom) PEG-PAsp(TEP)-based PMs incubated with sodium dextran sulfate (DS) at A/P ratio of 1.

PEG-PAsp(TET)-based PMs. On the other hand, any PEG-PAsp(TEP)-based PMs could not maintain the loaded mRNA in the core. In all PMs, following factors probably affected to determine the structural stability of PMs against exchange reaction with competitive anionic macromolecules; (i) the number of block copolymers binding to mRNA determines cross-linking efficiency in PM core, (ii) high introduction ratio of FPBA and GlcAm moieties enabled to form efficient cross-linking in PM core and finally stabilize PM structure, (iii) increasing FPBA moieties decreases charge density of cationic segment and inhibits electrostatic interaction between mRNA and block copolymers, and (iv) hydrophilicity of highly-introduced GlcAm moieties prevents mRNA condensation with dehydration. In case of PEG-PAsp(DET)-based PMs, factor (i) and (ii) had an advantage to accelerate FPBA/GlcAm cross-linking in the PM core, while factor (iii) and (iv) had a disadvantage to destabilize PM structure. Therefore, the optimal introduction ratio of FPBA and GlcAm moieties was derived from the balance of these factors. In case of PEG-PAsp(TET)-based PMs, factor (i) could greatly affect the tolerability of PMs. Because the number of protonated amino groups on PAsp(TET) side chain was estimated to decrease from two to one after FPBA or GlcAm installation, high introduction ratio of FPBA and GlcAm moieties dramatically increased cross-linkable units in PM core and finally improved the structural stability of PMs against exchange reaction with anionic macromolecules. The number of block copolymers binding to mRNA was also a critical factor for PEG-PAsp(TEP)-based PMs. The number of protonated amino groups on PAsp(TEP) side chain is estimated to be still kept two even after FPBA and GlcAm installation. In the PM preparation condition, at most 9 block copolymers contributed to PM formation on average, making it difficult to stabilize PM structure by cross-linking due to a smaller number of cross-linkable units. From these results, B58/G54 DET, B58/G87 DET, B85/G55 TET, and B85/G88

TET PMs were evaluated in following experiments.

Next, the chemical structure of block copolymers was optimized through ATP-responsiveness. Electrophoregram showed no migration of mRNA from non-cross-linked PMs (**Figure 3-3, (top, left) and (bottom, left)**), while PMs composed of FPBA modified block copolymers obviously released loaded mRNA in response to ATP. B58/G54 DET and B58/G87 DET PMs released loaded mRNA at 3 mM ATP, while these did not release at 0.4 mM ATP ((**Figure 3-3 (top, center) and (top, right)**)), which was consistent with the results of PMs loaded with pDNA in Chapter 2. On the other hand, mRNA encapsulated in B85/G55 TET or B85/G88 TET PMs was released in the presence of over 0.4 mM ATP concentration ((**Figure 3-3 (bottom, center) and (bottom, right)**)). Importantly, as the extracellular and intracellular ATP concentration is ~0.4 mM and ~3 mM respectively,⁴⁻⁶ B58/G54 DET and B58/G87 DET

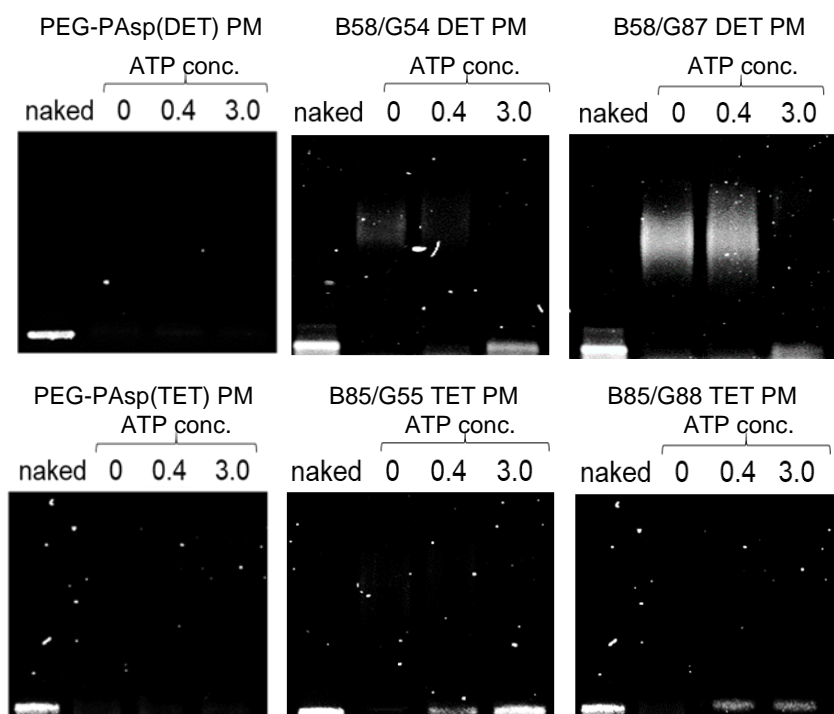


Figure 3-3. Electrophoregram of (top) PEG-PAsp(DET), 58/54 DET and 58/87 DET PMs, and (bottom) PEG-PAsp(TET), 85/55 TET and 85/88 TET PMs incubated for 2 h in the presence of various concentrated ATP (0, 0.4, and 3.0 mM).

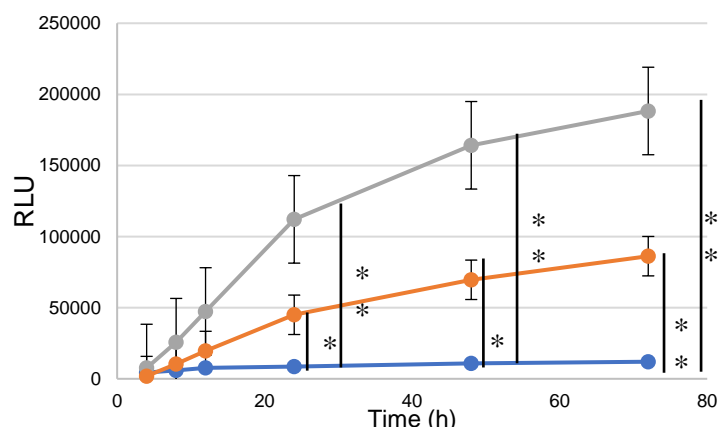


Figure 3-4. *Gluc expression profile from mRNA loaded in PEG-PAsp(DET) (blue), B58/G54 DET PM (gray), or B58/G87 DET (orange). Data were shown as means \pm SEM ($n = 4$). Statistical difference was analyzed by Student's unpaired 2-tailed test. (* $p < 0.05$, ** $p < 0.01$)*

PMs can maintain mRNA inside the PM core, but B85/G55 TET or B85/G88 TET PMs may be dissociated during delivery process. These release profile of mRNA from PMs may be explained by the introduction ratio of FPBA moieties. That is, ATP can bind to FPBA more efficiently with increasing the introduction ratio of FPBA moieties on cationic side chain, and finally trigger PM dissociation at low ATP concentration. From these results, B58/G54 DET and B58/G87 DET PMs were used in following experiments.

Finally, I compared protein expression profile of B58/G54 DET and B58/G87 DET PMs. As shown in **Figure 3-4**, cross-linked PMs showed dramatically higher Gluc expression than PEG-PAsp(DET) PMs, suggesting that integrating FPBA/GlcAm cross-linking in PM core was effective for achieving higher protein expression as is in pDNA delivery. Especially, the Gluc expression of B58/G54 DET PMs was approximately 13-fold higher than PEG-PAsp(DET) PMs after 24 h of transfection. Note that, as mRNA loaded in B58/G54 DET or B58/G87 DET PMs expressed Gluc at the early time point, it is safe to consider FPBA/GlcAm cross-linking in PM core does not disturb transition of mRNA to translational process inside the cells. In conclusion, the PMs composed of PEG-PAsp(DET-FPBA_{58%}) and PEG-

PAsp(DET-GlcAm_{54%}) was optimal condition in terms of stabilization of PM structure, ATP-responsiveness and Gluc expression.

3.3.4 Characterization of FPBA/GlcAm cross-linked PMs with cholesterol moieties

Nuclease resistance of mRNA is also an important factor to achieve efficient mRNA therapy. Thus, the nuclease resistance of mRNA loaded in PMs were evaluated by incubation in 10% FBS solution. Note that, mRNA degradation in FBS solution was caused by RNases because RNase inhibitor improved nuclease resistance of mRNA (**Figure 3-9**), indicating that the experiment incubating mRNA in FBS solution can reflect nuclease resistance of mRNA. Unfortunately, the amount of remained mRNA loaded in optimized B58/G54 DET PMs after incubation in 10% FBS condition was similar to that of PEG-PAsp(DET) PMs (**Figure 3-5**). Because the calculation of PEG shielding area on PM surface suggested RNase can easily passed through PEG-shielding (see “*Estimation of PEG density on PM surface*” section in *Appendix*), introduction of FPBA/GlcAm cross-linking into PM core did not improved nuclease resistance probably due to the approximately 10 nm size increase of B58/G54 DET PMs (**Table 3-1**). Thus, in order to make PMs smaller and to get nuclease resistance, cholesterol (Chol) moieties were installed into ω end of block copolymers, which can enhance core condensation of PMs.⁷ According to above optimization of cationic segment and introduction

Table 3-4. Cumulant diameter and polydispersity index of PMs evaluated by DLS measurement at 25 °C in 10 mM HEPES buffer (pH 7.4)

	Size (d. nm)/ PDI
PEG-PAsp(DET) PM	51/0.18
PEG-PAsp(DET)-Chol PM	54/0.14
B58/G54 DET PM	65/0.17
Chol-B56/G52 DET PM	55/0.15

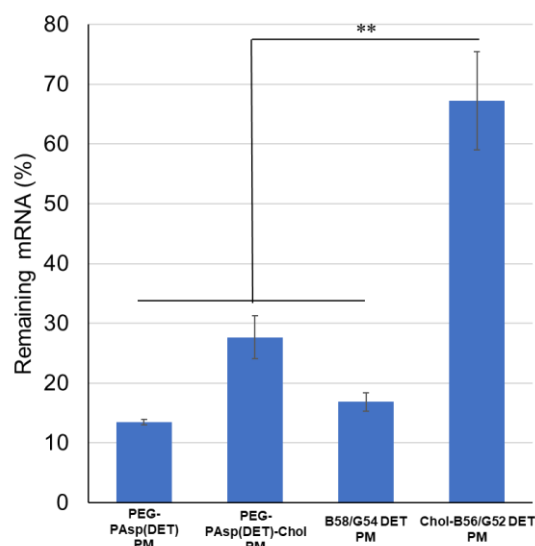


Figure 3-5. Nuclease resistance of PMs after incubation in 10% FBS solution. Data were shown as means \pm SEM ($n = 6$). Statistical difference was analyzed by Student's unpaired 2-tailed test. (** $p < 0.01$)

ratio of FPBA and GlcAm moieties, PEG-PAsp(DET-FPBA_{56%})₆₃-Chol and PEG-PAsp(DET-GlcAm_{52%})₆₃-Chol were synthesized, and PMs were prepared at residual charge ratio of 1.5 (Chol-B56/G52 DET PMs), which was the same condition to B58/G54 DET PMs. DLS measurement, as expected, showed size decrease of FPBA/GlcAm cross-linked PMs by installation of Chol moieties (**Table 3-4**), indicating that Chol groups accelerated mRNA condensation in PM core. Then, nuclease resistance of PMs was evaluated by incubation in 10% FBS condition. Obviously, the nuclease resistance of PMs was improved by introducing both FPBA/GlcAm cross-linking and Chol moieties into PM core (**Figure 3-5**), indicating synergetic effect between FPBA/GlcAm cross-linking and core condensation by Chol installation.

Although the stabilization of PMs by installing Chol moieties into PM core, Chol-B56/G52 DET PMs still possessed proper ATP-responsiveness (**Figure 3-6**). Note that, in this experiment, various concentrated ATP and competitive RNA molecules, which mimicked intracellular environment, were added to PMs loaded with Cy3-labeled mRNA. This

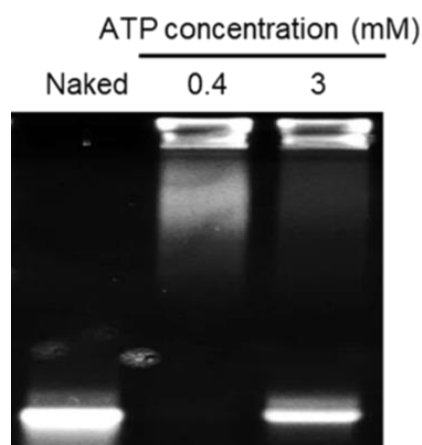


Figure 3-6. Electrophoregram of Chol-B56/G52 PMs incubated with various concentrated ATP (0.4, and 3 mM) and competitive RNA molecules (500 µg/mL).

experimental condition trigger unstable PM dissociation, such as PEG-PAsp(DET) PM. As shown in **Figure 3-6**, complete release of Cy3-labeled mRNA from Chol-B56/G52 DET PMs was observed in 3 mM ATP concentration. Because extracellular and intracellular ATP level is ~0.4 and ~3 mM, respectively,¹³⁻¹⁵ Chol-B56/G52 DET PMs can maintain PM structure during delivery process and can release loaded mRNA in response to cytosolic ATP level.

Finally, Gluc expression profile of PMs was monitored in HuH-7 cells (**Figure 3-7**

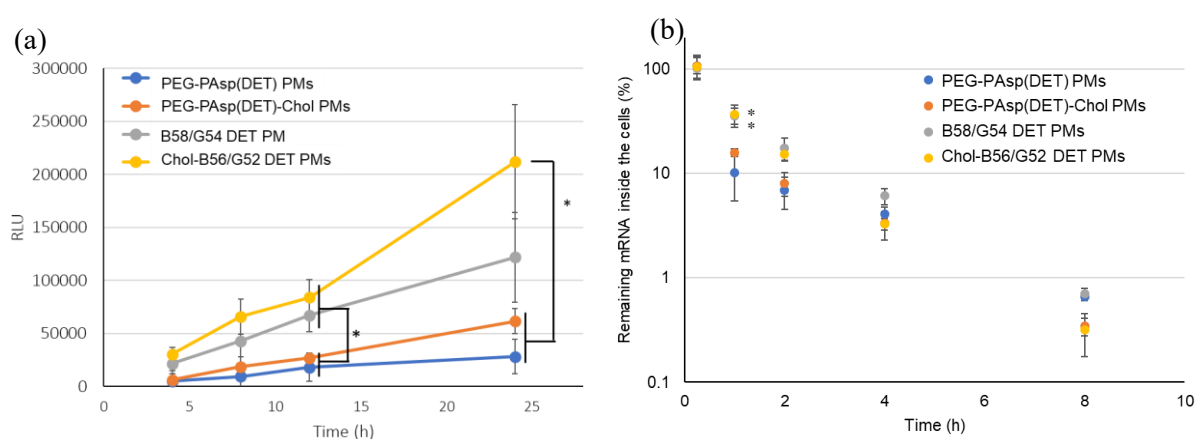


Figure 3-7. mRNA transfection into cultured HuH-7 cells. (a) Gluc expression efficiency from mRNA encapsulated in PMs after 4, 8, 12, and 24 h of transfection. Data were shown as means \pm SEM ($n = 4$). Statistical difference was analyzed by Student's unpaired 2-tailed test. (* $p < 0.05$). (b) The remaining mRNA inside the cells after 1, 2, 4, and 8 h of transfection. Data were shown as means \pm SEM ($n = 3$). Statistical difference to the PEG-PAsp(DET) PMs was analyzed by analysis of variance followed by Dunnett's test. (* $p < 0.05$).

(a)). FPBA/GlcAm cross-linked PMs indeed showed higher Gluc expression efficiency in spite of Chol-installation, but Gluc expression efficiency of Chol-B56/G52 DET PMs tended to be higher than that of B58/G54 DET. To get further insights of Gluc expression, the amount of remaining transfected *Gluc* mRNA inside the cells was quantified at several time points after transfection because more remaining mRNA inside the cells can bring higher Gluc expression at the later time point. As is different in nuclease resistance test, mRNA loaded in B58/G54 DET PMs or Chol-B56/G52 DET PMs was remained in the cells while mRNA in non-cross-linked PMs, immediately disappeared in the early time point (**Figure 3-7 (b)**). Noteworthy, half-life times of Chol-B56/G52 DET PMs were estimated to be 42 min by exponential approximation. The trend of the remaining amount of mRNA inside the cells was consistent with the Gluc expression profile, indicating that intracellular stability of PMs was an important factor for efficient protein expression.

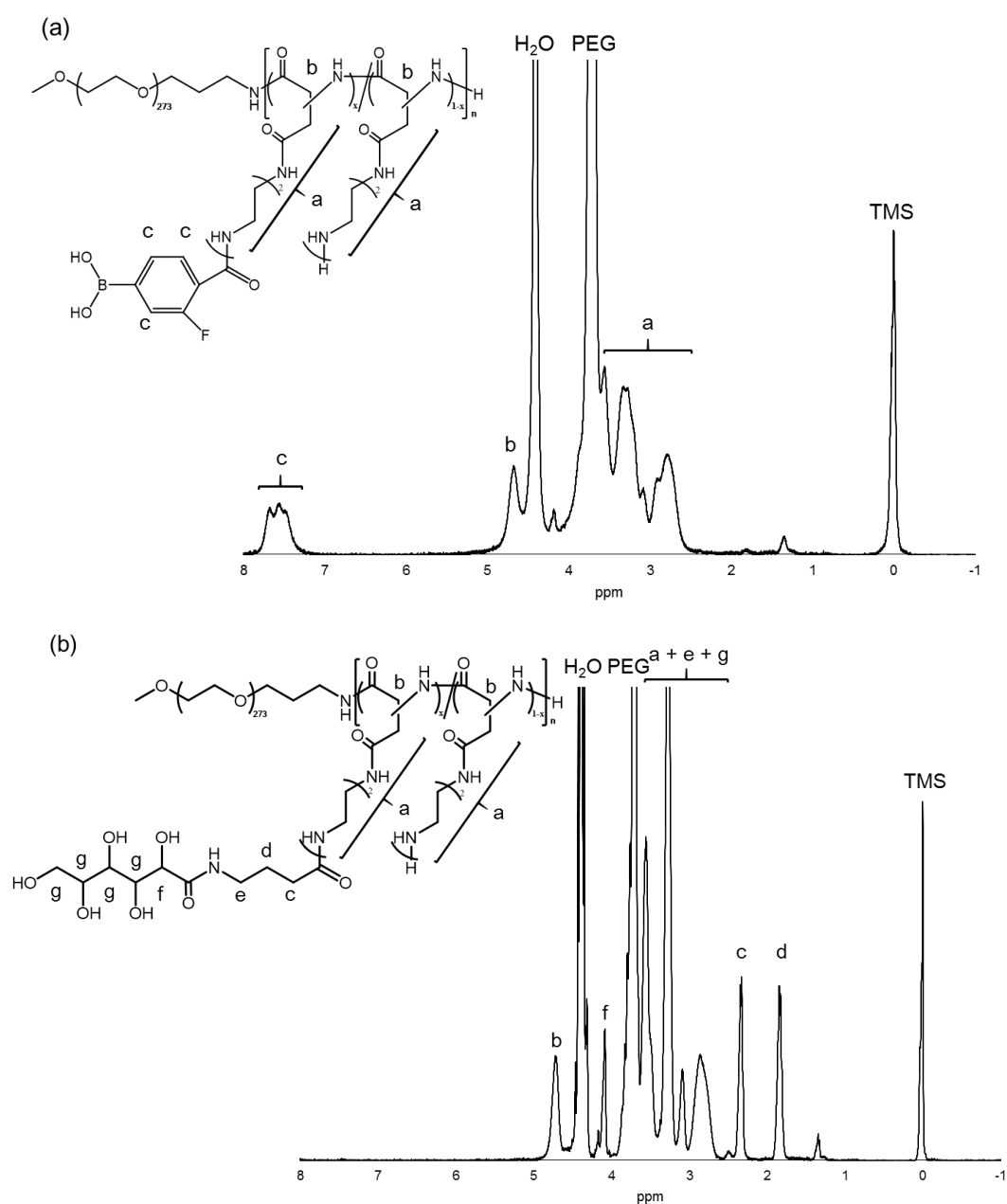
3.4 Conclusion

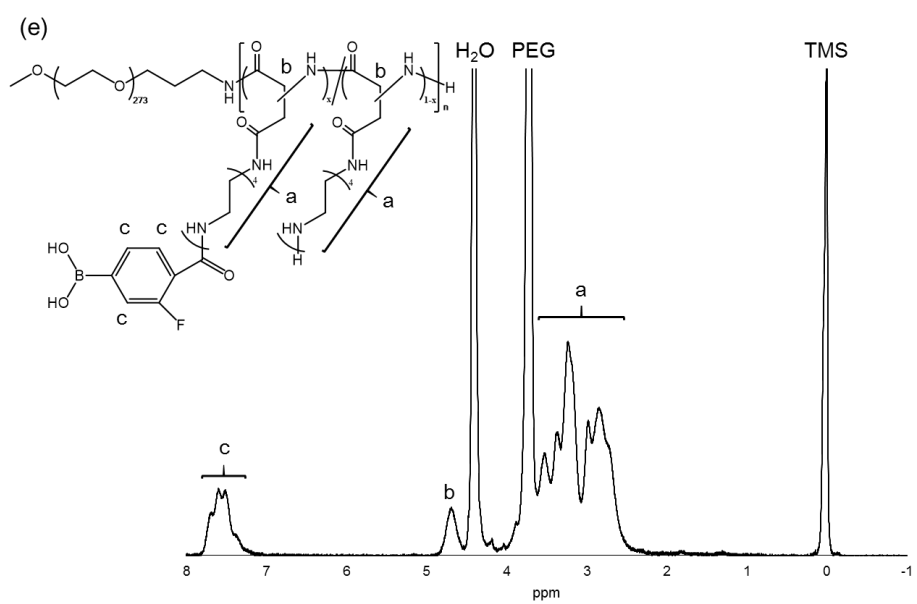
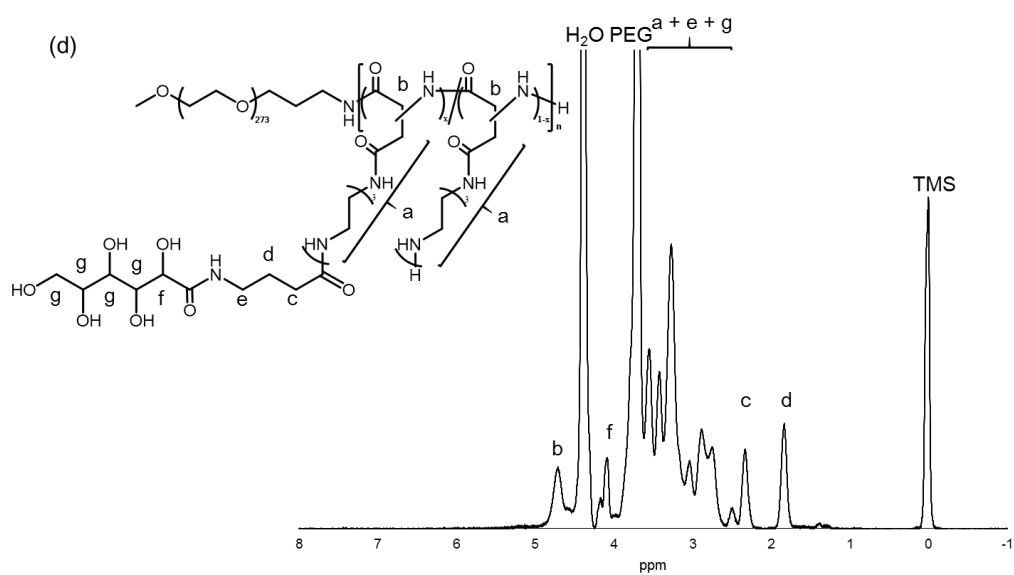
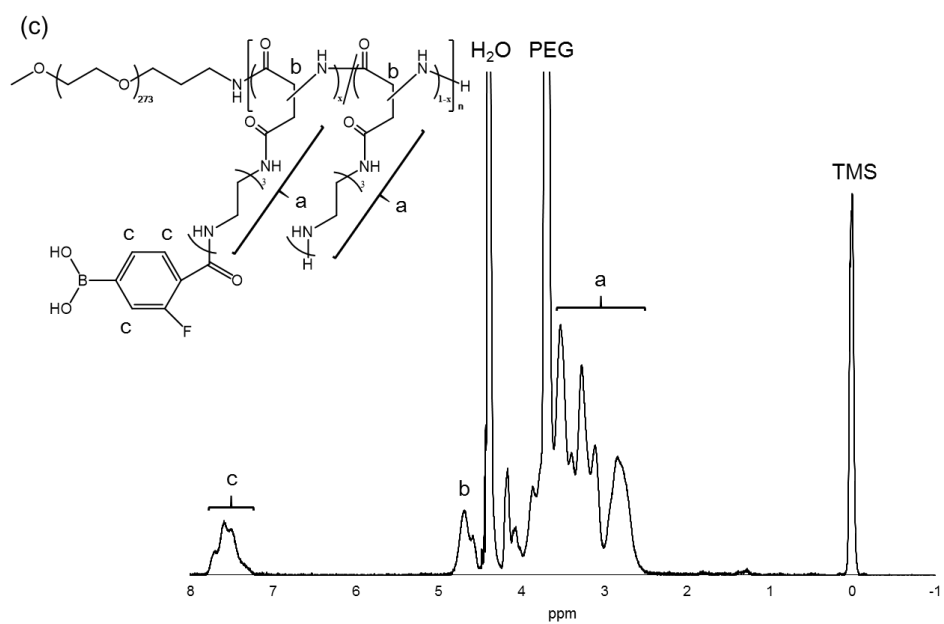
In this Chapter, cationic segment of block copolymer was fine-tuned for more efficient mRNA delivery by changing aminoethylene repeats of side chain and introduction ratio of cross-linking units. Engineering cationic side chain and cross-linking units affected charge density and cross-linking efficiency, and finally optimized chemical structure was determined through tolerability test against polyion exchange reaction, ATP-responsiveness, and protein expression efficiency. Based on the optimized structure, cholesterol moieties were installed into ω -end of the block copolymers for ensuring more efficient delivery. Both integration of FPBA/GlcAm cross-linking and cholesteryl moiety stabilized PM structure against nuclease attacks synergistically. In addition, introduction of FPBA/GlcAm cross-linking into PM core

improved not only extracellular stability but also intracellular tolerability, which led to efficient mRNA transfection. These results suggested that PM core condensation status was a key factor for nuclease resistance, and the effective strategy introducing cross-linking into PM core without core size increase is expected to contribute to more efficient mRNA delivery.

3.5 Appendix

3.5.1 ^1H -NMR spectra of synthesized block copolymers





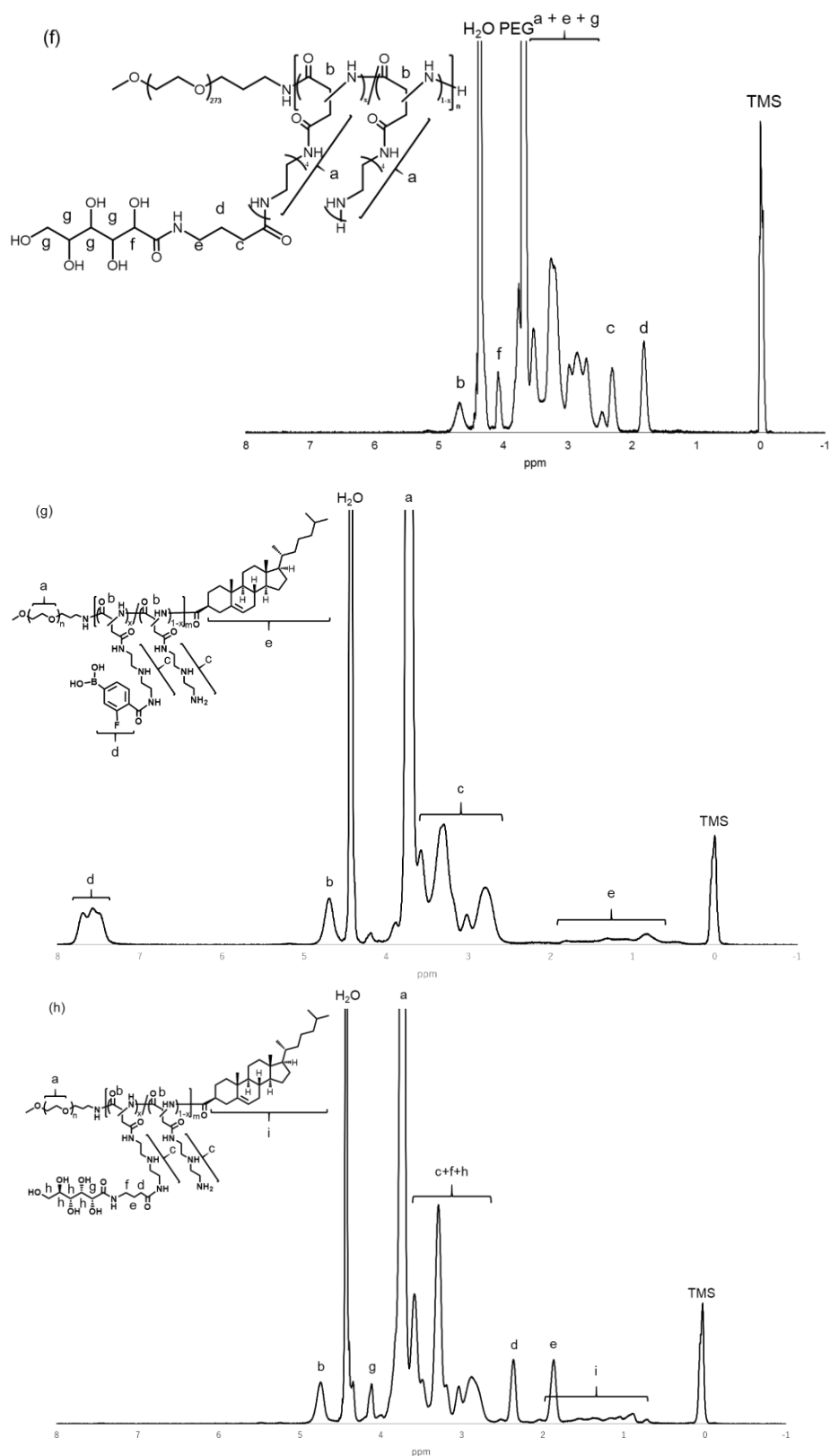


Figure 3-8. Representative ^1H -NMR spectra of (a) PEG-PAsp(DET-FPBA), (b) PEG-PAsp(DET-GlcAm), (c) PEG-PAsp(TEP-FPBA), (d) PEG-PAsp(TEP-GlcAm), (e) PEG-PAsp(TEP-FPBA), (f) PEG-PAsp(TEP-GlcAm), (g) PEG-PAsp(DET-FPBA)-Chol, and (h) PEG-PAsp(DET-GlcAm)-Chol

Representative ^1H -NMR spectra of PEG-PAsp(DET-FPBA), PEG-PAsp(DET-GlcAm), PEG-PAsp(TET-FPBA), PEG-PAsp(TET-GlcAm), PEG-PAsp(TEP-FPBA), PEG-PAsp(TEP-GlcAm) was shown in **Figure 3-8**. Also, ^1H -NMR spectra of PEG-PAsp(DET-FPBA)-Chol and PEG-PAsp(DET/GlcAm)-Chol were shown in **Figure 3-8**.

3.5.2 Nuclease resistance of mRNA incubated in FBS solution with RNase inhibitor

The nuclease resistance of naked mRNA was evaluated by the same protocol described in Materials and Methods section. With increasing the concentration of RNase inhibitor, the amount of remaining mRNA became larger as shown in **Figure 3-9**, indicating mRNA degradation was derived from RNase.

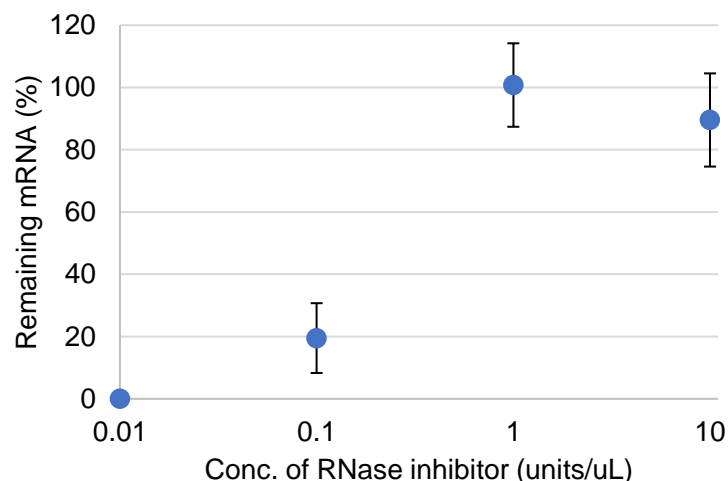


Figure 3-9. The amount of intact mRNA incubated in 10% FBS solution with various concentrated RNase inhibitor ($n = 4$). Data were shown as means \pm SEM.

3.5.3 Transmission electron microscopic (TEM) imaging

Copper TEM grids (Cu400, JEOL Ltd., Tokyo, Japan) were hydrophilized using an Eiko IB-3 ion coater (Eiko Engineering Co. Ltd., Tokyo, Japan). 2% w/v Uranyl acetate aqueous solution was added to the same volume of PM solution (10 mM HEPES buffer with

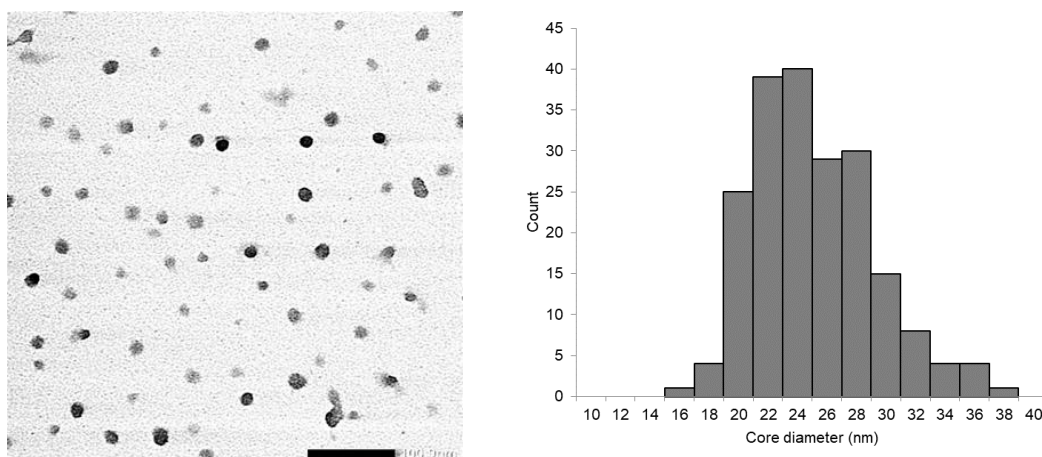


Figure 3-10. TEM image of PEG-PAsp(DET) PMs (left) and size distribution obtained from TEM images by counting 200 particles (right).

150 mM NaCl (pH 7.4)) on the hydrophilized grids. After 1 min incubation at room temperature, the mixture was removed with a filter paper. Then, TEM observation was performed using a JEM-1400 (JEOL Ltd., Tokyo, Japan) operated at 120 kV of acceleration voltage. The PM core size was estimated by counting 200 PMs in TEM images. Note that, uranyl acetate staining should make nucleic acid size 83.7% smaller than actual length.⁸ Thus, the actual length of PM core was calculated based on this report.

3.5.4 Quantification of the number of block copolymers binding to mRNA strand

PEG-PAsp(DET) was labeled by conjugating with CF594 succinimidyl ester according to the manufactures' procedure. PMs were prepared from mRNA and CF594-labeled PEG-PAsp(DET) with the same procedure described in the above section. Then, the PM solution was centrifuged for 90 min at 55,000 g using a polycarbonate tube with thick-wall and Beckman XL-1 ultracentrifuge with TLA-120.1 rotor. After ultracentrifugation, the fluorescence intensity of free block copolymers in the supernatant was analyzed using NanoDrop ND-3300 at a wavelength of 614 nm. The free block copolymer concentration was determined from the calibration curve of CF594-labeled block copolymer solution. The

experiment demonstrated that 11 block copolymers bound to one mRNA strand at pH 7.4.

3.5.5 Estimation of PEG density on PM surface

The size of RNase was reported around 3 ~ 4 nm in previous study.⁹ Thus, PEG shell surrounding PM core may not prevent RNase from invading into the core. The average PM core diameter, which was regarded as a spherical structure, estimated from TEM images was 24 ± 4.1 nm (average \pm standard deviation) (**Figure 3-10**). If single mRNA was encapsulated in one PM, 11 strands of PEG-PAsp(DET) was bound to mRNA. Therefore, the tethering PEG density (σ (chains/nm²)) on PM core was calculated to be 0.05 chains/nm². Also, the distance between the nearest PEG strands (T) was calculated as follows; $T = 1/\langle\sigma\rangle^{1/2}$ (nm). Because the radius gyration (R_g) of PEG (12 kDa) is estimated to be 4.7 nm,¹⁰ reduced tethering density ($\pi R_g^2 \sigma$) was calculated to be 0.35 (≤ 1). It means there may be much room between two neighboring PEG strands. Such a low PEG tethering density may allow nucleases to invade PM core without difficulty. Therefore, swelling of PM core observed in FPBA/GlcAm cross-linked PMs may cause no improvement in the tolerability test against nuclease attacks.

3.6 Reference

1. Uchida, H.; Itaka, K.; Nomoto, T.; Ishii, T.; Suma, T.; Ikegami, M.; Miyata, K.; Oba, M.; Nishiyama, N.; Kataoka, K., Modulated Protonation of Side Chain Aminoethylene Repeats in N-Substituted Polyaspartamides Promotes mRNA Transfection, *J. Am. Chem. Soc.* **2014**, 136, 12396-12405.
2. Oba, M.; Miyata, K.; Osada, K.; Christie, R. J.; Sanjoh, M.; Li, W.; Fukushima, S.; Ishii, T.; Kano, M. R.; Nishiyama, N.; Koyama, H.; Kataoka, K., Polyplex micelles prepared from

- ω -cholesteryl PEG-polycation block copolymers for systemic gene delivery, *Biomaterials* **2011**, 32, 652-663.
3. Uchida, H.; Miyata, K.; Oba, M.; Ishii, T.; Suma, T.; Itaka, K.; Nishiyama, N.; Kataoka, K., Odd-Even Effect of Repeating Aminoethylene Units in the Side Chain of N-Substituted Polyaspartamides on Gene Transfection Profiles, *J. Am. Chem. Soc.* **2011**, 133, 15524-15532.
4. Traut, T. W., Physiological concentrations of purines and pyrimidines, *Mol. Cell. Biochem.* **1994**, 140, 1-22.
5. Leist, M.; Single, B.; Castoldi, A. F.; Kuhnle, S.; Nicotera, P., Intracellular adenosine triphosphate (ATP) concentration: a switch in the decision between apoptosis and necrosis, *J. Exp. Med.* **1997**, 185, 1481-1486.
6. Gorman, M. W.; Feigl, E. O.; Buffington, C. W., Human plasma ATP concentration, *Clin. Chem.* **2007**, 53, 318-325.
7. Uchida, S.; Kinoh, H.; Ishii, T.; Matsui, A.; Tockary, T. A.; Takeda, K. M.; Uchida, H.; Osada, K.; Itaka, K.; Kataoka, K., Systemic delivery of messenger RNA for the treatment of pancreatic cancer using polyplex nanomicelles with a cholesterol moiety, *Biomaterials* **2016**, 82, 221-228.
8. Namork, E.; Johansen, B. V., Electron microscopy of nucleic acids: The effect of different post-treatments on contour-length measurements, *Micron* **1980**, 11, 85-90.
9. Kartha, G.; Bello, J.; Harker, D., Tertiary Structure of Ribonuclease, *Nature* **1967**, 213, 862-865.
10. Tockary, T. A.; Osada, K.; Chen, Q. X.; Machitani, K.; Dirisala, A.; Uchida, S.; Nomoto, T.; Toh, K.; Matsumoto, Y.; Itaka, K.; Nitta, K.; Nagayama, K.; Kataoka, K., Tethered PEG Crowdedness Determining Shape and Blood Circulation Profile of Polyplex Micelle Gene Carriers, *Macromolecules* **2013**, 46, 6585-6592.

Chapter 4

Development of mRNA/polymer direct cross-linked polyplex micelles
through phenylboronate ester linkage

4.1 Introduction

In order to improve the nuclease resistance of mRNA, many reports have paid attention to the molecular design of delivery carriers, which actually achieved to improve mRNA life time in harsh physiological condition.¹⁻⁸ However, there were few researches engineering mRNA molecule itself for improving nuclease resistance. Chemical modification of mRNA nucleoside has been investigated as a method to modulate mRNA strands to decrease immunogenicity, but previous studies reported that chemical modification of mRNA scarcely improved nuclease resistance. Moreover, chemical modification of nucleobase on mRNA can decrease protein expression efficiency.⁹⁻¹⁰

Herein, in order to achieve synergetic effects of designing both delivery carrier and mRNA for efficient delivery, I focused on the single strand structure of mRNA and attempted to modify mRNA through hybridization of RNA oligonucleotides (OligoRNA) complementary to mRNA sequences. In this design, 5'-end *N*-gluconamide (GlcAm) modified OligoRNAs

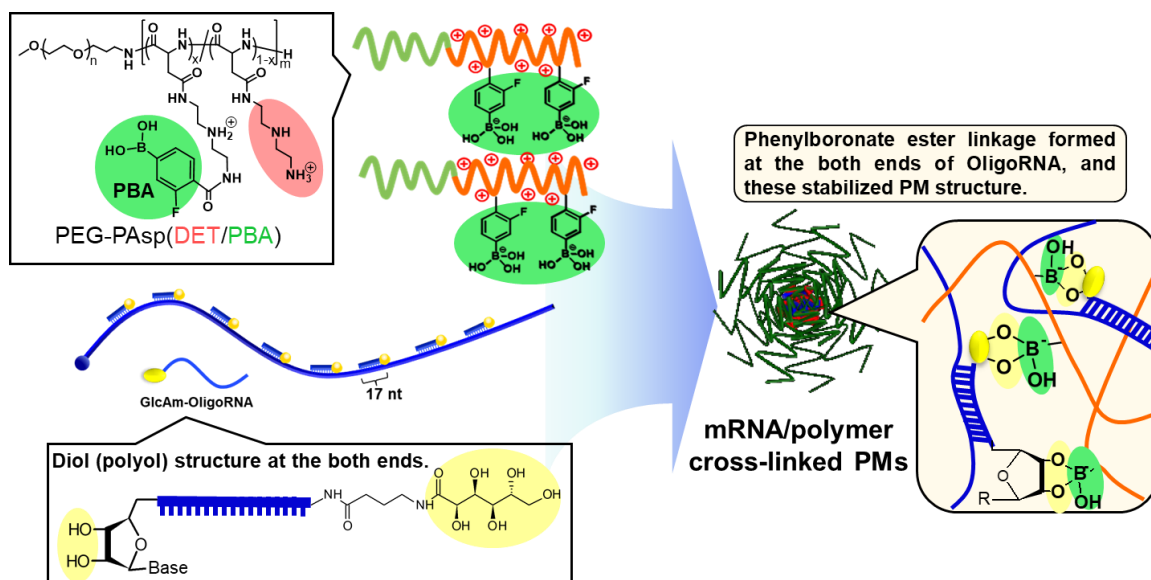


Figure 4-1. Schematic illustration of design of PMs; mRNA hybridized with GlcAm-OligoRNA can form phenylboronate ester cross-linking on OligoRNA with FPBA moieties on block copolymers.

(GlcAm-OligoRNAs) were hybridized with mRNA (GlcAm-mRNA), and PMs were prepared from the GlcAm-mRNA and PEG-PAsp(DET) modified with 3-fluoro-substituted phenylboronic acid (FPBA) in PAsp(DET) segments (PEG-PAsp(DET-FPBA)) (**Figure 4-1**). The formation of direct cross-linking between FPBA moieties on PAsp(DET) side chain and GlcAm moieties on mRNA was expected to suppress polyion exchange reaction and eventually to enhance nuclease resistance of PMs. Interestingly, the mRNA/polymer cross-linked PMs protected loaded mRNA from nuclease attacks more efficiently than polymer/polymer cross-linked PMs prepared from PEG-PAsp(DET-FPBA) and PEG-PAsp(DET-GlcAm), which was evaluated in Chapter 3.

4.2 Materials and methods

4.2.1 Materials

PEG-PAsp(DET), PEG-PAsp(DET-FPBA), and PEG-PAsp(DET-GlcAm) were synthesized according to the same protocol described in “*Chapter 2 and 3*.” mRNA was also prepared by the same procedure in “*Chapter 3*”. HEPES, hydrochloric acid (HCl), sodium acetate, sodium chloride (NaCl), sodium dextran sulfate (DS) (M_w : 50,000 g/mol), and acetic acid were purchased from Wako Pure Chemical Industrial Ltd. (Osaka, Japan). Sybr Green II and Agarose L03 TAKARA were purchased from TAKARA Bio Inc. (Shiga, Japan). Cell culture medium was prepared from 450 mL of Dulbecco’s modified Eagle’s medium (DMEM) (Sigma-Aldrich Co., Madison, WI), 50 mL of fetal bovine serum (FBS) (Dainippon Sumitomo Pharma Co., Ltd., Osaka, Japan) and 5 mL of Penicillin-Streptomycin Solution Stabilized (Sigma-Aldrich). Human Hepatocarcinoma cells (HuH-7), Human cervical cancer cells expressing firefly luciferase (Hela-luc cells), and mouse macrophage-derived cells (RAW264.7

cells) were obtained from RIKEN Cell Bank (Tsukuba, Japan). CF594 succinimidyl ester was purchased from Biotium, Inc. (Fremont, CA). Opti-MEM was purchased from Thermo Fisher Scientific Inc. (Tokyo, Japan). Renilla Luciferase Assay System Kit was purchased from Promega Co. (Madison, WI). Lipofectamine LTX was purchased from Invitrogen (Carlsbad, CA). Cy3/Cy5 double-labeled mRNA were prepared using Label IT Nucleic acid labeling kit (Mirus Bio Corporation, Madison, WI) according to manufactures' protocol with slight modification. Isoflurane was purchased from Pfizer Japan Inc. (Tokyo, Japan). ReverTra Ace qPCR RT Master Mix kit was purchased from TOYOBO Life Science (Osaka, Japan). The 96-well, 48-well, 24-well, and 12-well plates were purchased from Becton Dickinson (Franklin Lakes, NJ).

4.2.2 Hybridization of OligoRNA into mRNA

All of OligoRNAs except simple OligoRNA were purchased from GeneDesign Inc. (Osaka, Japan). Simple OligoRNAs were purchased from Hokkaido System Science Co. Ltd. (Hokkaido, Japan). The secondary structured region in *Gluc* mRNA estimated by IPknot software,¹⁶ can be possibly avoided to be selected as target sequences where OligoRNAs can bind. Sequences of OligoRNAs are in **Table 4-3**. For preparing GlcAm-OligoRNA, 500 µg of 5' end NH₂-OligoRNA (77 nmol) was dissolved in 800 µL of the mixture of 10 mM NaHCO₃ and methanol (1/3). DMT-MM (1 mg) and GlcAm (0.1 mg; 5 eq. to the primary amino group on OligoRNA) were added to the OligoRNA solution, and then reacted for 6 h in 4 °C with addition of 1 mg DMT-MM every 2 h. Sodium acetate solution (3 M) and NaCl solution (2 M) were added to the reacted mixture, and final concentration of sodium acetate and NaCl were set to be 0.3 mM and 0.2 mM, respectively. Then, twice volume of 2-propanol was added to

the mixture, followed by incubation for 1 h at -20 °C. After the incubation, the reacted solution was centrifuged for 30 min at 15,400 g, and the supernatant was removed. Then, the pellet of RNA oligonucleotide was washed three times by 1 mL of 70% ethanol. The conjugation efficiency of GlcAm with OligoRNA was determined from the calibration curve of fluorescence intensity of the mixture of fluorescamine and NH₂-OligoRNA.

In all experiments, #1, #5, #9, #13, and #17 OligoRNAs were used for 5*OligoRNA, #1, #3, #5, #7, #9, #11, #13, #15 and #17 OligoRNAs were for 10*OligoRNA, #1, #2, #3, #5, #6, #7, #9, #10, #11, #13, #14, #15, #17, #18, and #19 OligoRNAs were for 15*OligoRNAs and #1 ~ #20 OligoRNAs were for 20*OligoRNA.

mRNA solution (final conc.: 50 µg/mL) and OligoRNA solution (1 equimolar to mRNA strand) were mixed in 10 mM HEPES buffer (pH 7.4). The mixture was heated for 5 min at 65 °C, and then gradually cooled from 65 °C to 30 °C in 10 min for hybridization. The Hybridized solution was analyzed through 10% TBE poly(acrylamide) gel electrophoresis (Thermo Fisher Scientific Inc., Waltham, MA) to evaluate hybridization efficiency. The hybridized solution (10 µL) containing 5% glycerol was electrophoresed for 60 min at 100 V in TBE buffer. The migration of RNA in the poly(acrylamide) gel was imaged by Sybr Green II staining. Images were captured using PharosFX™ System.

4.2.3 Cell culturing

Cells were cultured in Opti-MEM or DMEM containing 10% FBS and 1% penicillin/streptomycin in a humidified atmosphere with 5% CO₂ at 37 °C, unless specifically described.

4.2.4 Effect of the length of OligoRNA hybridized to mRNA on translation efficiency and immune response

The length of OligoRNA was optimized in terms of protein expression efficiency and immunogenicity. OligoRNA with 17, 23, 40, or 60 nt was hybridized with *Gluc* mRNA, respectively. These mRNA was complexed with Lipofectamine LTX according to the manufactures' protocol. HuH-7 cells (5,000 cells/well) and RAW264.7 cells (10,000 cells/well) were seeded on 96-well plate, respectively, and incubated for 24 h. After the replacement of culture medium with 50 μ L of Opti-MEM, 50 μ L of mRNA/Lipofectamine LTX complex containing 250 ng of mRNA was added. After 4 h of transfection, 10 μ L of the supernatant of culture medium was evaluated using Renilla Luciferase Assay Kit and Lumat³ LB9508 (Berthold Japan co. Ltd., Osaka, Japan). Then, the Opti-MEM was exchanged for 100 μ L of fresh DMEM, and after 20 h post-incubation, luciferase assays were also conducted.

For evaluation of immune response, RAW264.7 cells (300,000 cells/well) were seeded on 12-well plate and cultured for 24 h. After removing culture medium, 900 μ L of Opti-MEM was added to each well. Then 100 μ L of mRNA/Lipofectamine LTX complexes comprising 1 μ g of mRNA were transfected. After 4 h of transfection, the cells were washed by cold D-PBS twice, and then RNAs were extracted using RNeasy Mini Kit from these cells. After reverse transcription of collected RNA using ReverTra Ace qPCR RT Master Mix kit, qRT-PCR measurement was conducted using TaqMan Gene Expression Assays (Applied Biosystems, Mm00446190_m1 for interleukin-6 (IL-6), Mm00439552_s1 for Interferon- β (IFN- β), and Mm00607939 for β -actin) and an ABI Prism 7500 sequence Detector.

4.2.5 Synthesis of block copolymers and preparation of PMs

FPBA and GlcAm moieties were installed into cationic side chain of PEG-PAsp(DET) (Mw of PEG: 12 kDa, DP of PAsp(DET): 70). The introduction ratio of FPBA and GlcAm was determined to be 27%, 49%, 87% for FPBA and 54% for GlcAm moiety from ^1H -NMR spectra, respectively.

PMs were prepared from these synthesized block copolymers and each mRNA with the same procedure described in “the Materials and Methods section of *Chapter 2* and *3*.” One-unit volume polymer solution was mixed with 2-unit volume mRNA solution (mRNA conc.: 50 $\mu\text{g/mL}$) at a residual charge ratio ([protonated amine group on PAsp(DET) (N^+) – negatively-charged boron atoms (B^-)]/[phosphate groups in both mRNA and OligoRNA (P)] (($\text{N}^+ - \text{B}^-$)/P ratio)) of 1.5. PMs were incubated overnight at 4 $^\circ\text{C}$ before all experiments. PM formation was confirmed through DLS measurement in 10 mM HEPES buffer (pH 7.4) at 25 $^\circ\text{C}$ using 532 nm laser.

4.2.6 Tolerability test of PMs against nuclease attacks

PMs containing 100 ng of *Gluc* mRNA were incubated in 24 μL of 10% FBS solution at 37 $^\circ\text{C}$ for 15 min. The samples were immediately diluted 1,250 times by RLT buffer with 1% mercaptoethanol in RNeasy Mini Kit. After 2h incubation at 37 $^\circ\text{C}$, mRNA was extracted using RNeasy Mini Kit, followed by reverse transcription of mRNA using ReverTra Ace qPCR RT Master Mix kit. Then, qRT-PCR measurement was conducted using a couple of primers for *Gluc* mRNA (Reverse sequence; GTCAGAACACTGCACGTTGG, and Forward sequence; TGAGATTCCTGGGTTCAAGG) and MicPCR (Bio Molecular Systems, Upper Coomera, Australia).

4.2.7 Förster resonance energy transfer (FRET) measurement

PMs were prepared from Cy3/Cy5 double-labeled mRNA as described above. PM solution was incubated for 1 h in the various concentrated ATP solution (0, 0.3, 1, and 3 mM), where mRNA concentration was 12.5 µg/mL. After incubation, the fluorescence intensity was obtained by Tecan Microplate Reader Infinite M1000 Pro at 488 nm wavelength for excitation, and 570 nm and 672 nm for Cy3 and Cy5 for emission, respectively. FRET efficiency of all samples was calculated by following equation.

$$\text{FRET efficiency} = (\text{Cy5 intensity (672 nm)}) / (\text{Cy3 intensity (570 nm)})$$

4.2.8 Tolerability test of PMs against exchange reaction by competitive anionic macromolecules

PM solutions containing 500 ng of mRNA were mixed with DS at various residual charge ratios of [sulfate groups in DS (A)]/[phosphate groups in mRNA (P)] (A/P ratios) in the 10 mM HEPES with 150 mM NaCl at physiological pH (pH 7.4). After 1 h incubation at 37 °C, the PM solution (20 µL) containing 5% glycerol was electrophoresed for 30 min at 100 V in TAE buffer. The migration of mRNA in the agarose gel was imaged by 0.5 mg/L of EtBr staining. Images were taken by using Pharos^{FXTM} System.

4.2.9 Quantification of the number of block copolymers binding to mRNA

Block copolymers were labeled by conjugating with CF594 succinimidyl ester reagent according to the manufactures' procedure. PM solution in 10 mM HEPES buffer with 150 mM NaCl at physiological pH (pH 7.4) was ultracentrifuged by the same condition and instrument described in Chapter 3 (55,000g and 1.5 h centrifuge). After ultracentrifugation, the

fluorescence intensity of free block copolymers in the supernatant was measured using NanoDrop ND-3300 at a wavelength of 614 nm. The number of free block copolymers was determined from the standard curve of CF594-labeled block copolymer solution, which was ultracentrifuged at the same condition. Same experiment was conducted in acetate buffer with 150 mM NaCl at pH 5.5.

4.2.10 Protein expression efficiency of PMs in cultured cells

HuH-7 cells (10,000 cells/well) were seeded onto 48-well plates, and incubated for 24 h. After replacing the culture medium with 200 μ L of fresh one, 15 μ L PM solution containing 500 ng of mRNA was transfected. After 24 h of transfection, luminescence intensity in 10 μ L of culture medium supernatant was evaluated using Renilla Luciferase Assay Kit and single tube luminometer (Lumat LB9508, Berthold Japan K. K., Tokyo, Japan).

4.2.11 Quantification of the remaining amount of transfected mRNA

PMs were prepared with the same procedure described the proceeding section. HuH-7 cells (20,000 cells/well) were seeded on 24-well plate and incubated for 24 h. After removing the culture medium, the cells were washed by cold D-PBS twice. Then, 125 μ L of PM solution containing 1 μ g of mRNA in 10 mM HEPES with 150 mM NaCl was transfected. After 15 min post-incubation, PMs were completely removed by washing cells once using D-PBS, and then 400 μ L of fresh DMEM was added to each well. At the indicated time points, cells were washed D-PBS twice, and lysed by RLT buffer in RNeasy kit (Quiagen) containing 1% 2-mercaptethanol. Total RNA in lysate was extracted using RNeasy Kit, followed by reverse transcription of the collected RNA. Then, the amount of *Gluc* mRNA in reverse-transcribed

samples was quantified by the same protocol described above using qRT-PCR. In each sample, the amount of mRNA after 15 min PM treatment was considered as 100%.

4.3 Results and Discussion

4.3.1 Optimization of the length of OligoRNA

First, the length of OligoRNA was optimized in terms of translational efficiency and immunogenicity of hybridized mRNA because undesirable effects by hybridization should be avoided for efficient mRNA delivery. Thus, translational activity and immune response of transfected mRNA to mouse macrophage derived RAW264.7 cells, which express various immune receptors,¹⁷ were examined by using mRNA encoding secretory luciferase (*Gaussian luciferase: Gluc*) as a reporter mRNA. Here OligoRNAs without any modification at the both ends were used to exclude other influence of functional groups on these assays, allowing to completely clarify the hybridized length effect. Twenty position throughout the *Gluc* mRNA sequence except poly A tail were chosen for OligoRNA hybridization (**Figure 4-2 (a)**, **Table 4-3**). Among these 20 positions, four OligoRNAs (#2, #6, #16, #19) were used to evaluate the effect of OligoRNA hybridization on translational efficiency and immunogenicity. A series of OligoRNAs possessing five different complementary sequence length (17, 23, 40, 60, and 80 nt) were hybridized with mRNA encoding *Gluc*, respectively. Note that, to guarantee efficient hybridization in physiological condition, 17 nt was chose as a minimum length of complementary sequence on OligoRNA, because estimated melting temperature (T_m) showed stable hybridization over 17 bp at 37 °C under physiological salt condition even in A/U rich sequences (more than 80%) (**Figure 4-9**).¹⁸⁻¹⁹ The hybridization efficiency of these OligoRNAs was confirmed thorough poly(acrylamide) gel electrophoresis (**Figure 4-10**).

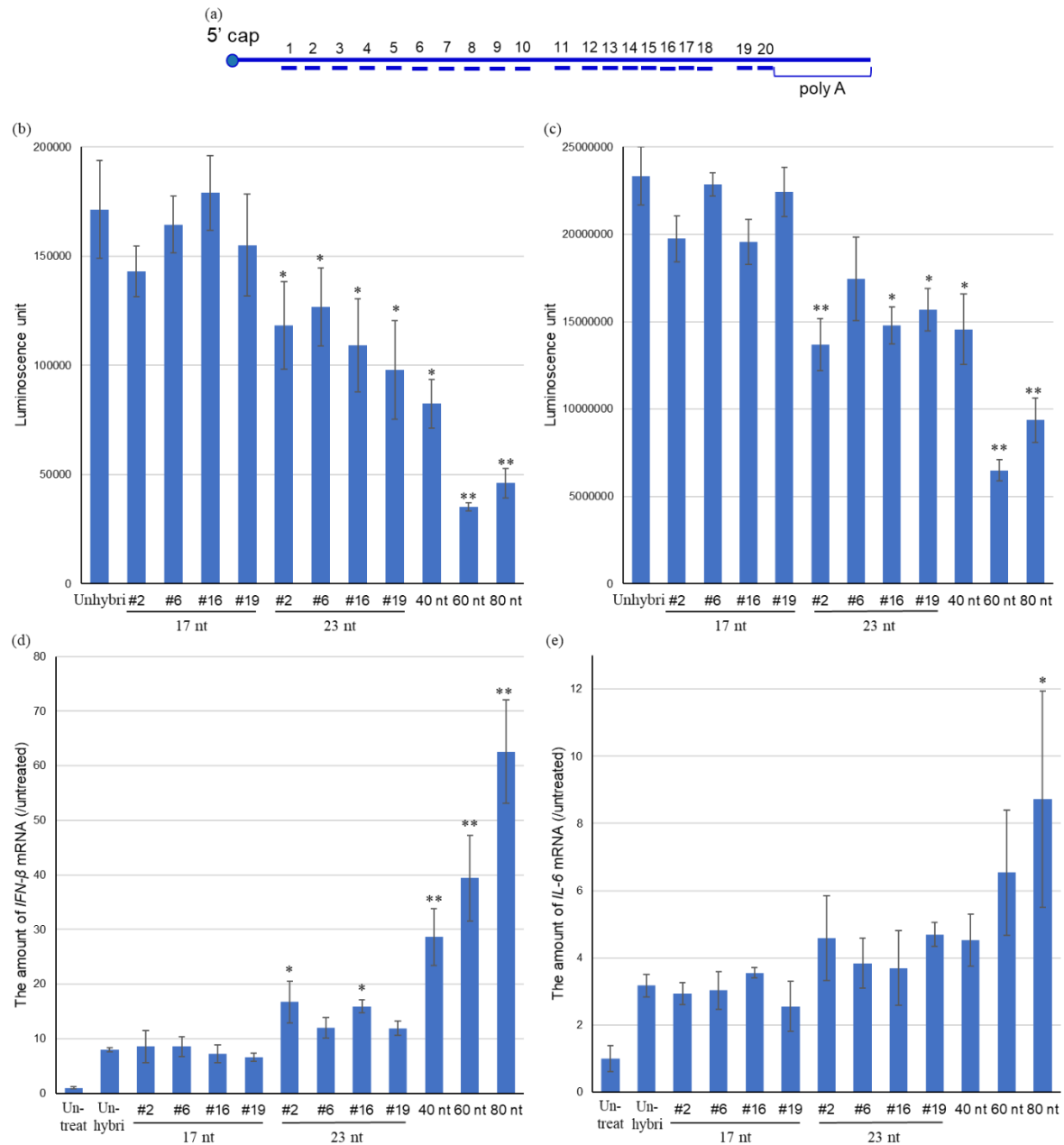


Figure 4-2. Optimization of the length of OligoRNA through translational activity and immunogenicity in RAW264.7 cells. (a) The hybridization positions of OligoRNA in Gluc mRNA. (b-c) Transfection activity of each mRNA complexed with Lipofectamine LTX reagent after (b) 4 and (c) 24 h of transfection. Data were shown as means \pm SEM ($n = 6$). (d-e) Proinflammatory transcripts ((d) IFN- β and (e) IL-6) levels after 4h of mRNA complexed with Lipofectamine LTX transfection. Abbreviation: “Untreat” means untreated control and “Unhybri” means unhybridized mRNA. Data were shown as means \pm SEM ($n = 4$). Statistical difference to “Unhybri” group was analyzed by analysis of variance followed by Dunnett’s test. (* $p < 0.05$, ** $p < 0.01$)

Then, these hybridized mRNA with different length OligoRNA were transfected to

RAW264.7 cells using lipofectamine LTX. As seen in **Figure 4-2 (b)**, the Gluc expression efficiency of mRNA hybridized with 17 nt OligoRNA was similar to that of unhybridized one after 4 h of transfection, indicating that 17 nt OligoRNA hybridization did not inhibit mRNA translation in cultured cells. On the other hand, mRNA with 23 nt or longer OligoRNA showed significant decrease of Gluc expression efficiency comparing to unhybridized mRNA. The similar trend was observed in Gluc expression efficiency of all samples after 24 h of transfection (**Figure 4-2 (c)**), suggesting that 17 nt OligoRNA did not induce RNAi process inside the cells. Another important problem to be considered from a view point of cytotoxicity was suppression of endogenous protein expression by RNAi that may happen if OligoRNA can bind to endogenous mRNA. For this issue, OligoRNAs complexed with Lipofectamine RNAiMax were transfected to luciferase-expressing Hela cells (Hela-Luc cells). Eventually, as seen in **Figure 4-11**, endogenous Luc expression was maintained by transfecting OligoRNA at the concentration used in the mRNA transfection experiment into cultured cells (8 nM). Note that, transfection of 0.5 nM siRNA decreased the Luc expression to 1/3, and approximately 1000-times higher concentration of OligoRNA was required to decrease the Luc expression at the similar level. These results indicated that the risk of introducing OligoRNA to endogenous expression can be ignored.

Next, the effect of OligoRNA hybridization on immunogenicity was evaluated by quantifying *IFN- β* and *IL-6*, which are proinflammatory transcripts, in RAW264.7 cells using qRT-PCR. The transfection of mRNA hybridized with 17 nt OligoRNA demonstrated no extra *IFN- β* and *IL-6* expression comparing to the unhybridized mRNA regardless of the hybridization sequences, while mRNA with over 23 nt OligoRNA induced significant increase of these proinflammatory transcripts (**Figure 4-2 (d)-(e)**). Such a hybridization length-

dependent induction of mRNA immunogenicity can be explained by receptor recognition length of dsRNA for its activation. For example, retinoic acid-inducible gene (RIG-I) recognizes 20 bp,¹⁴⁻¹⁵ Toll-like receptor (TLR) recognizes 50 bp.¹⁶ The sharp recognition of RIG-I receptor could explain the immunogenicity difference between mRNA hybridized with 17 nt OligoRNA and 23 nt OligoRNA of 23 bases as shown in **Figures 4-2 (d)-(e)**. The transfection and immunogenicity experiments indicated that using 17 nt complementary sequence was a satisfactory method to hybridize OligoRNA with mRNA without inhibiting translational activity and inducing immunogenicity. Thus, 17 nt OligoRNA was used for hybridization in the following experiments.

4.3.2 Preparation of PMs loading mRNA hybridized with GlcAm-OligoRNA

PEG-PAsp(DET), PEG-PAsp(DET-FPBA), and PEG-PAsp(DET-GlcAm) was synthesized according to the “*Materials and Methods section in Chapter 2*” (M_w of PEG: 12 kDa, Degree of polymerization of PAsp(DET): 70). The introduction ratio of FPBA and GlcAm was determined to be 27, 49, 88% for FPBA and 54% for GlcAm from ¹H-NMR spectra. FPBA-OligoRNA and GlcAm-OligoRNA were also synthesized through dehydration reaction using coupling reagent. The conjugation ratio of GlcAm was calculated from the residual primary amino groups at the end of OligoRNA detected by fluorescamine method. It was confirmed that almost all amino groups were reacted with FPBA and GlcAm (**Table 4-4**). mRNA with GlcAm-OligoRNA (GlcAm-mRNA) was prepared from these synthesized OligoRNAs by hybridization in 10 mM HEPES buffer at physiological pH (pH 7.4). PMs were prepared from synthesized block copolymers and mRNA at residual charge ratio ($(N^+-B^-)/P$) of 1.5 (See “*Materials Method*” Section). DLS measurement demonstrated 43-53 nm cumulant

diameter in the PMs composed of PEG-PAsp(DET-FPBA_{27%}) or PEG-PAsp(DET-FPBA_{49%}), while PMs prepared from PEG-PAsp(DET-FPBA_{88%}) showed around 100 nm of cumulant diameter (**Table 4-1**). The size increase of PMs from PEG-PAsp(DET-FPBA_{88%}) may be resulted from decreasing charge density of cationic segment due to negatively-charged FPBA moieties. To get the further insights of PM formation, FRET efficiency of PMs loaded with Cy3/Cy5 double-labeled mRNA was measured because previous study reported that FRET signal from double-labeled mRNA was an indicator representing condensation status of mRNA.⁶ Comparing to PMs composed of PEG-PAsp(DET-FPBA_{27%}) or PEG-PAsp(DET-

Table 4-1. Cumulant diameter and polydispersity index of PMs evaluated by DLS measurement at 25 °C in 10 mM HEPES buffer (pH 7.4)

	Size (d. nm)/PDI				
	The number of GlcAm-OligoRNA				
	0	5	10	15	20
PEG-PAsp(DET) PM	44/0.19	—	—	—	45/0.24
Polymer/polymer cross-linked PM	53/0.15	—	—	—	—
PEG-PAsp(DET/FPBA _{27%}) PM	45/0.22	—	49/0.23	—	43/0.14
PEG-PAsp(DET/FPBA _{49%}) PM	44/0.16	46/0.18	47/0.20	46/0.17	48/0.18
PEG-PAsp(DET/FPBA _{88%}) PM	102/0.20	—	96/0.23	—	95/0.23

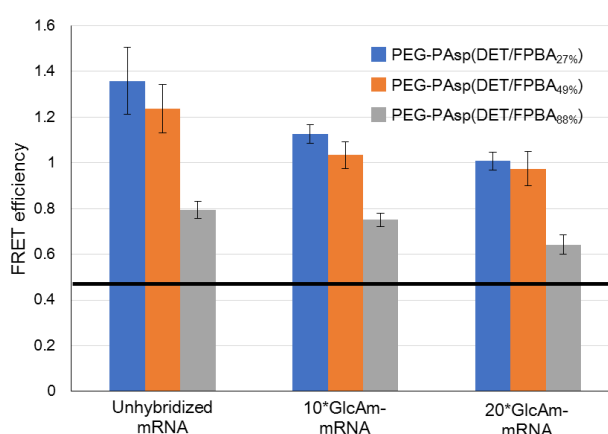


Figure 4-3. FRET efficiency of PMs loaded with Cy3/Cy5 double-labeled mRNA in 10 mM HEPES buffer containing 150 mM NaCl. Solid line represented FRET efficiency of naked Cy3/Cy5 double-labeled mRNA without hybridization in 10 mM HEPES buffer containing 150 mM NaCl. Data were shown as means \pm SEM ($n = 3$).

FPBA_{49%}), PEG-PAsp(DET-FPBA_{88%}) PMs showed quite lower FRET efficiency in physiological condition (**Figure 4-3**), strongly suggested that mRNA was hardly condensed in PEG-PAsp(DET-FPBA_{88%}) PM core. These results were consistent with DLS measurement in **Table 4-1**. Noteworthy, increasing the number of GlcAm-OligoRNA hybridized with mRNA decreased the FRET efficiency of PMs in spite of FPBA introduction ratio on block copolymers. Probably, hydrophilicity of GlcAm moieties inhibited mRNA condensation involving dehydration.

4.3.3 Characterization of PMs loaded with hybridized mRNA

Improving nuclease resistance of mRNA is an important factor for efficient mRNA delivery. Thus, the introduction ratio of FPBA moieties into PAsp(DET) side chain was optimized through the tolerability test of PMs against nuclease attacks. Quantification of mRNA loaded in PMs after incubation in 10% FBS solution demonstrated that more mRNA was remained with increasing the number of GlcAm-OligoRNA when it was encapsulated in

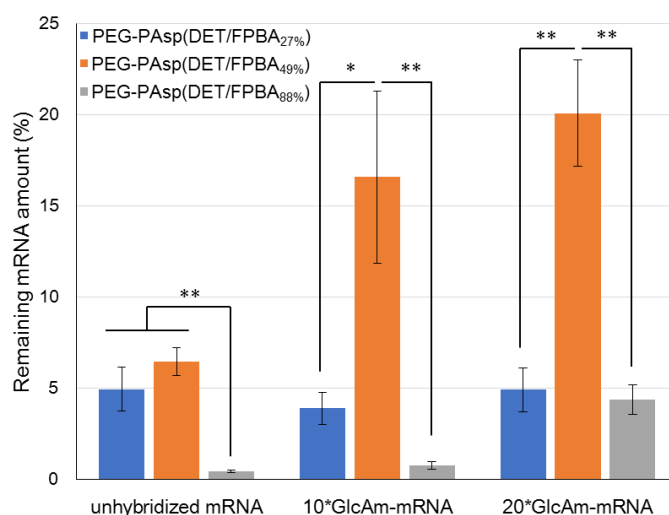


Figure 4-4. Nuclease resistance of PMs after incubation in 10% FBS solution. Data were shown as means \pm SEM ($n = 6$). Statistical difference was analyzed by Student's unpaired 2-tailed test. (* $p < 0.05$, ** $p < 0.01$)

the PMs prepared from PEG-PAsp(DTE/FPBA_{49%}) (**Figure 4-4**). Noteworthy, PMs prepared from PEG-PAsp(DET-GlcAm) and mRNA hybridized with FPBA-modified OligoRNA (FPBA-OligoRNA) did not show improvement of nuclease resistance comparing to simple PEG-PAsp(DET) PMs (**Figure 4-12**). Also, formation of PMs from PEG-PAsp(DET-FPBA_{88%}) slightly improved nuclease resistance by hybridizing 20 GlcAm-OligoRNA. In contrast, nuclease resistance of PMs composed of PEG-PAsp(DET) or PEG-PAsp(DET-FPBA_{27%}) was not affected by the number of GlcAm-OligoRNA. The optimal FPBA introduction ratio for nuclease resistance can be explained the balance of the number of FPBA moieties in PM core and charge density of PAsp(DET) segment. Increasing the introduction ratio of FPBA moieties can indeed enhance cross-linking efficiency in PM core, but, at the same time, decreases charge density of cationic segment due to negatively-charged FPBA moieties, which weakens electrostatic interaction between mRNA and block copolymers. In low introduction ratio, *i.e.*, PEG-PAsp(DET-FPBA_{27%}), FPBA moieties in PM core may not enough to form FPBA/GlcAm linkage effectively, and eventually stabilization effect did not achieve. Also, high modification of FPBA moieties on PAsp(DET) hardly induced mRNA condensation into PM core and allowed nucleases to pass PEG shell on PM because it was indicated that mRNA was degraded before PM dissociation (**Figure 4-13**). Therefore, middle FPBA introduction ratio of PAsp(DET) side chain, *i.e.*, 49% modification, showed higher nuclease resistance than other introduction ratios.

To confirm the formation of cross-linking between block copolymers and GlcAm-OligoRNAs, mRNA hybridized with three types of OligoRNAs (i; GlcAm-OligoRNA, ii; OligoRNA, iii; 3'-DeoxyoligoRNA) were prepared, and nuclease resistance of PMs loading mRNA hybridized with each OligoRNA was examined. GlcAm-OligoRNA can form

phenylboronate ester linkage at the both ends, simple OligoRNA can form at the only 3' end, and 3'-deoxyOligoRNA cannot form ester linkage (**Figure 4-5 (a)**). Actually, GlcAm-OligoRNA hybridization was efficiently improved nuclease resistance of PMs than other two OligoRNA, and the stabilization effect of 3'-DeoxyoligoRNA was quite limited (**Figure 4-5 (b)**). Obviously, it can be observed that the trend is in accordance with the number of the diol (polyol) functionalities, GlcAm-OligoRNA>OligoRNA>3'-DeoxyoligoRNA, indicating the order of cross-linking efficiency. Because the size of these PMs evaluated by DLS measurement was similar of all PMs (**Table 4-4**), it was safe to consider that the difference of nuclease resistance among three kinds of OligoRNAs resulted from PM core condition, especially cross-linking efficiency. Consequently, these results strongly suggested the formation of phenylboronate ester cross-linkings at the both ends of GlcAm-OligoRNA. Note that, hybridization of 20*3'-DeoxyoligoRNA to mRNA slightly improved nuclease resistance of PMs. Presumably, increasing the number of block copolymers associating to mRNA with OligoRNA, which increases the negative charge in PM core, resulted in higher PEG density protecting encapsulated mRNA more effectively. Moreover, the PMs prepared from PEG-PAsp(DET-FPBA_{49%}) and mRNA with 20*GlcAm-OligoRNA (mRNA/polymer cross-linked PMs) interestingly showed 3-fold higher nuclease resistance than the PMs prepared from unhybridized mRNA and the polymer mixture containing PEG-PAsp(DET-FPBA) and PEG-PAsp(DET-GlcAm) (Polymer/polymer cross-linked PMs) (**Figure 4-5 (c)**), which formed intermolecular cross-linking between block copolymers in PM core as described in Chapter 3. Noteworthy, the number of GlcAm and ribose structures was at most 40 groups in PMs encapsulating mRNA hybridized with GlcAm-OligoRNA while that in polymer/polymer cross-linked PMs was estimated to be 291 groups (**Table 4-2**, *details described in the following*

proteins, carbohydrates and nucleic acids.²⁰⁻²³ To evaluate the tolerability of PMs, PMs were mixed with dextran sulfate (DS), which is a negatively-charged carbohydrate, at residual charge ratios (A/P ratio) of 3. After 1 h incubation, the mixture was then evaluated through gel electrophoresis to quantify the amount of released mRNA from PM. In gel electrophoresis, mRNA hybridized with different OligoRNAs (OligoRNA, GlcAm-OligoRNA, and 3'-DeoxyoligoRNA) was compared to evaluate the effect of chemical structure at the ends of OligoRNA. Electrophoregrams showed suppression of migrated mRNA in accordance with the number of OligoRNAs (**Figure 4-6 (a)**). The trend that was in accordance with the number of the diol (polyol) functionalities was observed by comparing the three systems (GlcAm-

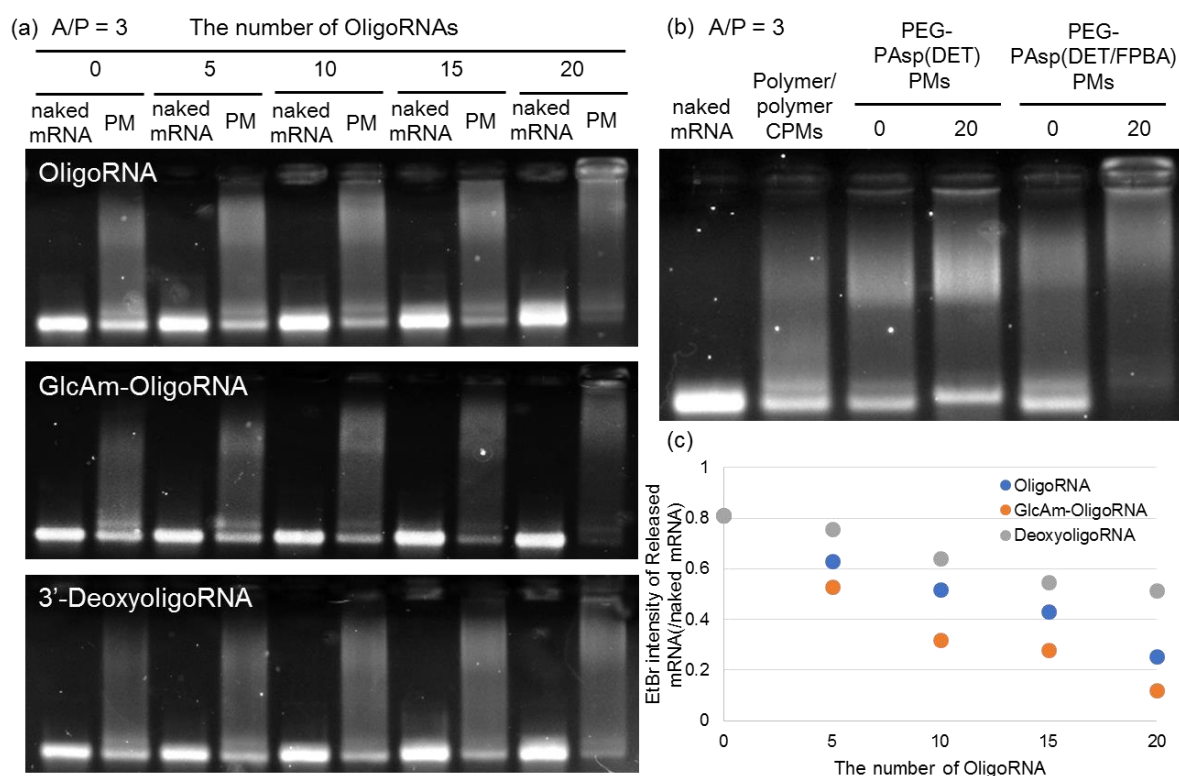


Figure 4-6. Tolerability test of PMs against polyion exchange reaction at A/P ratio of 3. (a) Electrophoregrams of PEG-PAsp(DET-FPBA) PMs loaded with mRNA hybridized with (top) OligoRNA, (middle) GlcAm-OligoRNA, and (bottom) 3'-DeoxyoligoRNA. (b) Electrophoregram of PMs prepared from different block copolymers. (c) Quantification of migrated mRNA released from PMs based on fluorescence intensity of EtBr. Abbreviation: Polymer/polymer CPM means PMs prepared from unhybridized mRNA and the mixture of PEG-PAsp(DET-FPBA) and PEG-PAsp(DET-GlcAm).

OligoRNA, OligoRNA, and 3'-DeoxyoligoRNA) (**Figure 4-6 (c)**). These results were consistent with the tolerability test against nuclease attacks shown in **Figure 4-5**, and indicated that cross-linking between GlcAm-OligoRNA and block copolymers was formed in PM core and suppressed polyion exchange reaction. Noteworthy, similarly to tolerability test against nucleases, the PMs prepared from PEG-PAsp(DET-FPBA_{49%}) and mRNA with 20*GlcAm-OligoRNA showed higher structural stability than the PMs prepared from unhybridized mRNA and the polymer mixture of PEG-PAsp(DET-FPBA) and PEG-PAsp(DET-GlcAm) (**Figure 4-6 (b)**). These results support an important role for the phenylboronate ester linkage in the stabilization of the complex.

4.3.4. pH- and ATP-responsiveness of mRNA/polymer cross-linked PMs

The pH-responsiveness of PMs was then assessed at pH 7.4 and 5.5, which are mimics of physiological and late endosomal/lysosomal pH. In response to pH drop, equilibrium shift of FPBA and subsequent cross-linking cleavage inside the PM core are expected to be occurred. At the same time, increasing protonation degree of aminoethylene units in the PAsp(DET) side chain triggered release of some PEG-PAsp(DET) from PM responding to pH decrease. Therefore, release of the block copolymers from the cross-linked PM is thought to be caused

Table 4-2. The number of block copolymers associating to mRNA at pH 7.4 and 5.5.

	Number of GlcAm-OligoRNA	pH 7.4	pH 5.5
PEG-PAsp(DET) PM	0	11	6
	20	18	11
Polymer/polymer Cross-linked PM	0	11(B)/7(G)	10(B)/6(G)
	0	22	18
	5	26	24
PEG-PAsp(DET/FPBA _{49%}) PM	10	29	26
	15	31	28
	20	34	31

in response to pH decrease. Then, block copolymer release from PM was evaluated by quantifying the amount of free block copolymers in supernatant after ultracentrifugation. It was confirmed that the block copolymers were certainly released from PM (**Table 4-2**). Note that, PEG-PAsp(DET-FPBA) was not released so as to conform to the stoichiometric charge ratio, probably because the hydrophobicity of FPBA at acidic pH conflicted with electrostatic repulsion and made the block copolymer tethering to PM.

The ATP responsiveness of PM was evaluated by observing the change in FRET efficiency under various concentrated ATP at pH 7.4. Regardless of the ATP concentration, the FRET efficiency of PMs composed of PEG-PAsp(DET) was kept in high efficiency by incubation in the presence of ATP (**Figure 4-7**). On the other hand, FRET efficiency of PMs prepared from PEG-PAsp(DET-FPBA) decreased depending on ATP concentration. These results indicated that ATP associated with FPBA moieties in PM core and triggered

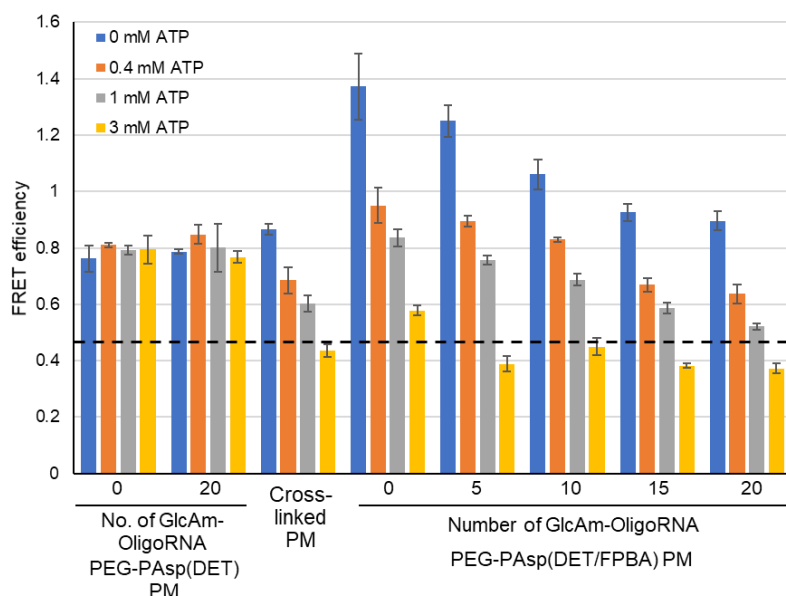


Figure 4-7. FRET efficiency of PMs loaded with Cy3/Cy5 double-labeled mRNA in 10 mM HEPES buffer containing 150 mM NaCl and various concentrated ATP (0, 0.4, 1, and 3 mM). Dotted line represented FRET efficiency of naked Cy3/Cy5 double-labeled mRNA without hybridization in 10 mM HEPES buffer containing 150 mM NaCl. Data were shown as means \pm SEM ($n = 3$).

decondensation of mRNA due to breaking charge balance in PM core.

4.3.5 Effect of mRNA/polymer cross-linking on mRNA expression and intracellular stability

Both improving tolerability of PM against nuclease degradation and polyion exchange reaction and providing pH- and ATP-responsiveness are expected to enhance mRNA transfection efficiency. Actually, increasing the number of GlcAm-OligoRNA hybridized with mRNA enhanced Gluc expression in HuH-7 cells (**Figure 4-8 (a)**). Especially, the Gluc expression of PMs prepared from PEG-PAsp(DET-FPBA) and mRNA hybridized with 20*GlcAm-OligoRNA was approximately 4-fold higher than that of PEG-PAsp(DET) PMs after 24 h of transfection. Interestingly, polymer/polymer cross-linked PM, which had less tolerability against nucleases and polyion exchange reaction comparing to mRNA/polymer cross-linked PMs shown in **Figure 4-5 (c)** and **4-6 (b)**, showed comparable Gluc expression efficiency to mRNA/polymer cross-linked PMs. In order to investigate transfection efficiency in detail, the degradation profile of transfected mRNA inside the cells was monitored by quantifying remained *Gluc* mRNA using qRT-PCR. The amount of remained mRNA encapsulated in PEG-PAsp(DET-FPBA) PM was increased in accordance to the number of GlcAm-OligoRNAs on mRNA as shown in **Figure 4-8 (c)**. In addition, polymer/polymer cross-linked PMs maintained more transfected mRNA inside the cells comparing to other unstable PMs, such as PEG-PAsp(DET) PMs. Probably, both nuclease resistance and block copolymer release during intracellular trafficking process, especially pH decrease in endosomes, resulted in the intracellular stability of mRNA loaded in PMs. The loss of some of block copolymers in PMs can accelerated mRNA decondensation, and may finally cause less tolerability against nuclease resistance. Actually, when incubated at pH 5.5, PMs composed of PEG-PAsp(DET)

showed both size increase and decrease of FRET efficiency, while other PMs kept these size and FRET efficiency (**Figure 4-14**). Consequently, the remaining amount of mRNA inside the cells was consistent with Gluc expression, indicating that intracellular life-time of mRNA was quite important factor to achieve efficient protein expression in cultured cells. Finally, in order

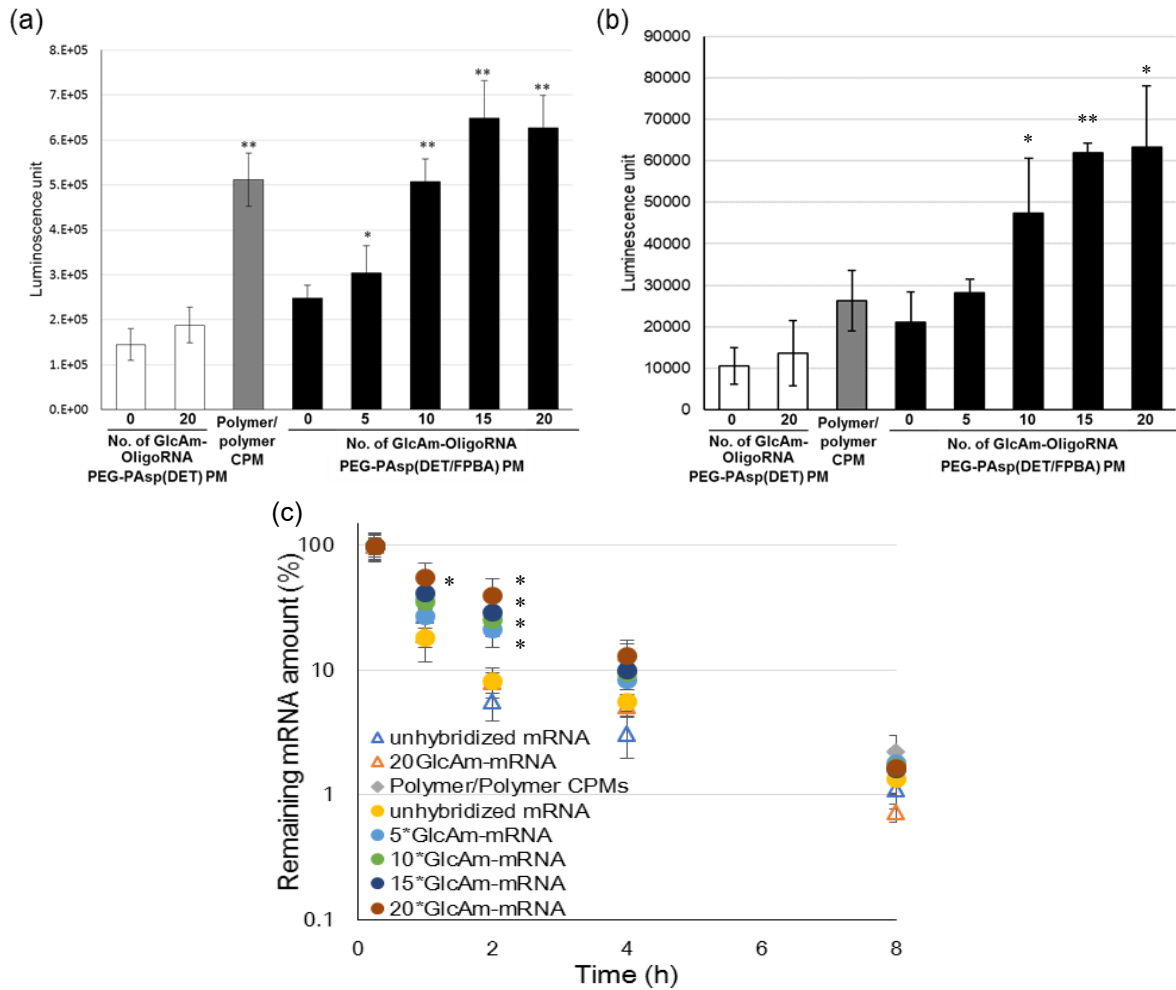


Figure 4-8. Transfection of mRNA loaded in PMs into HuH-7 cells. (a-b) Gluc expression efficiency of (a) PMs and (b) 5 min pre-incubated ones in 10% FBS solution after 24 h of transfection. Data were shown as means \pm SEM. ($n = 6$). (c) The amount of transfected mRNA loaded in PMs composed of (open triangle) PEG-PAsp(DET), (diamond) the mixture of PEG-PAsp(DET-FPBA) and PEG-PAsp(DET)/GlcAm, and (circle) PEG-PAsp(DET-FPBA). Data were shown as means \pm SEM. ($n = 3$). Abbreviation: Polymer/polymer CPM means PMs prepared from unhybridized mRNA and the mixture of PEG-PAsp(DET-FPBA) and PEG-PAsp(DET-GlcAm). Statistical difference to the PMs prepared from PEG-PAsp(DET) and unhybridized mRNA was analyzed by analysis of variance followed by Dunnett's test. ($*p < 0.05$)

to investigate the influence of PM tolerability on Gluc expression, PMs were pre-incubated in 10% FBS solution for 5 min. As shown in **Figure 4-8 (b)**, PMs prepared from PEG-PAsp(DET-FPBA) and mRNA hybridized with GlcAm-OligoRNA performed higher Gluc expression than polymer/polymer cross-linked PMs, suggesting that much mRNA was protected by mRNA/polymer cross-linking in 10% FBS solution and that nuclease resistance of PMs is necessary to get protein expression in harsh physiological condition.

4.4 Conclusion

In this Chapter, I attempted to modify mRNA for efficient mRNA delivery through hybridization of functionalized short OligoRNA. Hybridization of OligoRNA was thought to inhibit mRNA translational efficiency and to induce immunogenicity due to forming double strand RNA structure. However, by fine-tuning of the length of OligoRNA, I achieved to introduce OligoRNA with functional group without such side effects. Especially, hybridizing GlcAm-OligoRNA to mRNA, which increased the number of diol (polyol) structure on mRNA, allowed to efficiently form phenylboronate ester linkage with FPBA modified block copolymers, which could stabilize PM structure. Actually, the tolerability test of PMs against nuclease attacks and polyion exchange reaction demonstrated that formation of direct cross-linking between mRNA and block copolymers through phenylboronate ester linkage was more effective than cross-linking between block copolymers although the number of diol (polyol) moieties in PM loaded with GlcAm-mRNA was quite less than PMs with cross-linking between block copolymers in the core.

4.5 Appendix

4.5.1 List of OligoRNA sequences hybridizing to *Gluc* mRNA

Following OligoRNAs were used in each experiment.

Table 4-3 A. OligoRNAs used for optimizing the length of OligoRNA (Figure 4-2)

17 nt OligoRNA #2	5'-CUCGGCCACAGCGAUGC-3'
17 nt OligoRNA #6	5'-UCUUUGAGCACCUCAG-3'
17 nt OligoRNA #16	5'-GCGGCAGCCACUUCUUG-3'
17 nt OligoRNA #19	5'-CUCUAGAUGCAUGCUCG-3'
23 nt OligoRNA #2	5'-CUCGGCCACAGCGAUGCAGAUCA-3'
23 nt OligoRNA #6	5'-UCUUUGAGCACCUCAGCGGCAG-3'
23 nt OligoRNA #16	5'-GCGGCAGCCACUUCUUGAGCAGG-3'
23 nt OligoRNA #19	5'-CUCUAGAUGCAUGCUCGAGCGGC-3'
40 nt OligoRNA	5'-UCUUUGAGCACCUCAGCGGCAGCUUCUUGCCGGG CAACU-3'
60 nt OligoRNA	5'-UCUUUGAGCACCUCAGCGGCAGCUUCUUGCCGGG CAACUCCCCGCGGUCAGCAUCGAGA-3'
80 nt OligoRNA	5'-UCUUUGAGCACCUCAGCGGCAGCUUCUUGCCGGG CAACUCCCCGCGGUCAGCAUCGAGAUCCGUGGUCGCG AAGUUGCUGG-3'

Table 4-3 B. OligoRNAs used for evaluating gene silencing effect of OligoRNA (Figure 4-11)

OligoRNA (Luc)	5'-UCGAAGUACUCAGCGUAAG-3'
OligoRNA (Scr)	5'-ACGUGACACGUUCGGAGAA-3'
siRNA (Luc)	5'-CUUACGCUGAGUACUUCGAdTdT-3' (sense strand), 5'-UCGAAGUACUCAGCGUAAGdTdT-3' (antisense strand)
siRNA (Scr)	5' -UUCUCCGAACGUGUCACGUdTdT-3' (sense strand), 5'-ACGUGACACGUUCGGAGAAAdTdT-3' (antisense strand)

Table 4-3 C. GlcAm-OligoRNA used for stabilizing PM (Figure 3-8, Table 4-1)

GlcAm-OligoRNA #1	5'-(GlcAm)-AAAAACAGAACUUUGACUC-3'
GlcAm-OligoRNA #2	5'-(GlcAm)-AACUCGGCCACAGCGAUGC-3'
GlcAm-OligoRNA #3	5'-(GlcAm)-AAUUGAAGUCUUCGUUGUU-3'
GlcAm-OligoRNA #4	5'-(GlcAm)-AAGGUCGCGAAGUUGCUGG-3'
GlcAm-OligoRNA #5	5'-(GlcAm)-AAGGGCAACUCCCCGCGGU-3'
GlcAm-OligoRNA #6	5'-(GlcAm)-AAUCUUUGAGCACCUCAG-3'
GlcAm-OligoRNA #7	5'-(GlcAm)-AAGCAGCCAGCUUCCGGG-3'

GlcAm-OligoRNA #8	5'-(GlcAm)-UAGUGGGACAGGCAGAUCA-3'
GlcAm-OligoRNA #9	5'-(GlcAm)-AAGAUGAACUUCUUCAUCU-3'
GlcAm-OligoRNA #10	5'-(GlcAm)-AAACUCUUUGUCGCCUUCG-3'
GlcAm-OligoRNA #11	5'-(GlcAm)-AUAUCUCAGGAAUGUCGAC-3'
GlcAm-OligoRNA #12	5'-(GlcAm)-UUCUGCUCCAUGGGCUCCA-3'
GlcAm-OligoRNA #13	5'-(GlcAm)-AUCACACAGAUCGACCUGU-3'
GlcAm-OligoRNA #14	5'-(GlcAm)-AAUUGAGGCAGCCAGUUGU-3'
GlcAm-OligoRNA #15	5'-(GlcAm)-AAAGAACACUGCACGUUGG-3'
GlcAm-OligoRNA #16	5'-(GlcAm)-AAGCGGCAGCCACUUCUUG-3'
GlcAm-OligoRNA #17	5'-(GlcAm)-UACUUGCUGGCAAAGGUCG-3'
GlcAm-OligoRNA #18	5'-(GlcAm)-AAUGAUCUUGUCCACCUGG-3'
GlcAm-OligoRNA #19	5'-(GlcAm)-AACUCUAGAUGCAUGCUCG-3'
GlcAm-OligoRNA #20	5'-(GlcAm)-AAGAAUUCGAGCUCGGUAC-3'

Table 4-3 D. OligoRNA and 3'-DeoxyoligoRNA used for evaluating chemical structure of ends of OligoRNA (Figure 4-5, 4-6)

OligoRNA #1	5'-AAAAACAGAACUUUGACUC-3'
OligoRNA #2	5'-AACUCGGCCACAGCGAUGC-3'
OligoRNA #3	5'-AAUUGAAGUCUUCGUUGUU-3'
OligoRNA #4	5'-AAGGUCGCGAAGUUGCUGG-3'
OligoRNA #5	5'-AAGGGCAACUCCCCGCGGU-3'
OligoRNA #6	5'-AAUCUUUGAGCACCUCAG-3'
OligoRNA #7	5'-AAGCAGCCAGCUUCCGGG-3'
OligoRNA #8	5'-UAGUGGGACAGGCAGAUCA-3'
OligoRNA #9	5'-AAGAUGAACUUCUUCAUCU-3'
OligoRNA #10	5'-AAACUCUUUGUCGCCUUCG-3'
OligoRNA #11	5'-AUAUCUCAGGAAUGUCGAC-3'
OligoRNA #12	5'-UUCUGCUCCAUGGGCUCCA-3'
OligoRNA #13	5'-AUCACACAGAUCGACCUGU-3'
OligoRNA #14	5'-AAUUGAGGCAGCCAGUUGU-3'
OligoRNA #15	5'-AAAGAACACUGCACGUUGG-3'
OligoRNA #16	5'-AAGCGGCAGCCACUUCUUG-3'
OligoRNA #17	5'-UACUUGCUGGCAAAGGUCG-3'
OligoRNA #18	5'-AAUGAUCUUGUCCACCUGG-3'
OligoRNA #19	5'-AACUCUAGAUGCAUGCUCG-3'
OligoRNA #20	5'-AAGAAUUCGAGCUCGGUAC-3'
3'-DeoxyoligoRNA #1	5'-AAAAACAGAACUUUGACUdC-3'
3'-DeoxyoligoRNA #2	5'-AACUCGGCCACAGCGAUGdC-3'
3'-DeoxyoligoRNA #3	5'-AAUUGAAGUCUUCGUUGUdU-3'
3'-DeoxyoligoRNA #4	5'-AAGGUCGCGAAGUUGCUGdG-3'
3'-DeoxyoligoRNA #5	5'-AAGGGCAACUCCCCGCGGdU-3'
3'-DeoxyoligoRNA #6	5'-AAUCUUUGAGCACCUCAdG-3'
3'-DeoxyoligoRNA #7	5'-AAGCAGCCAGCUUCCGGdG-3'
3'-DeoxyoligoRNA #8	5'-UAGUGGGACAGGCAGAUcdA-3'

3'-DeoxyoligoRNA #9	5'-AAGAUGAACUUCUUCAUCdU-3'
3'-DeoxyoligoRNA #10	5'-AAACUCUUUGUCGCCUUCdG-3'
3'-DeoxyoligoRNA #11	5'-AUAUCUCAGGAAUGUCGAdC-3'
3'-DeoxyoligoRNA #12	5'-UUCUGCUCCAUGGGCUCdA-3'
3'-DeoxyoligoRNA #13	5'-AUCACACAGAUCGACCUGdU-3'
3'-DeoxyoligoRNA #14	5'-AAUUGAGGCAGCCAGUUGdU-3'
3'-DeoxyoligoRNA #15	5'-AAAGAACACUGCACGUUGdG-3'
3'-DeoxyoligoRNA #16	5'-AAGCGGCAGCCACUUCUdG-3'
3'-DeoxyoligoRNA #17	5'-UACUUGCUGGCAAAGGUCdG-3'
3'-DeoxyoligoRNA #18	5'-AAUGAUCUUGUCCACCUGdG-3'
3'-DeoxyoligoRNA #19	5'-AACUCUAGAUGCAUGCUCdG-3'
3'-DeoxyoligoRNA #20	5'-AAGAAUUCGAGCUCGGUAdC-3'

4.5.2 Calculation of melting temperature of double strand RNA

Melting temperature (T_m) of OligoRNA was calculated using parameters described in previous studies.¹⁸⁻¹⁹

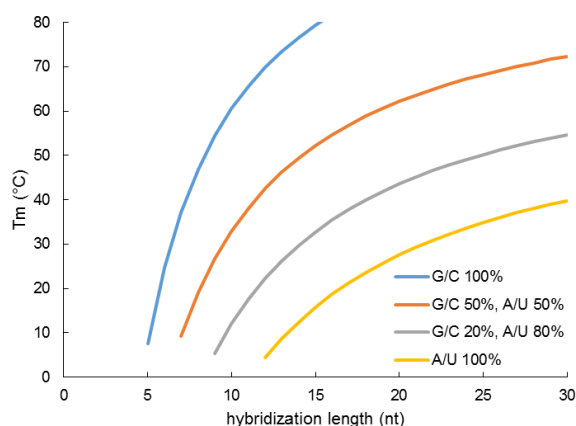


Figure 4-9. Calculated melting temperature (T_m) of double stranded RNA at the concentration of $0.5 \mu\text{M}$ in 150 mM NaCl condition. T_m of dsRNA with various ratios of G/C and A/U base pairs was plotted against hybridization lengths.

4.5.3 Confirmation of OligoRNA hybridization to mRNA

Hybridization efficiency of OligoRNA was evaluated through poly(acrylamide) gel electrophoresis. As shown in **Figure 4-10**, almost all OligoRNAs bound to mRNA in this hybridization protocol.

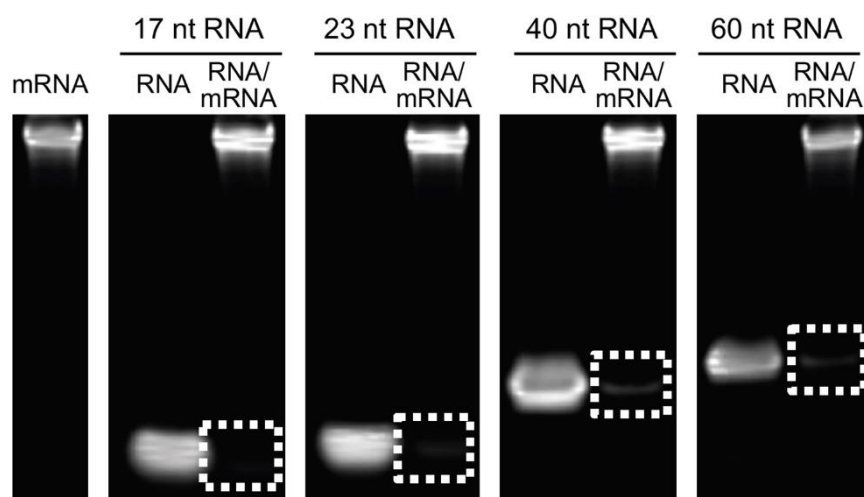


Figure 4-10. Electrophoregram of mRNA in poly(acrylamide) gel. Abbreviation: “mRNA” means unhybridized mRNA, “RNA” means OligoRNA without hybridization, and “RNA/mRNA” means mRNA hybridized with OligoRNA.

4.5.4 Gene silencing effect of OligoRNA

Gene silencing effect of OligoRNA was evaluated by transfecting into HeLa-Luc cells, which expresses luciferase constantly. HeLa-luc (5,000 cells/well) were seeded onto 96-well plates, and incubated for 24 h. After replacement of the cultured medium with 100 μ L of Opti-MEM, 19 nt OligoRNA and siRNA complexed with Lipofectamine RNAi MAX was added to

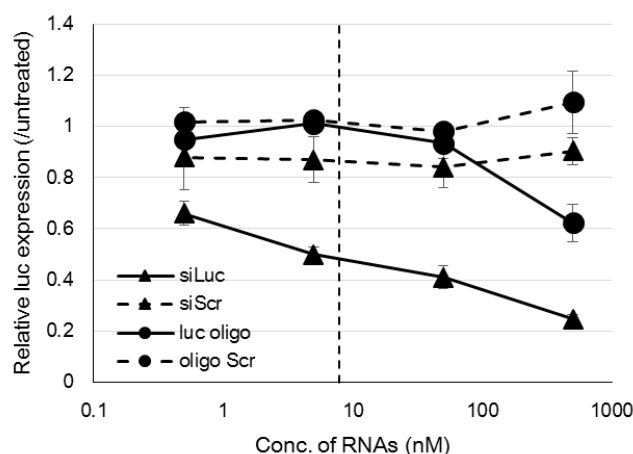


Figure 4-11. Gene silencing effect of OligoRNA (circle) and siRNA (triangle). Dotted line represents the OligoRNA concentration in mRNA transfection. Data were shown means \pm SEM. ($n = 5$).

each well. After 4 h of transfection, the Opti-MEM was exchanged for 100 μ L of DMEM, followed by 20 h of post-incubation. After washing cells by cold D-PBS twice, cells were lysed by 50 μ L of the Passive lysis buffer (Promega Co.). Luciferase expression in 20 μ L of the lysate was evaluated using Luciferase Assay System Kit (Promega Co.), and Luminometer Glomax 96. OligoRNA did not show gene silencing effect at the concentration in transfection after hybridization (8 nM).

4.5.5 Conjugation efficiency of GlcAm moiety with NH₂-OligoRNA

Conjugation efficiency of GlcAm moiety with NH₂-OligoRNA was evaluated fluorescamine method. After purification of GlcAm-OligoRNA, 3 μ L of fluorescamine solution in DMSO was mixed with 9 μ L of GlcAm-OligoRNA solution. After 15 min incubation at 25 °C, fluorescence intensity of each sample was measured using NanoDrop ND-3300 at a wavelength of 495 nm. The concentration of amine groups on NH₂-OligoRNA was determined from the calibration curve of unreacted NH₂-OligoRNA solution. From the calculation, over 91% of amine group was reacted with GlcAm molecule.

Figure 4-4. Conjugation ratio of GlcAm moieties with NH₂-OligoRNA

Introduction ratio of GlcAm to NH ₂ -OligoRNA (%)									
#1	#2	#3	#4	#5	#6	#7	#8	#9	#10
96	93	97	98	96	93	96	96	94	99
Introduction ratio of GlcAm to NH ₂ -OligoRNA									
#11	#12	#13	#14	#15	#16	#17	#18	#19	#20
92	97	95	92	95	91	97	97	92	95

4.5.6 Comparing the nuclease resistance of PMs encapsulating mRNA hybridized with FPBA-OligoRNA or GlcAm-OligoRNA

Two type of PM design forming phenylboronate ester linkage between mRNA and block copolymers can be considered; one is PM prepared from PEG-PAsp(DET-FPBA) and mRNA hybridized with GlcAm-OligoRNA and the other is PM prepared from PEG-PAsp(DET-GlcAm) and mRNA with FPBA-OligoRNA. Thus, these chemical structures were optimized by evaluating the tolerability of PMs in 10% FBS solution. In the experiment, mRNA hybridized with 5 number of each OligoRNA was prepared. As shown in **Figure 4-13**, PMs prepared from PEG-PAsp(DET-FPBA_{49%}) and 5*GlcAm-mRNA showed improvement of nuclease resistance comparing with other PMs. Therefore, PMs prepared from PEG-PAsp(DET-FPBA) and GlcAm-mRNA were used in other experiments.

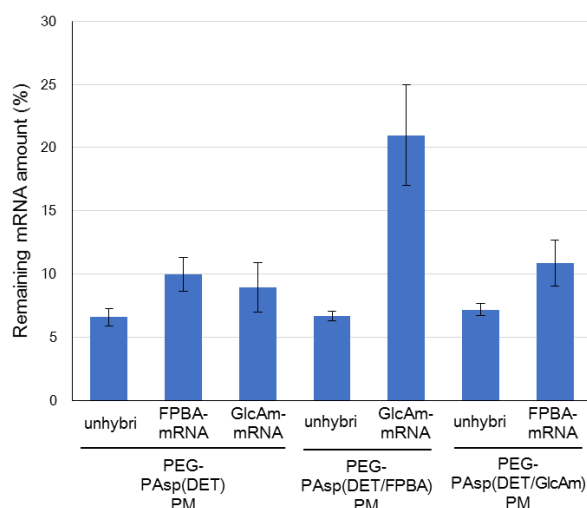


Figure 4-12. The amount of remaining mRNA loaded in PM after 15 min incubation in 10% FBS solution. Five number of FPBA-OligoRNA or GlcAm-OligoRNA were hybridized with mRNA. Abbreviation: unhybri means unhybridized mRNA. Data were shown means \pm SEM. ($n = 4$).

4.5.7 FRET efficiency of mRNA loaded in PMs incubated in 10% FBS and RNase inhibitor

PEG-PAsp(DET) PM solution was diluted 10 mM HEPES buffer with 150 mM NaCl or that containing 10% FBS. To avoid degradation, RNase inhibitor (RNasin (Promega)) was

added to both PM solutions according to manufactures' protocol. The fluorescence intensity was measured by the same method described in Materials and Methods section. The FRET efficiency of PMs in 10% FBS solution was comparable to that in HEPES buffer, indicating that mRNA was degraded by nucleases before PM dissociation.

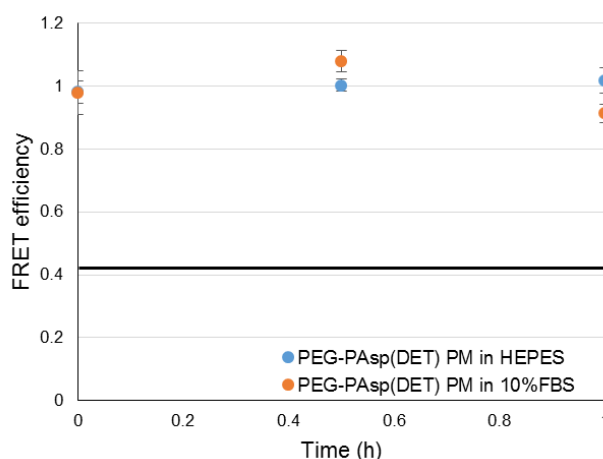


Figure 4-13. FRET efficiency of PEG-PAsp(DET) PMs incubated in 10 mM HEPES buffer with or without 10% FBS containing RNase inhibitor. Solid line represents the FRET efficiency of Cy3/Cy5 double-labeled mRNA in 10 mM HEPES buffer containing 150 mM NaCl. Data were shown means \pm SEM. ($n = 3$).

4.5.8 DLS measurement of PMs loaded with mRNA hybridized with OligoRNA or 3'-deoxyOligoRNA

DLS measurement was performed with the same protocol described in Materials and Methods section. All PMs showed 45-50 nm cumulant diameter, which was comparable to PMs loaded with unhybridized or GlcAm-OligoRNA hybridized mRNA.

Table 4-5. Cumulant diameter and polydispersity index of PMs evaluated by DLS measurement at 25 °C in 10 mM HEPES buffer (pH 7.4)

	Size (d. nm)/ PDI			
	The number of OligoRNA			
	5	10	15	20
OligoRNA	50/0.23	47/0.21	45/0.16	49/0.17
3'-DeoxyoligoRNA	46/0.15	46/0.10	46/0.12	48/0.16

4.5.9 pH-dependent change of PM structure

To make PMs experience intracellular trafficking process, PMs were incubated at pH 5.5, followed by conducting FRET measurement. PMs were incubated in 10 mM HEPES buffer at pH 7.4 or 10 mM acetate buffer at pH 5.5 containing 150 mM NaCl, respectively. Then buffer solution was exchanged to 10 mM HEPES buffer containing 150 mM NaCl at pH 7.4 using a VIVASPIN 500 (MWCO: 30 kDa) (Sartorius Stedim Biotech, Goettingen, Germany). FRET measurement was performed in the PM solutions. FRET efficiency decrease was observed in only PEG-PAsp(DET) PMs probably because PEG-PAsp(DET) PMs lost approximately half block copolymers binding to mRNA in response to pH drop (**Table 4-2**). Therefore, PEG-PAsp(DET) PMs showed swelled structure after experiencing pH change mimicking intracellular trafficking.

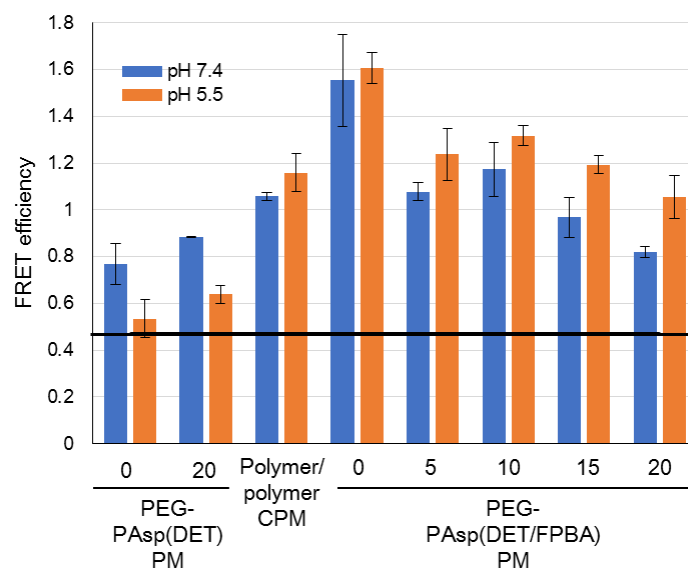


Figure 4-14. FRET efficiency of PMs after experiencing pH modulation of intracellular trafficking process. Solid line represents the FRET efficiency of Cy3/Cy5 double-labeled mRNA in 10 mM HEPES buffer containing 150 mM NaCl. Data were shown means \pm SEM. ($n = 3$).

4-6 References

1. Uchida, S.; Kinoh, H.; Ishii, T.; Matsui, A.; Tockary, T. A.; Takeda, K. M.; Uchida, H.; Osada, K.; Itaka, K.; Kataoka, K., Systemic delivery of messenger RNA for the treatment of pancreatic cancer using polyplex nanomicelles with a cholesterol moiety, *Biomaterials* **2016**, 82, 221-228.
2. Hajj, K. A.; Whitehead, K. A., Tools for translation: non-viral materials for therapeutic mRNA delivery, *Nat. Rev. Mat.* **2017**, 2.
3. Fenton, O. S.; Kauffman, K. J.; Kaczmarek, J. C.; McClellan, R. L.; Jhunjunwala, S.; Tibbitt, M. W.; Zeng, M. D.; Appel, E. A.; Dorkin, J. R.; Mir, F. F.; Yang, J. H.; Oberli, M. A.; Heartlein, M. W.; DeRosa, F.; Langer, R.; Anderson, D. G., Synthesis and Biological Evaluation of Ionizable Lipid Materials for the In Vivo Delivery of Messenger RNA to B Lymphocytes, *Advanced materials (Deerfield Beach, Fla.)* **2017**, 29.
4. McKinlay, C. J.; Vargas, J. R.; Blake, T. R.; Hardy, J. W.; Kanada, M.; Contag, C. H.; Wender, P. A.; Waymouth, R. M., Charge-altering releasable transporters (CARTs) for the delivery and release of mRNA in living animals, *Proc. Natl. Acad. Sci. U S A* **2017**, 114, E448-E456.
5. Tanaka, H.; Nakatani, T.; Furihata, T.; Tange, K.; Nakai, Y.; Yoshioka, H.; Harashima, H.; Akita, H., In Vivo Introduction of mRNA Encapsulated in Lipid Nanoparticles to Brain Neuronal Cells and Astrocytes via Intracerebroventricular Administration, *Mol. Pharm.* **2018**, 15, 2060-2067.
6. Uchida, H.; Itaka, K.; Nomoto, T.; Ishii, T.; Suma, T.; Ikegami, M.; Miyata, K.; Oba, M.; Nishiyama, N.; Kataoka, K., Modulated protonation of side chain aminoethylene repeats in Nsubstituted polyaspartamides promotes mRNA transfection, *J. Am. Chem. Soc.* **2014**, 136, 12396-12405.
7. Uchida, H.; Itaka, K.; Uchida, S.; Ishii, T.; Suma, T.; Miyata, K.; Oba, M.; Nishiyama, N.;

Kataoka, K., Synthetic Polyamines to Regulate mRNA Translation through the Preservative Binding of Eukaryotic Initiation Factor 4E to the Cap Structure, *J. Am. Chem. Soc.* **2016**, 138, 1478-1481.

8. Li, J.; Wang, W.; He, Y.; Li, Y.; Yan, E. Z.; Zhang, K.; Irvine, D. J.; Hammond, P. T., Structurally Programmed Assembly of Translation Initiation Nanoplex for Superior mRNA Delivery, *ACS Nano* **2017**, 11, 2531-2544.

9. Kariko, K.; Buckstein, M.; Ni, H.; Weissman, D., Suppression of RNA recognition by Toll-like receptors: the impact of nucleoside modification and the evolutionary origin of RNA, *Immunity* **2005**, 23, 165-175.

10. Kormann, M. S.; Hasenpusch, G.; Aneja, M. K.; Nica, G.; Flemmer, A. W.; Herber-Jonat, S.; Huppmann, M.; Mays, L. E.; Illenyi, M.; Schams, A.; Griesse, M.; Bittmann, I.; Handgretinger, R.; Hartl, D.; Rosenecker, J.; Rudolph, C., Expression of therapeutic proteins after delivery of chemically modified mRNA in mice, *Nat. Biotechnol.* **2011**, 29, 154-157.

11. Chu, C. Y.; Rana, T. M., Potent RNAi by short RNA triggers, *RNA* **2008**, 14, 1714-1719.

12. Kato, H.; Takeuchi, O.; Mikamo-Satoh, E.; Hirai, R.; Kawai, T.; Matsushita, K.; Hiiragi, A.; Dermody, T. S.; Fujita, T.; Akira, S., Length-dependent recognition of double-stranded ribonucleic acids by retinoic acid-inducible gene-I and melanoma differentiation-associated gene 5, *J. Exp. Med.* **2008**, 205, 1601-10.

13. Botos, I.; Liu, L.; Wang, Y.; Segal, D. M.; Davies, D. R., The toll-like receptor 3:dsRNA signaling complex, *Biochim. Biophys. Acta* **2009**, 1789, 667-674.

14. Schlee, M.; Roth, A.; Hornung, V.; Hagmann, C. A.; Wimmenauer, V.; Barchet, W.; Coch, C.; Janke, M.; Mihailovic, A.; Wardle, G.; Juranek, S.; Kato, H.; Kawai, T.; Poeck, H.; Fitzgerald, K. A.; Takeuchi, O.; Akira, S.; Tuschl, T.; Latz, E.; Ludwig, J.; Hartmann, G.,

Recognition of 5' triphosphate by RIG-I helicase requires short blunt double-stranded RNA as contained in panhandle of negative-strand virus, *Immunity* **2009**, 31, 25-34.

15. Binder, M.; Eberle, F.; Seitz, S.; Mucke, N.; Huber, C. M.; Kiani, N.; Kaderali, L.; Lohmann, V.; Dalpke, A.; Bartenschlager, R., Molecular mechanism of signal perception and integration by the innate immune sensor retinoic acid-inducible gene-I (RIG-I), *J. Biol. Chem.* **2011**, 286, 27278-27287.

16. Kato, Y.; Sato, K.; Asai, K.; Akutsu, T., Rtips: fast and accurate tools for RNA 2D structure prediction using integer programming, *Nucleic. Acids. Res.* **2012**, 40 (Web Server issue), W29-34.

17. Cui, W. Y.; Zhao, S.; Polanowska-Grabowska, R.; Wang, J.; Wei, J.; Dash, B.; Chang, S. L.; Saucerman, J. J.; Gu, J.; Li, M. D., Identification and characterization of poly(I:C)-induced molecular responses attenuated by nicotine in mouse macrophages, *Mol. Pharmacol.* **2013**, 83, 61-72.

18. Freier, S. M.; Kierzek, R.; Jaeger, J. A.; Sugimoto, N.; Caruthers, M. H.; Neilson, T.; Turner, D. H., Improved free-energy parameters for predictions of RNA duplex stability, *Proc. Natl. Acad. Sci. U S A* **1986**, 83, 9373-9377.

19. Chen, Z.; Znosko, B. M., Effect of sodium ions on RNA duplex stability, *Biochemistry* **2013**, 52, 7477-7485.

20. Li, S.; Tseng, W. C.; Stolz, D. B.; Wu, S. P.; Watkins, S. C.; Huang, L., Dynamic changes in the characteristics of cationic lipidic vectors after exposure to mouse serum: implications for intravenous lipofection, *Gene Ther.* **1999**, 6, 585-594.

21. Burke, R. S.; Pun, S. H., Extracellular barriers to in Vivo PEI and PEGylated PEI polyplexmediated gene delivery to the liver, *Bioconjug. Chem.* **2008**, 19, 693-704.

22. Zuckerman, J. E.; Choi, C. H.; Han, H.; Davis, M. E., Polycation-siRNA nanoparticles can disassemble at the kidney glomerular basement membrane, *Proc. Natl. Acad. Sci. U S A* **2012**, 109, 3137-3142.
23. Sanders, N.; Rudolph, C.; Braeckmans, K.; De Smedt, S. C.; Demeester, J., Extracellular barriers in respiratory gene therapy, *Adv. Drug. Deliv. Rev.* **2009**, 61, 115-127.

Chapter 5

Promotion of mRNA condensation in polyplex micelle core through hybridization of cholesteryl RNA oligonucleotides to get synergetic effect with phenylboronate ester cross-linking

5.1 Introduction

Chapter 3 and 4 demonstrated the utility of introducing phenylboronate ester linkage in polyplex micelle (PM) core and anchoring block copolymers on messenger RNA (mRNA) through covalent bond for efficient mRNA delivery. Especially, combination of introduction of phenylboronate ester cross-linking and installation of cholesterol (Chol) moieties in PM (PBA cross-linked Chol-PMs) dramatically improved PM-loading mRNA nuclease resistance, which is believed to be an important factor in mRNA delivery. Therefore, enhancing the interaction between mRNA and block copolymers in PBA cross-linked Chol-PMs except electrostatic interaction is expected to more improve the tolerability of PMs.

Herein, I designed 5' end Chol installed OligoRNA (Chol-OligoRNA) and combined two strategies; phenylboronate ester cross-linking and anchoring block copolymers on mRNA.

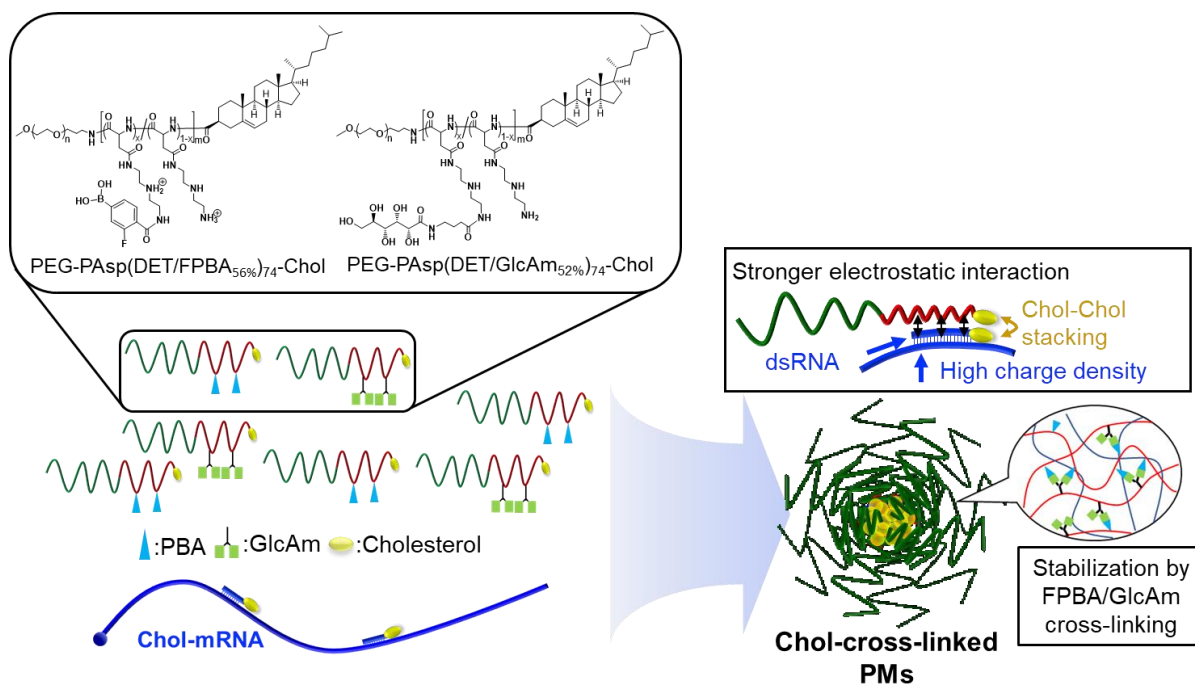


Figure 5-1. Schematic illustration of PBA cross-linked Chol-PMs. PBA cross-linked Chol-PMs were prepared from mRNA with Chol-OligoRNA and block copolymer mixture of PEG-PAsp(DET-FPBA)-Chol and PEG-PAsp(DET-GlcAm)-Chol. FPBA/GlcAm cross-linking formed in the highly concentrated PM core, and hydrophobic interaction between cholesterol moieties on mRNA and block copolymers accelerated PM core condensation.

In this design, PM structure is expected to be stabilized by not only phenylboronate ester cross-linking between block copolymers but also hydrophobic interaction between Chol-OligoRNA and Chol moiety on block copolymers (**Figure 5-1**). Firstly, the effect of hydrophobic interaction between cholesterol moieties on Chol-OligoRNA and block copolymers was confirmed by using PMs prepared from PEG-PAsp(DET)-Chol and Chol-OligoRNA hybridized mRNA (Chol-mRNA). Interestingly, a few Chol-OligoRNA hybridization enhanced PM core condensation status and improved nuclease resistance of mRNA, indicating that Chol-OligoRNA behaved as a node and that Chol installed block copolymers was gathered on the Chol-OligoRNA. Then, the system was combined with phenylboronate ester cross-linking (PBA cross-linked Chol-PMs with Chol-mRNA). The PMs showed high tolerability and proper ATP-responsiveness after Chol-Oligo hybridization. Eventually, PBA cross-linked Chol-PMs with Chol-mRNA performed approximately 20-fold higher protein expression comparing to PMs without any modification.

5.2 Materials and Methods

5.2.1 Materials

All block copolymers were synthesized according to the previous chapters. Agarose L03 TAKARA and Sybr green II were purchased from TAKARA Bio Inc. Cell culture medium was prepared similarly to previous chapters. Human Hepatocarcinoma cells (HuH-7) was obtained from RIKEN Cell Bank (Tsukuba, Japan). Renilla Luciferase Assay System Kit was purchased from Promega Co. (Madison, WI). Isoflurane was purchased from Pfizer Japan Inc. (Tokyo, Japan). mRNA was prepared using mMESSAGE mMACHINE T7 Ultra Kit according to Chapter 3. 10% TBE poly(acrylamide) gel was purchased from Thermo Fisher Scientific Inc.

(Waltham, MA). The 96-well, 48-well, 24-well and 12-well plates were purchased from Becton Dickinson (Franklin Lakes, NJ).

5.2.2 Animals

BALB/c mice were purchased from Charles River Laboratories Japan Inc. (Kanagawa, Japan). All animal experiments were conducted according to the approval of the Animal Care and Use Committee of the Innovation Center of NanoMedicine, Kawasaki Institute of Industrial Promotion (Kanagawa, Japan).

5.2.3 Hybridization of OligoRNA into mRNA

All of OligoRNAs were purchased from Hokkaido System Science Co. Ltd. (Hokkaido, Japan). The potentially forming secondary structure sequences in *Gluc* mRNA estimated by IPknot software¹ was avoided to be chose as target sequences where OligoRNAs can bind. Sequences of OligoRNAs are in **Table 5-2**. In all experiments, #5 OligoRNA was used for 1*OligoRNA, #1, #3, #5, #7, #10 OligoRNAs were used for 5*OligoRNA, and #1, #2, #3, #4, #5, #6, #7, #8, #10 OligoRNAs were for 9*OligoRNA.

Hybridization was conducted by the same procedure described in Chapter 4. The amount of hybridized OligoRNAs was determined through 10% TBE poly(acrylamide) gel electrophoresis. The migration of RNA in the poly(acrylamide) gel was imaged by Sybr Green II staining. Images were captured using PharosFXTM System.

5.2.4 Cell culturing

Cells were cultured in prepared DMEM in a humidified atmosphere with 5% CO₂ at

37 °C, unless specifically described.

5.2.5 Synthesis of block copolymers and preparation polyplex micelles

All of block copolymers were synthesized according to the procedure described in Materials and Methods section of Chapter 3. ^1H -NMR spectra showed the degree of polymerization of PAsp(DET) segment to be 70 and 63 for PEG-PAsp(DET) and PEG-PAsp(DET)-Chol by ^1H -NMR analyses (400 MHz, JEOL ECS-400), respectively. Cholesterol conjugation efficiency was also determined to be 98%. FPBA and GlcAm moieties were installed into the PAsp(DET) side chain, respectively. The introduction ratio of FPBA and GlcAm moieties was determined by ^1H -NMR.

PMs were prepared from these synthesized block copolymers and mRNA. One-unit volume block copolymer solution was mixed with 2-unit volume mRNA solution at a residual charge ratio ($(\text{N}^+ - \text{B}^-)/\text{P}$ ratio) of 1.5 (Details described in Chapter 3).

5.2.6 Characterization of PMs

ζ -potential of PMs at 25 °C in 10 mM HEPES buffer was measured through laser-doppler electrophoresis using Möbius ζ^{TM} (Wyatt Technology Corporation, CA) equipped with 532 nm laser. The ζ -potential of PMs was calculated based on the Smoluchowski's equation. The hydrodynamic diameter was estimated by DLS measurement in 10 mM HEPES buffer using an Ar laser ($\lambda = 532$ nm) with scattering angle of 173° at 25 °C (Zetasizer Nano-ZS) with cumulant method.

5.2.7 Nuclease resistance of mRNA loaded in PMs

PM solutions containing 100 ng of *Gluc* mRNA were incubated in 10% FBS solution at 37 °C for 15 min. From these samples, mRNA was immediately purified using RNeasy Mini Kit. After reverse transcription by ReverTra Ace qPCR RT Master Mix kit, the amount of intact mRNA was quantified by qRT-PCR analysis using a couple of primers for *Gluc* mRNA (Reverse sequence; GTCAGAACACTGCACGTTGG, and Forward sequence; TGAGATTCCTGGGTTCAAGG) and MicPCR.

5.2.8 Stability of PMs against exchange reaction with competitive anionic macromolecules

PM solutions containing 500 ng of mRNA were mixed with DS at various A/P ratios in the 10 mM HEPES with 150 mM NaCl (Details described in previous Chapters). For 1 h incubation at 37 °C, the PM solution (20 µL) containing 5% glycerol was electrophoresed for 30 min at 100 V in TAE buffer. The migration of mRNA in the agarose gel was imaged by 0.5 mg/L of EtBr staining. Images were taken by using PharosFX™ System.

5.2.9 Förster resonance energy transfer (FRET) measurement

PMs were prepared from Cy3/Cy5 double-labeled mRNA as described above. PM solution was incubated for 1 h in the various concentrated ATP solution (0, 0.3, 1, and 3 mM), where mRNA concentration was 12.5 µg/mL. After incubation, the fluorescence intensity was obtained by Tecan Microplate Reader Infinite M1000 Pro at 488 nm wavelength for excitation, and 570 nm and 672 nm for Cy3 and Cy5 for emission, respectively. FRET efficiency of all samples was calculated by following equation.

$$\text{FRET efficiency} = (\text{Cy5 intensity (672 nm)}) / (\text{Cy3 intensity (570 nm)})$$

5.2.10 Longitudinal relaxation time measurement

PM solution were purified using a 30 kDa MWCO Amicon Ultra-0.5 (Millipore, Billerica, MA) to remove free block copolymers and to replace buffer solution with D₂O containing 160 mM NaCl. The final concentration of RNA was set to 166.7 µg/mL. The longitudinal relaxation time (T_1) of block copolymer was measured by the inversion-recovery method using a double-pulse sequence at several delay time between 180° pulse and 90° pulse (0.1, 0.2, 5, 1, 2, and 10 s) at 25 °C (Accumulation = 128). The T_1 values were calculated by single-exponential fitting.

5.2.11 ATP-responsiveness of PMs

PMs loaded with Cy3-labeled mRNA (final mRNA conc.: 25 µg/mL) were incubated with various concentration of ATP (0, 0.4 and 3 mM) and non-labeled competitive *Gluc* mRNA (500 µg/mL) in 10 mM HEPES containing 150 mM NaCl for 2 h at 37 °C. After incubation, migration of mRNA was observed through gel electrophoresis using the same procedure described in the preceding section.

5.2.12 Transfection efficiency of PMs in cultured cells

HuH-7 cells (10,000 cells/well) were seeded onto 48-well plates, and incubated for 24 h. After replacement of DMEM with 200 µL of fresh one, 15 µL of PM solution containing 500 ng of mRNA was transfected. 10 µL of supernatant of culture medium was evaluated using Renilla Luciferase Assay Kit and Luminometer Glomax 96 at several time points.

5.2.13 Intracellular stability of transfected mRNA

HuH-7 cells (20,000 cells/well) were seeded on 24-well plate, and incubated for 24 h. After removing DMEM, cells were washed by cold D-PBS twice, followed by directly adding PM solution containing 1 μ g of mRNA in 10 mM HEPES with 150 mM NaCl. After 15 min post-incubation, PMs were completely washed out by D-PBS. Then, each well was filled by 400 μ L of fresh DMEM. At the several time points from transfection, cells were lysed by RLT buffer in RNeasy kit containing 1% 2-mercaptethanol. The remaining mRNA was extracted and quantified by the same protocol described above. The amount of mRNA after 15 min PM treatment was considered as 100% in each sample.

5.2.14 Intratracheal administration of mRNA to mouse lung

PMs, mRNA complexed with Lipofectamine LTX or *l*-PEI (*in vivo* jet PEI, Polyplus transfection, Illkirch, France) was prepared. Balb/c mice (6-week old, female) was fed for 1 week before the experiment. After tracheotomy under anesthesia by isoflurane inhalation, by using microspray (Model IA-1C-R, Penn Century, Philadelphia, PA), 50 μ L of sample solution containing 1.67 μ g of mRNA was administered. The lung was excised after 24 h of administration and then homogenized in 500 μ L of lysis buffer using Multibeads Shocker (Yasui Kikai Co., Osaka, Japan). Gluc expression in 10 μ L of the homogenate was evaluated using Renilla luciferase Assay System Kit and Lumat LB 9507 (Berthold Technologies).

To measure remaining amount of administered *Gluc* mRNA and inflammatory transcripts, mouse lung was excised after 4 h of administration. The excised lungs were homogenized in 500 μ L of RLT buffer in RNeasy Mini Kit containing 1% 2-mercaptoethanol using Multibeads Shocker. Then, RNA in the homogenate was purified using RNeasy Mini Kit. After reverse transcription of extracted RNA, qRT-PCR analysis with the same protocol as

described above.

5.2.15 Structural stability of PMs in blood circulation of mouse

PM solution (200 μ L) in 10 mM HEPES buffer (pH 7.4) with 150 mM NaCl containing 20 μ g of mRNA was administrated to BALB/c mouse (female, 7 weeks old, Charles River Laboratories Japan Inc., Kanagawa, Japan) from tail vein. After 2.5, 5, 10 min of administration, 2 μ L of blood was collected from tail vein and immediately mixed with 350 μ L 1% 2-mercaptoethanol containing RLT buffer in RNeasy kit. The mixture was diluted by 350-times using the same buffer, and the diluted solution was incubated at 37 °C for 2 h. After the incubation, mRNA was purified using RNeasy MiNI Kit, followed by reverse transcription of mRNA using ReverTra Ace qPCR RT Master Mix Kit. Then, qRT-PCR analysis was performed by SYBR green intercalator method using a primer pair for GLuc mRNA (Forward; TGCAAAAGATCCTCAACGTG, and Reverse; AATGGGAAGTCACGAAGGTG) and ABI Prism 7500 Sequence Detector (Applied Biosystems, Foster City, CA).

5.3 Results and Discussion

5.3.1 Preparation and characterization of PMs loaded with Chol-OligoRNA hybridized mRNA

The sequences of Chol-OligoRNAs were designed from 5' end to 3' end of mRNA except poly A tail (**Figure 5-2 (a)**). It should be noted that the hybridization positions avoided the secondary structure in Gluc mRNA itself as much as possible. I attempted to improve the nuclease tolerability of PMs prepared from mRNA hybridized with Chol-OligoRNA. Chol-RNA oligonucleotide having a mismatch sequence between hybridizing sequence and cholesterol group (overhang sequence) was also designed because the distance of cholesterol

group from mRNA main chain was considered as an important factor for enhancement of PM core condensation (**Figure 5-2 (b)**). To form PMs, PEG-PAsp(DET) solution was mixed with mRNA solution at N^+/P ratio of 1.5. The physicochemical values of each PM were summarized in **Table 5-3**. There was no remarkable difference of all prepared PMs. To evaluate the nuclease tolerability of PMs, the amount of remaining mRNA after incubation in 10% FBS solution at 37 °C for 15 min was quantified through qRT-PCR. Among Chol-OligoRNAs having a length of 0 to 5 nt overhang sequence between the Chol group and the complementary region, Chol-OligoRNA with 2 nt overhang has a tendency to improve nuclease resistance compared with those with 5 nt overhang and without overhang (**Figure 5-2 (c)**). From these results, Chol-OligoRNA with 2 nt overhang was used in the following experiments. The cholesterol group modification of block copolymers significantly improved the tolerability against nucleases comparing to PMs prepared from PEG-PAsp(DET) (**Figure 5-2 (d)**). Furthermore, the combination uses of PEG-PAsp(DET)-Chol and Chol-mRNA showed 2-fold more remaining mRNA than PMs loaded with unhybridized mRNA even though just one Chol-OligoRNA was hybridized with mRNA. Note that, no improvement of the tolerability against FBS was observed by adding uncomplimentary Chol-RNA oligonucleotide or unmodified RNA oligonucleotide. Therefore, it was preferable that the Chol-RNA oligonucleotide hybridization to mRNA was important to provide PM with high tolerability against FBS including nuclease. Increasing the number of Chol-OligoRNA on mRNA was expected to further improve the nuclease tolerability of PMs. Actually, the tolerability of PMs against FBS was improved with increasing the number of Chol-RNA oligonucleotides increased, and especially PMs prepared from mRNA hybridized with 9*Chol-RNA oligonucleotides showed 4-fold higher tolerability than PMs prepared from unhybridized mRNA (**Figure 5-2 (e)**). Note that, fluorescence

correlation spectroscopy (FCS) measurement confirmed that the diffusion coefficient of Chol-mRNA was slightly larger than that of unhybridized mRNA (**Figure 5-10**). These results indicated that Chol-mRNA formed smaller structure than unhybridized mRNA and that cholesterol installation into mRNA induced arrangement of mRNA structure. Also, FCS measurements showed no intermolecular interaction between Chol-mRNAs even after 9 Chol-OligoRNA hybridization.

An exchange reaction between polyanionic compounds and mRNA is one of the main

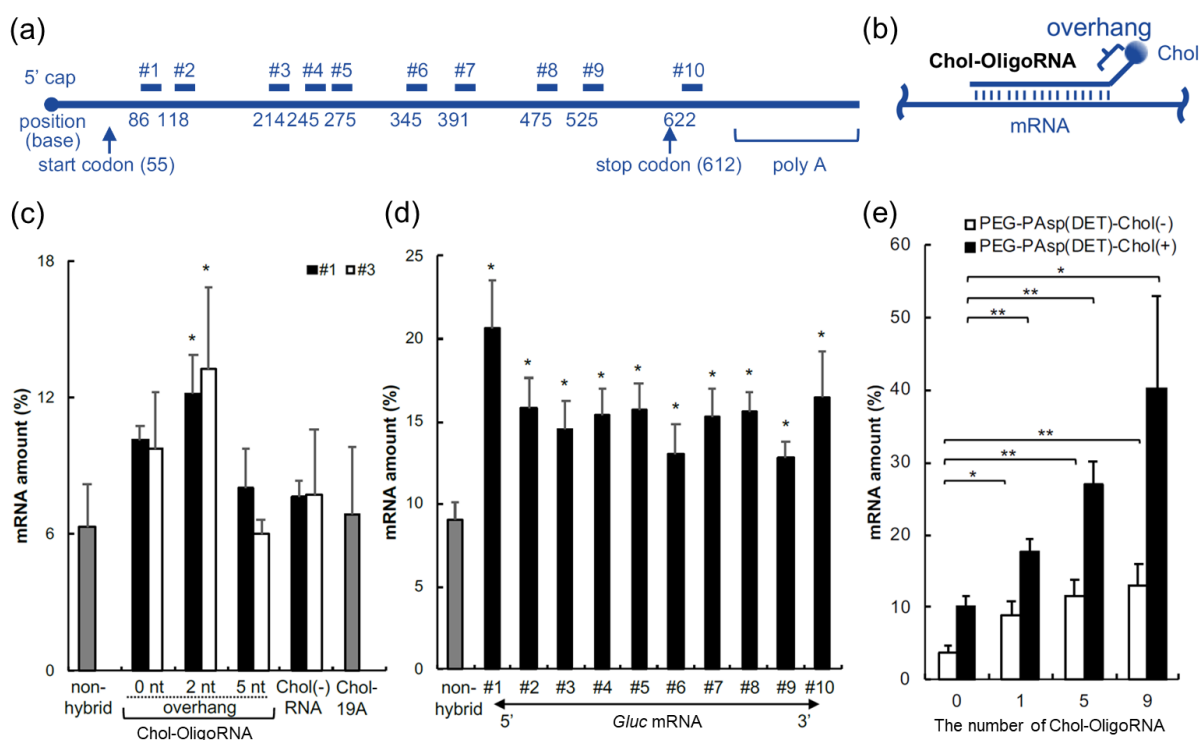


Figure 5-2. Tolerability test of PMs against nucleases. (a) The location of OligoRNA sequences on Gluc encoding mRNA. (b) Schematic illustration of Chol-OligoRNA with several mismatch sequence as overhang structure. (c)-(e) The amount of remaining mRNA in PMs after incubation in 10% FBS solution. (c) Comparing PMs loading mRNA hybridized with Chol-OligoRNA (closed bar: #1, open bar: #3) with different overhang length. (d) Influence of the location of Chol-OligoRNA on mRNA. (e) The number effect of Chol-OligoRNA on nuclease resistance. Abbreviation: non-hybrid means PMs loading unhybridized mRNA. Data were shown as mean \pm SEM ($n = 3$ for (c), 10 for (d), and 6 for (e)). Statistical difference to the “non-hybrid” group was analyzed by analysis of variance followed by Dunnett’s tests. * $p < 0.05$, ** $p < 0.01$.

barriers to disrupt PMs in physiological condition, such as glycosaminoglycan. Thus, the tolerability of PMs against polyion exchange reaction, *i.e.* dextran sulfate, was examined through gel electrophoresis. Electrophoregrams in **Figure 5-3** revealed that the migration of mRNA from PMs induced by the addition of DS at A/P ratio of 6. Obviously, mRNA release was suppressed in accordance with the number of Chol-OligoRNA, indicating that hydrophobic interaction between mRNA block copolymers stabilized PM structure against polyion exchange reaction.

The installation of cholesterol moieties into PMs might affect the PM core condensation. To tackle this issue, FRET efficiency of Cy3/Cy5 double-labeled mRNA was evaluated for estimating mRNA condensation status. Loading double-labeled mRNA into PM induced increase of FRET signal from a pair of fluorescent dye compared to the free form of double-labeled mRNA due to the condensation of mRNA in PM core. Apparently, higher FRET signal of PMs prepared from PEG-PAsp(DET)-Chol and Chol-mRNA was observed (**Figure 5-4 (a)**), indicating that hydrophobic interaction between Chol-OligoRNA and PEG-PAsp(DET)-Chol facilitated mRNA condensation in PM core. In PEG-PAsp(DET) PMs, the increase of FRET efficiency was not observed even though 9*Chol-RNA oligonucleotide was

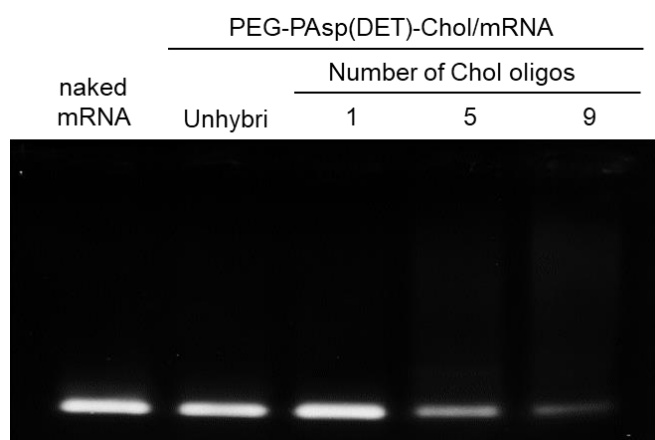


Figure 5-3. Electrophoregram of PEG-PAsp(DET)-Chol PMs loaded with different Chol-mRNA after incubation with dextran sulfate at A/P ratio of 6.

hybridized with mRNA. Also, the FRET efficiency of PEG-PAsp(DET) PMs loaded with Chol-mRNA was similar to that of PMs prepared from PEG-PAsp(DET)-Chol and unhybridized mRNA. The mechanism is still not clear, but it could be inferred that the block copolymers first bound to a double stranded part with a high charge density and then Chol moieties on block copolymer interacted with Chol moieties on mRNA derived from OligoRNA during PM formation. As the PM core condensation occurred around such an area, there seemed to be a difference in the condensation process and the condensed condition of PM core. In previous report claimed that the enhancement of core condensation is one of the important factors to improve the nuclease tolerability of nucleic acids,³ and actually the FBS tolerability was improved by modifying cholesterol group to both block copolymer and mRNA as shown in **Figure 5-3**. It indicated the importance of this design to introduce cholesterol group into both

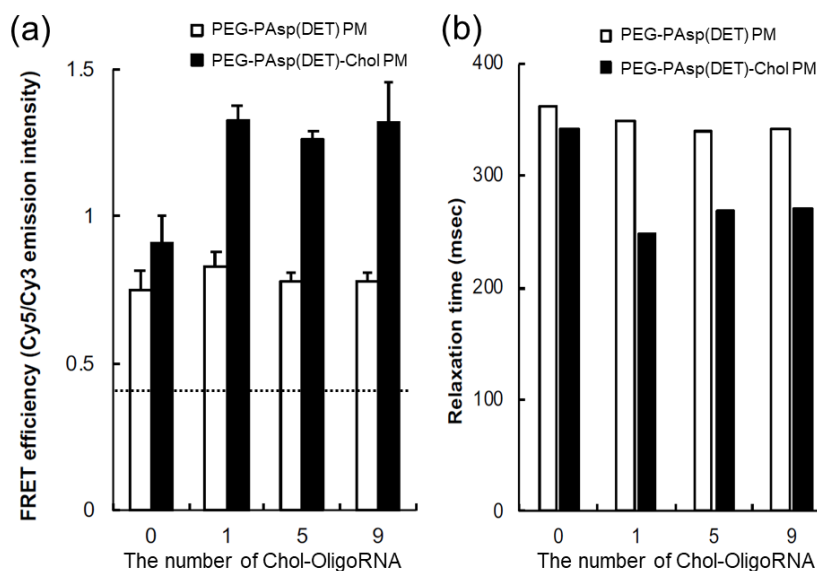


Figure 5-4. Evaluation of PM core condensation status. (a) FRET efficiency of (open bar) PEG-PAsp(DET) or (closed bar) PEG-PAsp(DET)-Chol PMs loaded with Cy3/Cy5 double-labeled mRNA. Dotted line represents the FRET efficiency of naked double-labeled mRNA. Data were shown as means \pm SEM ($n = 3$). (b) Longitudinal relaxation time (T_1) measurement of PAsp(DET) segment in (open bar) PEG-PAsp(DET) or (closed bar) PEG-PAsp(DET)-Chol PM core.

block copolymers and mRNA.

In order to get further insights into the structure of the PM core, the mobility of the block copolymers in PM was estimated by measuring T_1 value of each segment, which correlates with mobility of dissolved polymer chains.⁴⁻⁵ In particular, since the ion pair between the cationic segment on block copolymer and mRNA may be still hydrated, the ion composite PM core has considerable water molecules. Thus, T_1 measurement can indicate the movement of PAsp(DET) segment in PM core. Here, the T_1 value of the proton in PEG and PAsp(DET) segment was measured (for details, refer to **Figure 5-10**). As in the case of FRET measurements, single Chol-OligoRNA hybridization significantly reduced T_1 value of PAsp(DET) segment in PM composed of PEG-PAsp(DET)-Chol, while PEG-PAsp(DET) PM did not show such a decrease in T_1 even after 9*Chol-OligoRNA hybridization (**Figure 5-4 (b)**). Therefore, the introduction of the Chol moiety into both the mRNA and the block copolymer was necessary to get such a reduction in T_1 value. As explained in the Chapter 3 and 4, RNase can invade PM core and then degrade mRNA even encapsulated in the PM core. Therefore, FRET and T_1 measurement indicated that enhanced condensation status of mRNA in the PM core resulted in improvement of nuclease resistance.

5.3.2 Effect of cholesterol modification to mRNA in transfection efficiency of PMs

The PMs prepared from Chol-mRNA and PEG-PAsp(DET)-Chol showed significantly higher transfection efficiency than PMs loaded with unhybridized mRNA (**Figure 5-5 (a), (b)**). In addition, the effect of Chol-OligoRNA complementary to various sequences on mRNA from the 5' end to the 3' end (**Figure 5-2 (a)**) was examined, and all of the Chol-OligoRNA hybridization tended to improve the transfection efficiency although there were

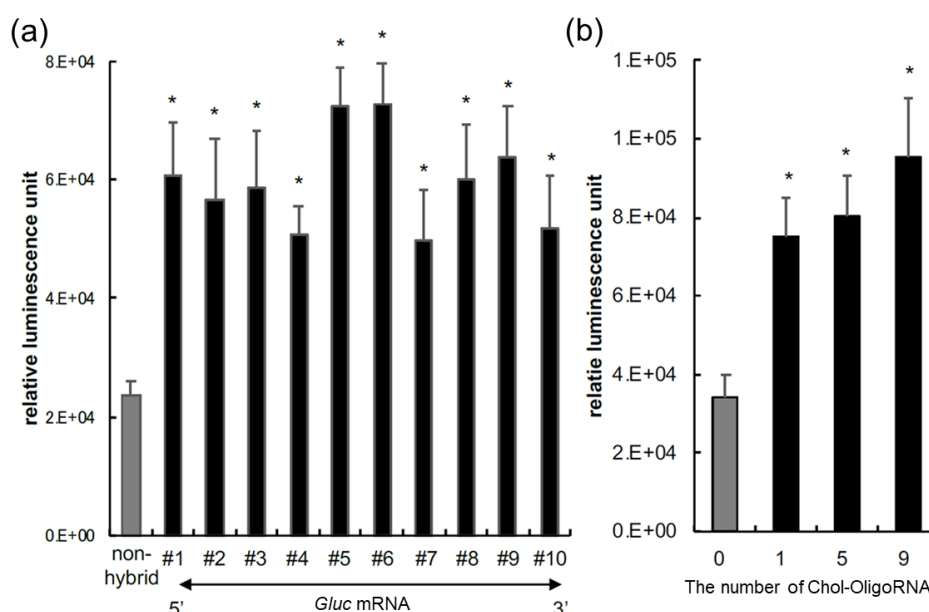


Figure 5-5. Transfection efficiency of PEG-PAsp(DET)-Chol PMs into HuH-7 cells. The effect of (a) the location (b) and number of Chol-OligoRNA hybridized with mRNA on transfection efficiency. Abbreviation: non-hybrid means PMs. Data were shown as means \pm SEM ($n = 8$). Statistical difference to the (a) “non-hybrid” or (b) “0” group was analyzed by analysis of variance followed by Dunnett’s tests. * $p < 0.05$.

variations (**Figure 5-5 (a)**). Such an increase in efficiency correlates well with the improvement in the structural and biological stability of PM after Chol-OligoRNA hybridization as seen in **Figure 5-2**. The increasing tendency of Gluc expression was observed to increase the hybridization number of Chol-OligoRNA from 1 to 9 (**Figure 5-5 (b)**), but not statistically significant. Note that, PM transfection did not show remarkable cytotoxicity and induced immune response in HuH-7 cells (**Figure 5-11**).

5.3.3 *In vivo* intratracheal administration into a mouse lung

To evaluate *in vivo* activity of PMs prepared from Chol-mRNA, we conducted intratracheal administration of PMs into mice lung. Intratracheal administration to lung has been extensively studied because it can be used to pulmonary diseases, such as cystic fibrosis⁶ and surfactant deficiency,⁷ and also applied to the therapeutic applications such as expressing

a secretory protein in the lung and effecting it on the whole body.⁸⁻¹⁰ On the other hand, lung is known as a severe environment. A defense mechanism to prevent the infection is developed,

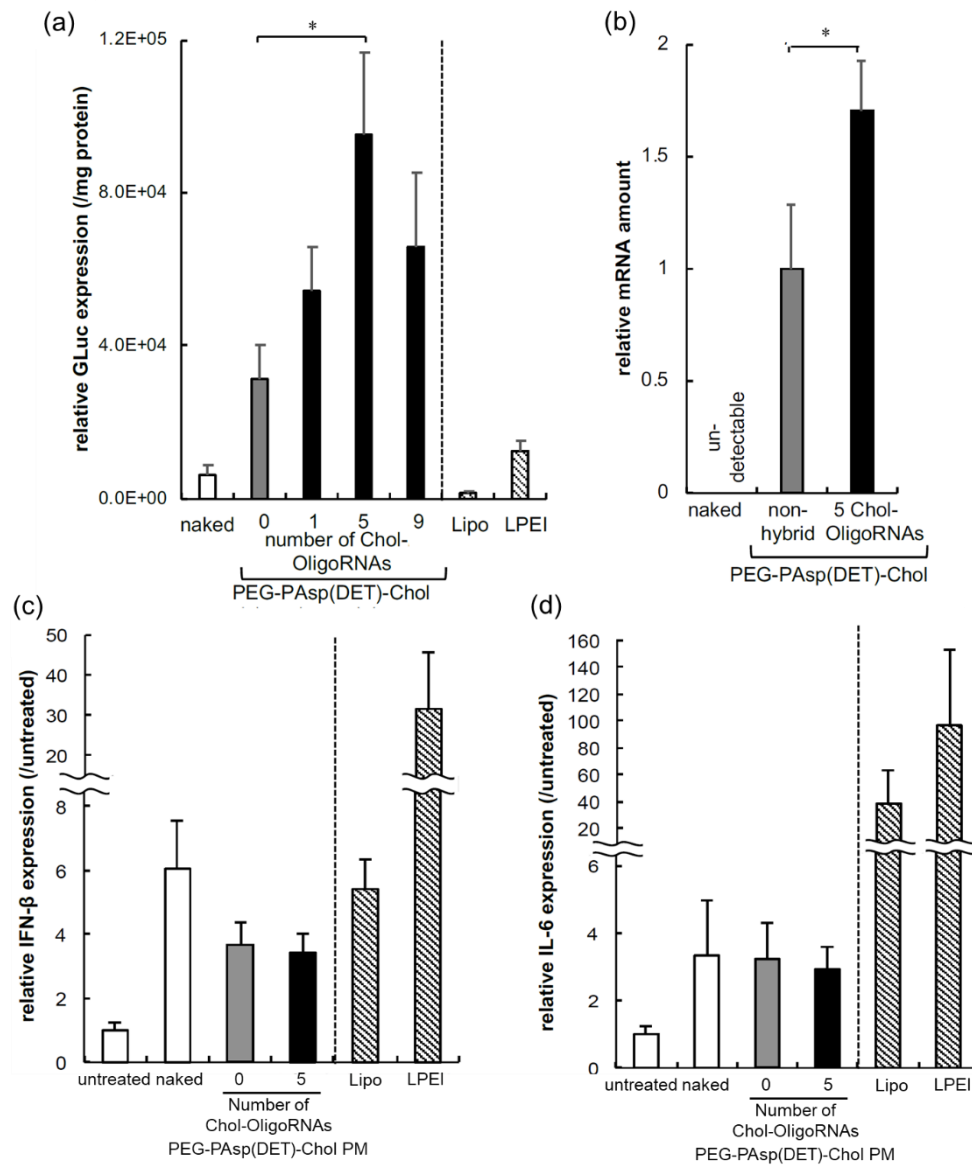


Figure 5-6. Intratracheal administration of PMs to mouse lung. (a) Transfection efficiency of mRNA loaded in PMs and complexed with Lipofectamine LTX or LPEI after 24 h of administration. (b) The amount of remaining mRNA loaded in PMs in mouse lung after 4 h of administration. (c) The amount of pre-inflammatory transcript ((c) IFN-β and (d) IL-6) in mouse lung after 4 h of administration. Abbreviation: non-hybrid; unhybridized mRNA, Lipo: Lipofectamine LTX/mRNA complexes, LPEI: linear polyethyleneimine/mRNA complexes. Data were shown as means and \pm SEM. ($n = 9$ for PMs samples in (a) and $n = 6$ for other groups, $n = 10$ for (b), and $n = 6$ for (c) and (d)). Statistical analyses were performed using analysis of variance followed by Dunnett's tests in (A) and Student's unpaired 2-tailed test in (B).

and lots of anionic biomacromolecules on mucous membrane covering respiratory epithelium of trachea and bronchi are believed to destabilize mRNA delivery carriers.¹¹ Thus, PMs prepared from PEG-PAsp(DET)-Chol and Chol-mRNA were administered into Balb/c mice lung. After 24 h of administration, PMs showed much higher mRNA expression in mice lung than naked mRNA, and the expression efficiency was further improved by hybridizing 5*Chol-OligoRNA (**Figure 5-6 (a)**). Moreover, by the quantification of remaining mRNA in mouse lung, 5*Chol-mRNA loaded with PMs was higher than unhybridized one after 4 h of administration (**Figure 5-6 (b)**). It indicated that the improvement of stability of PMs contributed to effective transfection efficiency.

Considering the effect on immune response, the amount of mRNA encoding *IFN-β* and *IL-6* was quantified after 4 h of administration using qRT-PCR. Despite of Chol-RNA oligonucleotide hybridization, PMs induced comparable amount of proinflammatory transcripts mRNA to naked mRNA (**Figure 5-6 (c), (d)**). Noteworthy, mRNA complexed with lipofectamine or linear polyethyleneimine, a polycation commonly used as transfection reagent, induced more these inflammatory cytokines encoding mRNA expression compared with PMs. From these results, it was indicated that the PMs loaded with Chol-mRNA was a promising method to introduce mRNA into lungs.

5.3.4 Combination of Chol-OligoRNA system and phenylboronate ester cross-linking - Characterization and tolerability test of PMs-

A series of block copolymers were synthesized with the same protocol described in the “*Materials and methods section in Chapter 3*”. According to the optimization of introduction ratio of FPBA and GlcAm moieties in Chapter 3, these were aimed to be around

60% to PAsp(DET) side chain. Actually, introduction ratio of FPBA and GlcAm moieties was determined to be 56% for FPBA and 52% for GlcAm, respectively (PEG-PAsp(DET-FPBA_{56%})₆₃-Chol and PEG-PAsp(DET-GlcAm_{52%})₆₃-Chol). Note that, PEG-PAsp(DET-FPBA)-Chol was dissolved in 10 mM HEPES buffer (pH 7.4) and showed comparable scattering intensity with PEG-PAsp(DET)-Chol solution even though hydrophobic moieties were on a block copolymer.

PMs were prepared from mRNA and these synthesized block copolymers at residual charge ratio of 1.5. Chol moieties were introduced to mRNA through Chol-OligoRNA hybridization. DLS measurement demonstrated that all of PMs showed 51-65 nm of cumulant diameter (**Table 5-1**). Note that, cross-linked PMs prepared from PEG-PAsp(DET-FPBA) and PEG-PAsp(DET-GlcAm), which does not have cholesterol moiety at the ω end, still showed approximately 10 nm larger diameter than other PMs, indicating that the PM core was still swelled even Chol-OligoRNA hybridization.

FPBA/GlcAm cross-linking and Chol installation into ω end of block copolymers and mRNA was aimed to improve tolerability of PMs against nuclease attacks and polyion exchange reaction. First, structural stability of PM was evaluated by observing polyion exchange reaction through gel electrophoresis. PMs were incubated with dextran sulfate (DS) at A/P ratio of 40, where no previous studies used such a high concentration. Obviously, the **Table 5-1. Cumulant diameter and polydispersity index of PMs evaluated by DLS measurement at 25 °C in 10 mM HEPES buffer (pH 7.4)**

	Size (d. nm)/ PDI		
	Number of Chol-OligoRNA		
	0	1	9
PEG-PAsp(DET) PMs	51/0.18	50/0.19	53/0.19
PEG-PAsp(DET)-Chol PMs	54/0.14	52/0.15	59/0.18
Cross-linked PMs	65/0.17	65/0.12	65/0.13
Chol-crosslinked PMs	55/0.15	56/0.19	57/0.20

migration of mRNA was suppressed in accordance with the number of Chol-OligoRNA hybridized with mRNA (**Figure 5-7 (a)**). Then, nuclease resistance was evaluated by incubating PM in the presence of 10% FBS solution. The remaining mRNA loaded in not only Chol installed block copolymers but also PEG-PAsp(DET)-based block copolymers was increased by Chol-OligoRNA hybridization (**Figure 5-7 (b)**). It indicates that Chol moieties on mRNA interacted with one another in the highly condensed PM core, and eventually improved nuclease resistance of PMs. Although the high stabilization of PMs by all combining phenylboronate ester linkage, Chol installation into ω end of block copolymers, and Chol-OligoRNA hybridization, PBA cross-linked Chol-PMs with Chol-mRNA still possessed proper ATP-responsiveness (**Figure 5-8**). Note that, in this experiment, various concentrated ATP and competitive RNA molecules, which mimicked intracellular environment, were added to PMs loaded with Cy3-labeled mRNA. This experimental condition trigger unstable PM dissociation, such as PEG-PAsp(DET) PM. As shown in **Figure 5-8**, complete release of Cy3-labeled mRNA

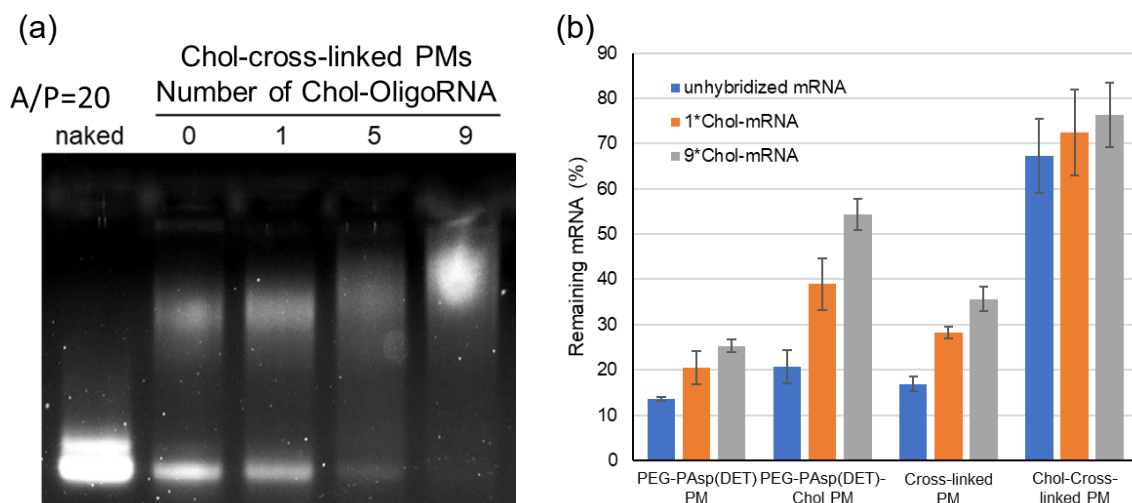


Figure 5-7. Tolerability test of PMs against polyion exchange reaction and nuclease attacks. (a) Electrophoregram of PMs prepared from each mRNA and the mixture of PEG-PAsp(DET-FPBA)-Chol and PEG-PAsp(DET-GlcAm)-Chol incubated with dextran sulfate at A/P ratio of 20. (b) The amount of remaining mRNA loaded in PMs after incubation in 10% FBS solution. Data were shown as means \pm SEM ($n = 4$).

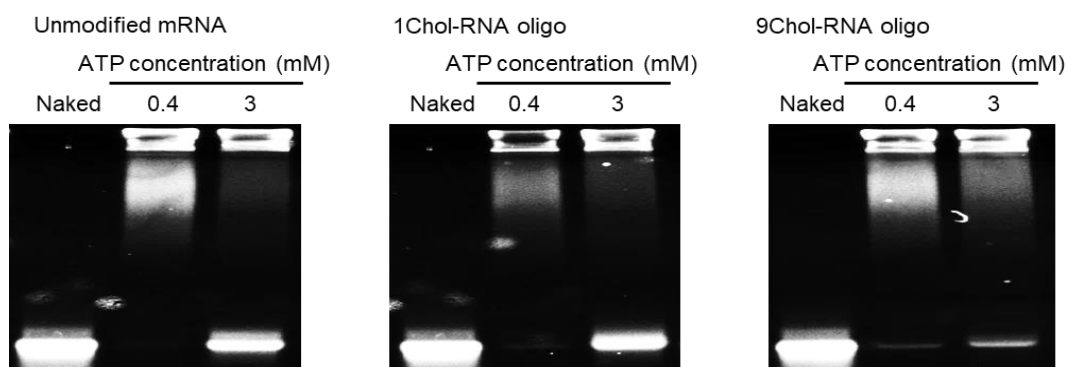


Figure 5-8. Electrophoregram of PBA cross-linked Chol-PMs incubated in the presence of 0.4 or 3 mM ATP and 500 ng/ μ L of competitive mRNA strands.

from Chol-B56/G52 DET PMs was observed in the presence 3 mM ATP concentration. Because extracellular and intracellular ATP concentration is \sim 0.4 and \sim 3 mM, respectively,¹²⁻¹⁴ the PBA cross-linked Chol-PMs with Chol-mRNA can maintain PM structure during delivery process and can release loaded mRNA in response to cytosolic ATP level. Actually, the released mRNA from PBA cross-linked Chol-PMs with 9*Chol-mRNA was decreased even though PMs were incubated in 3 mM ATP solution. Probably, the highly stabilized PM core especially by hydrophobic interaction between cholesterol moieties prevented ATP, which is a negatively-charged hydrophilic small compound, from invading into PM core and being replaced with GlcAm moieties. However, it may be an advantage to achieve gradual release of mRNA in target cells. From these results, higher cellular uptake and transfection efficiency were expected in PBA cross-linked Chol-PMs with 9*Chol-mRNA.

5.3.5 Effect of combination strategy of phenylboronate ester cross-linking and Chol-OligoRNA on transfection efficiency

Gluc expression profile was evaluated into cultured HuH-7 cells (**Figure 5-9 (a)-(c)**). As described in above section (**Figure 5-5**), the transfection efficiency of PMs prepared from PEG-PAsp(DET)-Chol was improved by just one Chol-OligoRNA hybridization with mRNA.

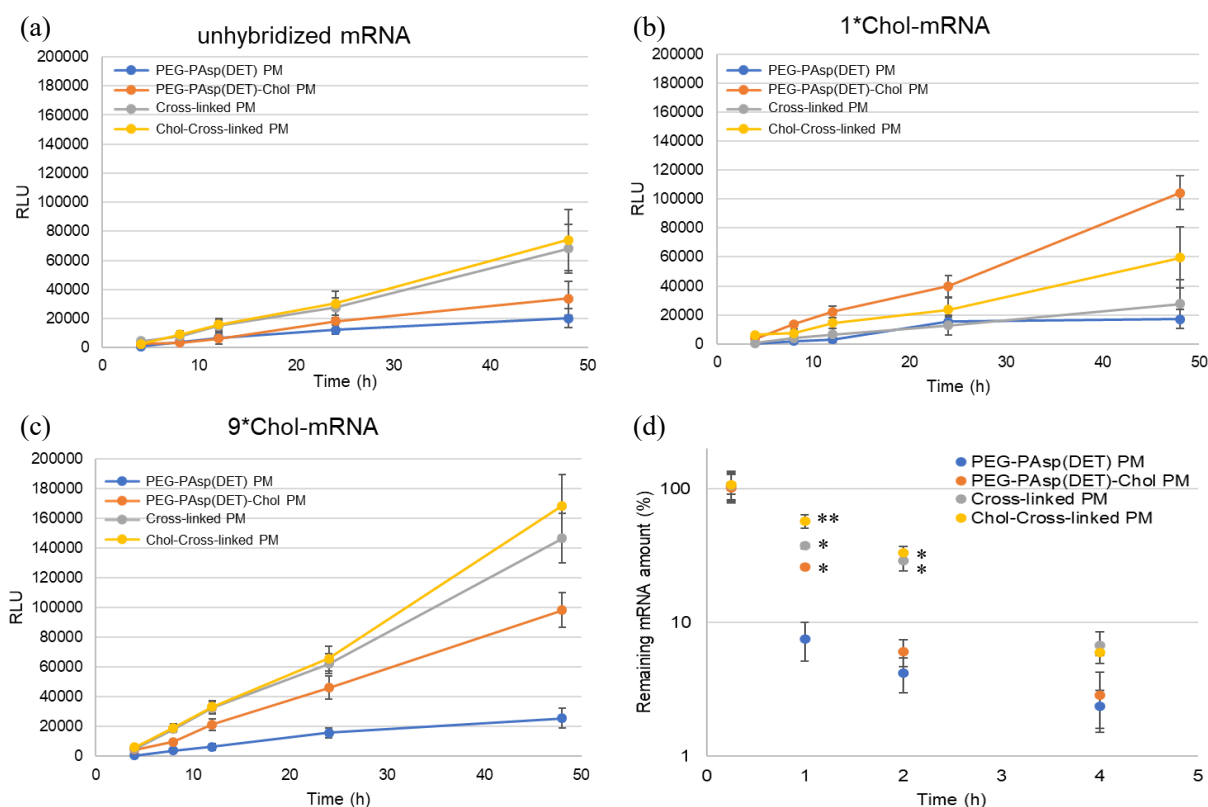


Figure 5-9. Intracellular behavior of PMs. (a-c) Gluc expression efficiency of PMs loaded with (a) unhybridized mRNA, (b) 1*Chol-mRNA, and (c) 9*Chol-mRNA in cultured HuH-7 cells after 4, 8, 12, 24, and 48 h of transfection. (d) The remaining amount of transfected 9*Chol-mRNA using PMs after 1, 2, 4 h of transfection. Data were shown as means and \pm SEM. ($n = 4$ for (a-c), and $n = 3$ for (d)). Statistical difference to the “PEG-PAsp(DET) PM” group was analyzed by analysis of variance followed by Dunnett’s tests. * $p < 0.05$, ** $p < 0.01$.

While PEG-PAsp(DET) PMs did not show any improvement of transfection efficiency despite Chol-OligoRNA hybridization. In case of cross-linked PMs, in spite of Chol installation to ω end of block copolymers, 9*Chol-OligoRNA hybridization dramatically improved transfection efficiency, but just one Chol-OligoRNA introduction into mRNA did not enhanced Gluc expression unlike PEG-PAsp(DET)-Chol PMs. Intracellular stability of mRNA loaded in PMs can be considered to cause these protein expression efficiencies. Then, the remaining amount of transfected 9*Chol-mRNA using PMs was quantified by qRT-PCR. Both cross-linked PMs kept intact mRNA after 2 h of transfection, probably during endocytosis.¹⁵ Considering the

tolerability of PMs against 10% FBS solution as shown in **Figure 5-7 (b)**, which showed comparable nuclease resistance in PBA cross-linked Chol-PMs, intracellular stability of mRNA may be more important factor to get efficient transfection of mRNA in cultured cells. Note that, the half-life time of PBA cross-linked Chol-PMs with 9*Chol-mRNA inside the cells was calculated to be 77 min based on exponential approximation. The half-life time of PBA cross-linked Chol-PMs with unhybridized mRNA was calculated to be 42 min as explained in Chapter 3, so that combination strategy of both phenylboronate ester cross-linking and Chol-OligoRNA hybridization prolonged mRNA half-life time approximately twice.

5.3.6 Stabilization effect of phenylboronate ester cross-linking and cholesterol installation on blood circulation

Finally, the stability of PMs in blood circulation was evaluated by quantifying the remaining mRNA in blood samples. As shown in **Figure 5-10**, PBA cross-linked Chol-PMs maintained over 10% and 1% of loaded mRNA in the PM core after 2.5 and 10 min of intravenous administration respectively while other less stable PMs showed smaller amount of remaining mRNA in mouse blood. Note that, PBA cross-linked Chol-PMs showed longer half-life time than commercially available lipid-based reagent for *in vivo* experiment (Invivofectamine), suggesting the utility of the system combining phenylboronate ester cross-linking and enhanced interaction between mRNA and block copolymers. In spite of dramatical improvement of PM stability by introducing cross-linking into PM core, α phase of blood circulation profile was observed in PBA cross-linked Chol-PMs. Probably, both PM dissociation and accumulation in reticuloendothelial system was happened in the α phase even after stabilization, indicating that there is still room to improve the stability of PMs. However,

importantly, the half-life time of PBA cross-linked Chol-PMs was longer than the previously reported PMs, which achieved antitumor effect on pancreatic cancer,³ strongly indicating that the PBA cross-linked Chol-PMs can attain therapeutic effect by intravenous administration at least on pancreatic cancer. Moreover, the half-life time of PBA cross-linked Chol-PMs was calculated to be 1.3 min from **Figure 3-10**. As one-rap of blood circulation in mouse is estimated to be 0.54 sec, 99% of mRNA loaded in PBA cross-linked Chol-PMs was maintained during one-rap blood circulation. From these calculations, it can be safe to consider that PBA cross-linked Chol-PMs deliver loading mRNA to target sites when ligand molecules are installed on PM surface.

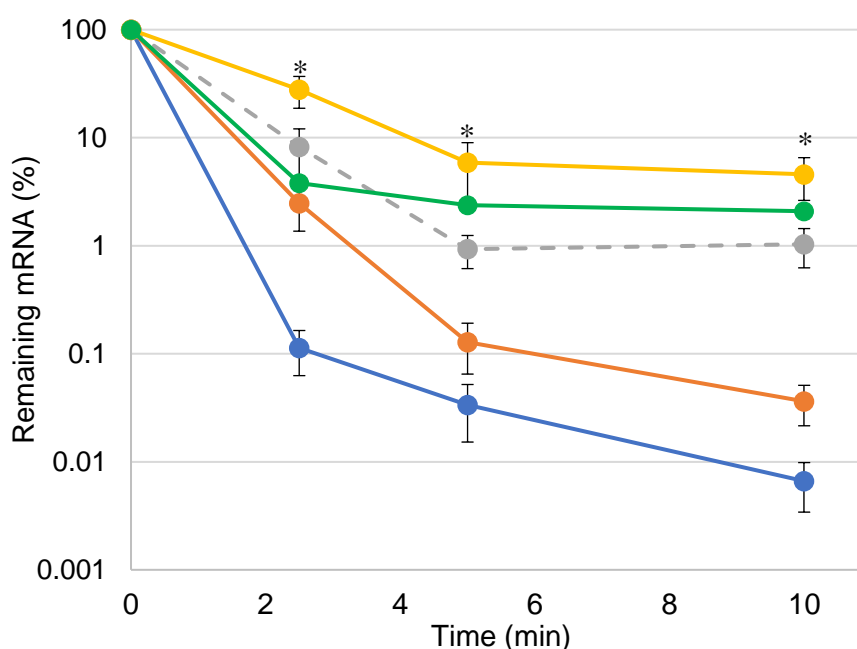


Figure 5-10. The remaining amount of mRNA in mouse blood. PMs were prepared from (blue line) PEG-PAsp(DET) and unhybridized mRNA, (orange line) PEG-PAsp(DET)-Chol and 9*Chol-mRNA, (green line) PEG-PAsp(DET-FPBA), PEG-PAsp(DET-GlcAm) and unhybridized mRNA, and (yellow line) PEG-PAsp(DET-FPBA)-Chol, PEG-PAsp(DET-GlcAm)-Chol and 9*Chol-mRNA. Dotted line denotes the mRNA complexed with InvivoFectamine. Data were shown as means and \pm SEM. ($n = 5$). Statistical difference to the “PEG-PAsp(DET) and unhybridized mRNA PMs (blue line)” group was analyzed by analysis of variance followed by Dunnett’s tests. * $p < 0.05$.

5.4 Conclusion

In this Chapter, I developed a quite stable PMs by combining phenylboronate ester cross-linking and enhancement of mRNA/polymer interaction except electrostatic interaction through introducing cholesterol moieties into both mRNA and block copolymers. First, the strategy of accelerated interaction between Chol moieties on block copolymers and OligoRNA hybridized with mRNA was evaluated. Interestingly, hybridization of even one Chol-OligoRNA with 17 nt, whose length is one forty sixth of mRNA strand, induced effective mRNA condensation in PM core, and provided PMs with higher tolerability against nuclease attacks and polyion exchange reaction. Finally, PMs prepared from PEG-PAsp(DET)-Chol and 5*Chol-mRNA demonstrated significantly higher protein expression efficiency in mouse lung without specific immune response. Moreover, introducing phenylboronate ester cross-linking in the Chol-OligoRNA system further improved stability of PM structure and derived much higher transfection efficiency in cultured cells. Eventually, the PMs with phenylboronate ester cross-linking and Chol-Chol interaction between mRNA and block copolymers dramatically improved the stability of PMs in mouse blood. The quite stable PMs loaded with mRNA are expected to maintain its structure in harsh physiological condition and finally to achieve efficient therapeutic effect to cure life-threatening diseases.

5.5 Appendix

5.5.1 List of OligoRNA sequences hybridizing to *Gluc* mRNA

Following OligoRNAs were used in each experiment.

Table 5-2A. OligoRNAs used for optimizing the length of mismatch overhang between complementary sequence and Chol moiety (**Figure 5-2 (c)**).

Chol-OligoRNA without overhang #1	5'-(Chol)-CUCGGCCACAGCGAUGC-3'
Chol-OligoRNA with 2 nt overhang #1	5'-(Chol)-AACUCGGCCACAGCGAUGC-3'
Chol-OligoRNA with 5 nt overhang #1	5'-(Chol)-AAAAACUCGGCCACAGCGAUGC-3'
OligoRNA #1	5'-AACUCGGCCACAGCGAUGC-3'
Chol-OligoRNA without overhang #3	5'-(Chol)-UCUUUGAGCACCUCAG-3'
Chol-OligoRNA with 2 nt overhang #3	5'-(Chol)-AAUCUUUGAGCACCUCAG-3
Chol-OligoRNA with 5 nt overhang #3	5'-(Chol)-AAUAAUCUUUGAGCACCUCAG-3
OligoRNA #3	5'-AAUCUUUGAGCACCUCAG-3
Chol-OligoA	5'-(Chol)-AAAAAAAAAAAAAAAAAAAAA-3

Table 5-2B. Chol-OligoRNAs with 2 nt overhang used for stabilizing PM.

Chol-OligoRNA #1	5'-(Chol)-AACUCGGCCACAGCGAUGC-3'
Chol-OligoRNA #2	5'-(Chol)-AAUUGAAGUCUUCGUUGUU-3'
Chol-OligoRNA #3	5'-(Chol)-AAUCUUUGAGCACCUCAG-3
Chol-OligoRNA #4	5'-(Chol)-AAGCAGCCAGCUUCCGGG-3'
Chol-OligoRNA #5	5'-(Chol)-UAGUGGGACAGGCAGAUCA-3'
Chol-OligoRNA #6	5'-(Chol)-AAACUCUUUGUCGCCUUCG-3'
Chol-OligoRNA #7	5'-(Chol)-AUAUCUCAGGAAUGUCGAC-3'
Chol-OligoRNA #8	5'-(Chol)-AAUUGAGGCAGCCAGUUGU-3'
Chol-OligoRNA #9	5'-(Chol)-AAGCGGCAGCCACUUCUUG-3'
Chol-OligoRNA #10	5'-(Chol)-AACUCUAGAUGCAUGCUCG-3'

5.5.2 Physicochemical values of PMs loaded with mRNA

DLS and ζ -potential measurement were conducted for PMs. As in **Table 5-3**, all PMs showed 59~68 nm of cumulant diameter and 0.11~0.20 PDI regardless of Chol installation to

Table 5-3. Cumulant diameter, polydispersity index, and ζ -potential of PMs in 10 mM HEPES buffer (pH 7.4) at 25 °C.

		The number of Chol-OligoRNA			
		0	1	5	9
PEG-PAsp(DET)	Cumulant diameter/PDI	65/0.13	60/0.16	59/0.20	62/0.20
	ζ -potential	-4.8	-4.6	-4.6	-5.0
PEG-PAsp(DET)-Chol	Cumulant diameter/PDI	65/0.11	59/0.15	63/0.16	68/0.18
	ζ -potential	1.2	1.1	1.7	1.6

block copolymer and mRNA. On the other hand, ζ -potential of PMs was different between block copolymers depending on Chol moiety at the ω end. PEG-PAsp(DET) PMs showed slightly negative ζ -potential (-5.0~-4.6 mV) while that of PEG-PAsp(DET)-Chol was slightly positive (1.1~1.7 mV).

5.3.3 Fluorescence correlation spectroscopy (FCS) measurement

mRNA was labelled with Label IT Tracker™ Cy5 Kit (Mirus, Madison, WI, USA), and Chol-mRNA oligonucleotide hybridization were prepared. The Chol-mRNA solution was diluted by distilled water. The final mRNA concentration was set to 2.5 ng/ μ L, followed by FCS measurement using MF-20 system (Olympus, Tokyo, Japan). The sample was excited at the wavelength of 633 nm, and detected at the wavelength of 665 nm. Autocorrelation curves were converted into diffusion coefficient using a standard dye (ATTO633) with MF Master software.

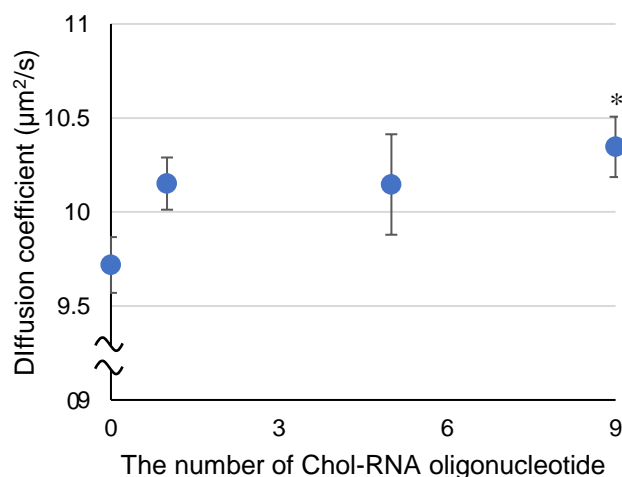


Figure 5-10. Diffusion coefficient measured of different numbers of Chol-RNA oligonucleotide were hybridized to Cy5-labeled mRNA by fluorescence correlation spectroscopy (FCS). Data were shown as means \pm SEM ($n = 3$). Statistical difference to the “unhybridized mRNA” group was analyzed by analysis of variance followed by Dunnett’s tests. * $p < 0.05$.

5.5.4 ^1H -NMR spectrum of PMs for T_1 measurement

To calculate T_1 value of PEG and PAsp(DET) segment, the peak of ethylene structure was selected as shown in **Figure 5-11**.

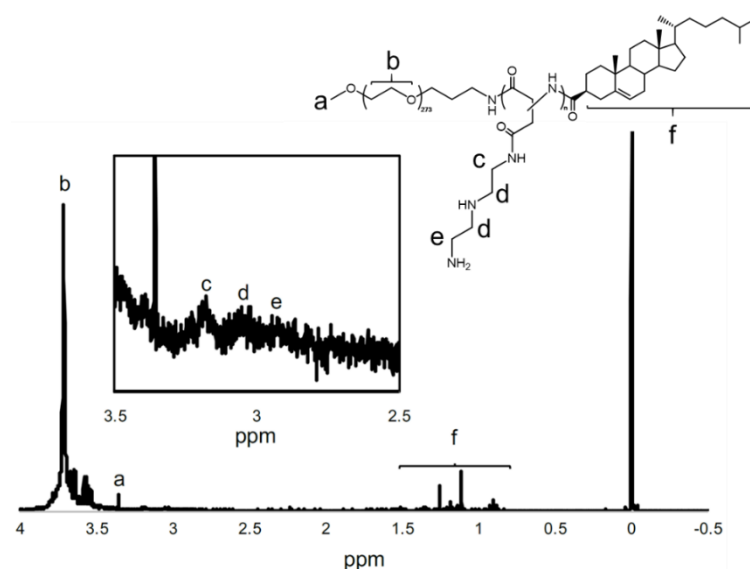


Figure 5-10. Representative ^1H -NMR spectrum of PEG-PAsp(DET)-Chol PMs loaded with 9*Chol-mRNA. Peaks “c-e” were used for calculating T_1 value of PAsp(DET) segment by inversion-recovery method.

5.5.4 Cytotoxicity of PMs in cultured cells

Cytotoxicity of PMs was evaluated by using CCK-8 kit. The viability of PM-treated

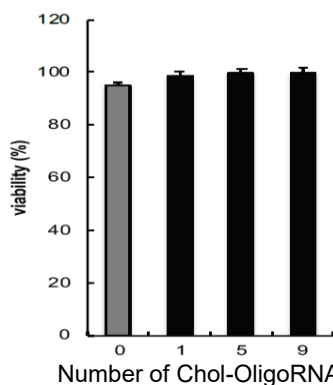


Figure 5-11. Cellular viability after 24 h of PEG-PAsp(DET)-Chol PMs treatment. Data were shown as means \pm SEM ($n = 4$).

cells was comparable to untreated cells, suggesting no remarkable cytotoxicity of PMs.

5.6 References

1. Kato, Y.; Sato, K.; Asai, K.; Akutsu, T., Rtips: fast and accurate tools for RNA 2D structure prediction using integer programming, *Nucleic. Acids. Res.* **2012**, 40 (Web Server issue), W29-34.
2. Uchida, H.; Itaka, K.; Nomoto, T.; Ishii, T.; Suma, T.; Ikegami, M.; Miyata, K.; Oba, M.; Nishiyama, N.; Kataoka, K., Modulated protonation of side chain aminoethylene repeats in *N*-substituted polyaspartamides promotes mRNA transfection, *J. Am. Chem. Soc.* **2014**, 136, 12396-12405.
3. Uchida, S.; Kinoh, H.; Ishii, T.; Matsui, A.; Tockary, T. A.; Takeda, K. M.; Uchida, H.; Osada, K.; Itaka, K.; Kataoka, K., Systemic delivery of messenger RNA for the treatment of pancreatic cancer using polyplex nanomicelles with a cholesterol moiety, *Biomaterials* **2016**, 82, 221-228.
4. Seki, M.; Morishima, Y.; Kamachi, M., Characterization of the complexes of amphiphilic polyanions and double-chain cationic surfactants, *Macromolecules* **1992**, 25, 6540-6546.
5. Nakai, K.; Nishiuchi, M.; Inoue, M.; Ishihara, K.; Sanada, Y.; Sakurai, K.; Yusa, S., Preparation and characterization of polyion complex micelles with phosphobetaine shells, *Langmuir* **2013**, 29, 9651-9661.
6. Yoshimura, K.; Rosenfeld, M. A.; Nakamura, H.; Scherer, E. M.; Pavirani, A.; Lecocq, J.-P.; Crystal, R. G., Expression of the human cystic fibrosis transmembrane conductance regulator gene in the mouse lung after in vivo intratracheal plasmid-mediated gene transfer, *Nucleic Acids Res.* **1992**, 20, 3233-3240.
7. Kormann, M. S.; Hasenpusch, G.; Aneja, M. K.; Nica, G.; Flemmer, A. W.; Herber-Jonat, S.;

- Huppmann, M.; Mays, L. E.; Illenyi, M.; Schams, A.; Griesse, M.; Bittmann, I.; Handgretinger, R.; Hartl, D.; Rosenecker, J.; Rudolph, C., Expression of therapeutic proteins after delivery of chemically modified mRNA in mice, *Nat. Biotechnol.* **2011**, 29, 154-157.
8. Blezinger, P.; Freimark, B. D.; Matar, M.; Wilson, E.; Singhal, A.; Min, W.; Nordstrom, J. L.; Pericle, F.; Intratracheal Administration of Interleukin 12 Plasmid-Cationic Lipid Complexes Inhibits Murine Lung Metastasis, *Hum. Gene Ther.* **1999**, 10, 723-731.
9. Abruzzese, R. V.; Godin, D.; Mehta, V.; Perrard, J. L.; French, M.; Nelson, W.; Howell, G.; Coleman, M.; O'Malley, B. W.; Nordstorm, J. L., Ligand-Dependent Regulation of Vascular Endothelial Growth Factor and Erythropoietin Expression by a Plasmid-Based Autoinducible GeneSwitch System, *Mol. Ther.* **2000**, 2, 276-287.
10. Mulugeta, S.; Beers, M. F., Surfactant protein C: Its unique properties and emerging immunomodulatory role in the lung, *Microbes Infect.* **2006**, 8, 2317-2323.
11. Sanders, N.; Rudolph, C.; Braeckmans, K.; De Smedt, S. C.; Demeester, J., Extracellular barriers in respiratory gene therapy, *Adv. Drug Deliv. Rev.* **2009**, 61, 115-27.
12. Traut, T. W., Physiological concentrations of purines and pyrimidines, *Mol. Cell. Biochem.* **1994**, 140, 1-22.
13. Leist, M.; Single, B.; Castoldi, A. F.; Kuhnle, S.; Nicotera, P., Intracellular adenosine triphosphate (ATP) concentration: a switch in the decision between apoptosis and necrosis, *J. Exp. Med.* **1997**, 185, 1481-1486.
14. Gorman, M. W.; Feigl, E. O.; Buffington, C. W., Human plasma ATP concentration, *Clin. Chem.* **2007**, 53, 318-325.
15. Bire, S.; Gosset, D.; Jégot, G.; Midoux, P.; Pichon, C.; Rouleux-Bonnin, F., Exogenous mRNA delivery and bioavailability in gene transfer mediated by piggyBac transposition, *BMC*

Chapter 6

Summary and perspectives

6.1 Summary

A lot of researches about nucleic acid delivery system have been reported. Especially, the number of studies about non-viral carriers has been increasing recently. Most of studies about non-viral carriers use cationic lipid or polycation as a component of delivery carrier and focus on designing these cationic carrier components. Although many efforts have been devoted to developing functional delivery carriers, few researches achieved three or more functions without complicated preparation method. In this study, by simple mixing of functional block copolymers and nucleic acid in aqueous solution, smart carrier design enables to provide delivery carriers with three functions, *i.e.* stability en route to target site for ensuring secure delivery, endosomal escapability for avoiding lysosomal degradation, and release property inside the cells for efficient protein expression. Also, modification of nucleic acids is another method to improve the nucleic acid delivery efficiency. However, chemical modification of nucleobase has been applied to siRNA or antisense oligonucleotides, which perform therapeutic effect by binding to target mRNA in target cells, because translational efficiency is inhibited by chemical modification. Herein, alternative method to modify mRNA was developed using complementary RNA oligonucleotides (OligoRNA) with functional moiety at the end.

In Chapter 2, I designed a novel phenylboronate ester cross-linked PMs to integrate three functions for enhanced transfection efficiency. In this design, two type of block copolymers were synthesized based on PEG-PAsp(DET); one with 3-fluoro substituted phenylboronic acid (FPBA) moieties on the PAsp(DET) side chain and the other with *N*-gluconamide (GlcAm) as a counterpart of phenylboronate ester cross-linking. The cross-linked PMs were prepared by simple mixing of pDNA and the block copolymer mixture. The strategy

using two type of block copolymers allowed to form cross-linking after PM preparation, which was an important advantage to avoid aggregation of only block copolymers. The formation of phenylboronate cross-linking in PM core stabilized PM structure and improved cellular uptake efficiency. After cellular uptake by endocytosis, cross-linked PMs performed efficient endosomal escape due to shift of equilibrium of FPBA moiety from hydrophilic structure to hydrophilic structure and increase of the number cationic charge of PAsp(DET) side chain responding to pH drop in endosomes/lysosomes. Inside the cells, cross-linked PMs released loaded pDNA responding to highly concentrated ATP, and eventually demonstrated facilitated gene expression.

It was confirmed that phenylboronate ester cross-linking was a promising method to enhance pDNA delivery efficiency in Chapter 2. mRNA is a more attractive nucleic acid drug because of its various advantages to get therapeutic protein expression. In Chapter 3, phenylboronate ester cross-linked PMs were applied to mRNA delivery. To achieve further efficient mRNA transfection efficiency, cationic segment of block copolymer was first optimized in terms of PM stability, ATP-responsiveness and protein expression efficiency. These screening experiments confirmed that PEG-PAsp(DET)-based PMs for introducing phenylboronate ester cross-linking into PM core. Moreover, cholesteryl moiety (Chol) was installed into ω end of block copolymer to improve nuclease resistance, which is believed to be a quite important factor for efficient mRNA delivery in harsh physiological condition. Chol-installation into block copolymer dramatically improved nuclease resistance. Nevertheless, Chol-installed cross-linked PMs still possessed proper ATP-responsiveness, which allowed mRNA release in the intracellular ATP concentration. Also, I found that intracellular stability of mRNA was one of the critical factors for high protein expression efficiency. Quantification

of intact transfected mRNA revealed that phenylboronate ester cross-linking prolonged life-time of loaded mRNA and achieved efficient protein expression.

Modification of mRNA itself is another fruitful strategy to improve nuclease resistance, but conventional modification method, such as chemical modification of nucleobase, is known to decrease translation efficiency. Thus, in Chapter 4, I designed an end-functionalize RNA oligonucleotide (OligoRNA) with complementary sequence to mRNA for introducing functional groups by hybridization. Indeed, there was concern that OligoRNA hybridization may also inhibit mRNA translation and, in addition, induce immune response due to double-strand RNA formation. However, these concerns can be avoided by fine-tuning of the length of complementary OligoRNA sequences. Hybridization of 17 nt OligoRNA achieved to functionalize mRNA without preventing mRNA translation and inducing immune response. By using this method, GlcAm moieties were introduced to mRNA (GlcAm-mRNA), and PMs were prepared from GlcAm-mRNA and PEG-PAsp(DET-FPBA) to form direct cross-linking between mRNA and block copolymers. Interestingly, facilitated interaction between mRNA and block copolymers by phenylboronate ester cross-linking dramatically stabilized PM structure and improved nuclease resistance comparing to cross-linked PMs between block copolymers as evaluated in Chapter 3, even though the number of GlcAm moieties in cross-linked PMs loaded with GlcAm-mRNA was quite smaller. These results strongly suggested that enhancement of mRNA/polymer interaction by additional force was a promising strategy to improve mRNA delivery efficiency.

Finally, in Chapter 4, I attempted to combine two strategies, phenylboronate ester cross-linking between block copolymers and facilitating interaction between mRNA and block copolymers by additional force, for much efficient mRNA delivery. To enhance

mRNA/polymer interaction, Chol modified OligoRNA (Chol-OligoRNA) and Chol-installed block copolymers were used. Chol-OligoRNA hybridization also improved nuclease resistance of PMs even without cross-linking. Interestingly, it was confirmed that hybridization of a small number of Chol-OligoRNAs was enough to enhance PM core condensation, which is one of the critical factors to improve nuclease resistance. In addition, PMs prepared from PEG-PAsp(DET)-Chol and 5*Chol-mRNA performed higher protein expression in mouse lung through intratracheal administration. Moreover, phenylboronate ester cross-linking was combined with the Chol-OligoRNA system for further improvement of the tolerability of PM. The cross-linked PMs loaded with Chol-mRNA showed remarkable stability against polyanion exchange reaction in the never reported high polyanion concentration. Although excess stabilization of PM structure took place, the PMs released loaded Chol-mRNA in response to intracellular ATP concentration, indicating that the quite stable PMs still possessed appropriate ATP-responsiveness. Eventually, the cross-linked PMs loaded with 9*Chol-mRNA performed efficient mRNA transfection in cultured cells.

6.2 Future perspectives

Recently, gene therapy by expression of therapeutic proteins from nucleic acid, especially mRNA, has been garnering much attention. For example, Moderna Therapeutics Inc., which is a venture company developing mRNA medicine for clinical use, raised 500 million dollars in funding by issuing shares in February 2018. While mRNA therapy has gathered much more attention, developing *in vivo* mRNA medicine is still challenging. Actually, clinical trials using mRNA focuses on *ex vivo* transfection or RNA vaccines [Hajj, K. A.; Whitehead, K. A., *Nat. Rev. Mat.* **2017**, 2, 17056]. In order to realize widespread usage of mRNA to cure various

diseases, delivering mRNA to target site through intravenous administration is preferable. Therefore, it is necessary to develop delivery carriers robustly protecting biologically fragile mRNA in harsh physiological condition.

As described in Chapter 5, extremely stable PMs were developed by fully using phenylboronate ester linkage and hydrophobic interaction between cholesterol moieties on mRNA and block copolymers in PM core (PBA-cross-linked Chol-PMs). The quite stable PBA-cross-linked Chol-PMs can be applied *in vivo* applications to cure various diseases, and actually the PBA-cross-linked Chol-PMs maintained loaded mRNA in the PM core in mouse blood. These results indicated that the PBA-cross-linked Chol-PMs developed is promising for delivering mRNA to disease site through intravenous injection. Future studies for the practical use of the quite stable PBA-cross-linked Chol-PMs will involve evaluating detailed pharmacokinetics and pharmacodynamics of the PMs because the PMs showed β phase in blood circulation profile, which suggested that the PMs kept loaded mRNA completely inside the core after several minutes from intravenous injection. As the possibility of the interaction of biological components with the PBA-cross-linked PMs is considered, evaluating interaction between PBA-cross-linked PMs and biological compounds can provide useful insights for mRNA delivery system using PMs. Of course, the stable PMs can be used not only for intravenous injection but also local injection, which allow delivery carriers to reach target sites directly. For example, local injection of mRNA encoding vascular endothelial growth factor (VEGF)-165 to mouse and mini pig after complexing with lipid-based carriers dramatically improved cardiac function of those animals [L. Carlsson, J. C. Clarke, C. Yen et al., *Mol. Ther. Methods Clin. Dev.* 2018, 9, 330]. The important point is that critical factors demanded for efficient mRNA delivery through local injection depends on organs. Because the PBA cross-

linked Chol-PMs possessed not only structural stability but also intracellular-specific functions, such as pH- and ATP-responsiveness, the PBA-cross-linked Chol-PMs can be used for getting further insights into effective mRNA delivery through local injection.

Thus, I believe that this research greatly expands the possibilities of mRNA medicine and makes a great contribution to the spread of mRNA therapy field.

List of publications

For this dissertation

1. Yoshinaga, N.; Ishii, T.; Naito, M.; Endo, T.; Uchida, S.; Cabral, H.; Osada, K.; Kataoka, K., Polyplex micelles with phenylboronate/gluconamide crosslinking in the core exerting promoted gene transfection through spatiotemporal responsiveness to intracellular pH and ATP concentration, *J. Am. Chem. Soc.* **2017**, 139, 18567-18575.
2. Yoshinaga, N.; Uchida, S.; Naito, M.; Osada, K.; Cabral, H.; Kataoka, K., Induced packaging of mRNA into nano-polyplex core through regulated hybridization with minimal number of cholesteryl RNA oligonucleotides directing to enhanced introduction to lung, *Biomaterials* **2019**, 197, 255-267.
3. N. Yoshinaga, S. Uchida, M. Naito, K. Osada, H. Cabral, K. Kataoka, "Fine-tuning of phenylboronate ester cross-linking in mRNA polyplex micelles for prolonged blood circulation," *Manuscript in preparation*.
4. Yoshinaga, N.; Uchida, S.; Naito, M.; Osada, K.; Cabral, H.; Kataoka, K., Enhancing the stability of mRNA loaded polyplex micelles by polymer/mRNA cross-linking through phenylboronate ester linkage for exerting mRNA transfection efficiency, *Manuscript in preparation*.

Other publications

1. Dirisala, A.; Uchida, S.; Tockary, T. A.; Yoshinaga, N., Li, J.; Osawa, S.; Gorantla, L.; Fukushima, S.; Osada, K., Kataoka, K., Precise tuning of disulfide crosslinking in mRNA polyplex micelles for optimizing extracellular and intracellular nuclease tolerability. *J. Drug Target.* *in press*.

2. Naito, M.; Yoshinaga, N.; Ishii, T.; Matsumoto, A.; Miyahara, Y.; Miyata, K.; Kataoka, K., Enhanced intracellular delivery of siRNA by controlling ATP-responsiveness of phenylboronic acid-functionalized polyion complex micelles, *Macromol. Biosci.* **2018**, 1, 1700357.
3. Uchida, S.; Yoshinaga, N.; Yanagihara, K.; Yuba, E.; Kataoka, K.; Itaka, K., Designing immunostimulatory double stranded messenger RNA with maintained translational activity through hybridization with poly A sequences for effective vaccination, *Biomaterials* **2018**, 150, 162-170.
4. Lee, D.-J.; Kessel, E.; Lehto, T.; Liu, X.; Yoshinaga, N.; Padari, K.; Chen, Y.-C.; Kempter, S.; Uchida, S.; Rädler, J. O.; Pooga, M.; Sheu, M.-T.; Kataoka, K.; Wagner, E.; Systemic delivery of folate-PEG siRNA lipopolyplexes with enhanced intracellular stability for in vivo gene silencing in leukemia, *Bioconjugate Chem.* **2017**, 28, 2393-2409.
5. Naito, M.; Azuma, R.; Takemoto, H.; Hori, M.; Yoshinaga, N.; Osawa, S.; Kamegawa, R.; Kim, H.-J.; Ishii, T.; Nishiyama, N.; Miyata, K.; Kataoka, K., Multilayered polyion complexes with dissolvable silica layer covered by controlling densities of cRGD-conjugated PEG chains for cancer-targeted siRNA delivery, *J. Biomater. Sci. Polym. Ed.* **2017**, 28, Issue10-12, 1109-1123.

Conferences

[International Meetings, Oral]

1. N. Yoshinaga, M. Naito, S. Uchida, H. Cabral, K. Osada, K. Kataoka, The 256th ACS National Meeting, (Boston Convention and Exhibition Center, Aug. 19th-23th, 2018).
2. N. Yoshinaga, T. Ishii, T. Endo, M. Naito, S. Uchida, H. Cabral, K. Osada, K. Kataoka, Chile-Japan Academic Forum at Patagonia 2016 (Hotel Remota, Nov. 7th-11th, 2016)

[International Meetings, Poster]

1. N. Yoshinaga, M. Naito, S. Uchida, H. Cabral, K. Osada, K. Kataoka, The 11th Annual Symposium on Nanobiotechnology 2017, P-32 (Kawasaki City Industrial Promotion Hall, Feb. 27th-28th, 2017)
2. N. Yoshinaga, T. Ishii, T. Endo, M. Naito, S. Uchida, H. Cabral, K. Osada, K. Kataoka, The 11th International Polymer Conference, 14P-S4-019a (Fukuoka International Conference Center, Dec. 13th-16th, 2016)
3. N. Yoshinaga, M. Naito, S. Uchida, H. Cabral, K. Osada, K. Kataoka, 3rd International Conference on Biomaterials Science in Tokyo, P039 (The University of Tokyo, Nov. 28th-30th, 2016)
4. N. Yoshinaga, T. Ishii, T. Endo, M. Naito, S. Uchida, K. Osada, K. Kataoka, The 10th International Polymer Conference, 3P-G6-111a (International Conference Center Epochal Tsukuba, Dec. 2nd-5th, 2014)

[Domestic Meetings, Oral]

1. 吉永直人、内田智士、長田健介、位高啓史、Cabral Horacio、片岡一則、第 34 回日本 DDS 学会学術集会、2D21 (長崎ブリックホール、6 月 21 日~22 日、2018 年)
2. 吉永直人、内田智士、Cabral Horacio、長田健介、片岡一則、第 67 回高分子学会年次大会、3H05 (名古屋国際会議場、5 月 23 日~25 日、2018 年)
3. 吉永直人、内藤瑞、内田智士、Cabral Horacio、長田健介、片岡一則、第 66 回高分子討論会、2W08 (愛媛大学城北キャンパス、9 月 20 日~22 日、2017 年)
4. 吉永直人、石井武彦、遠藤泰輔、内藤瑞、内田智士、長田健介、片岡一則、第 64 回高分子討論会、2W08、(東北大学川内キャンパス、9 月 15 日~17 日、2015 年)
5. 吉永直人、石井武彦、遠藤泰輔、内藤瑞、内田智士、長田健介、片岡一則、第 24 回インテリ

ジェント材料・システムシンポジウム、A-01 (東京女子医科大学 先端生命医科学研究所 TWIns,
1 月 19 日, 2015 年)

6. 吉永直人、石井武彦、遠藤泰輔、内藤瑞、内田智士、長田健介、片岡一則、第 36 回日本バイ
オマテリアル学会、2C-03 (タワーホール船堀, 11 月 17 日~18 日, 2014 年)

[Domestic Meetings, Poster]

1. 吉永直人、内藤瑞、内田智士、Cabral Horacio、長田健介、片岡一則、理研/iCONM/物材機構
医工学ネットワーク P6 (川崎生命科学・環境研究センター, 12 月 12 日, 2017 年)

2. 吉永直人、内藤瑞、内田智士、Cabral Horacio、長田健介、片岡一則、第 66 回高分子学会年
次大会, 1Pc097 (幕張メッセ, 5 月 29 日~31 日, 2017 年)

3. 吉永直人、石井武彦、遠藤泰輔、内藤瑞、内田智士、Cabral Horacio、長田健介、片岡一則、
第 26 回バイオ高分子シンポジウム, P1 (東京工業大学大岡山キャンパス, 7 月 28 日~29 日, 2016
年)

4. 吉永直人、石井武彦、遠藤泰輔、内藤瑞、内田智士、Cabral Horacio、長田健介、片岡一則、
第 16 回遺伝子・デリバリー研究会シンポジウム, P14 (川崎生命科学・環境研究センター, 5 月 16
日, 2016 年)

5. 吉永直人、石井武彦、遠藤泰輔、内藤瑞、内田智士、長田健介、片岡一則、第 64 回高分子学
会年次大会, 1Pa115 (札幌コンベンションセンター, 5 月 27 日~29 日, 2015 年)

6. 吉永直人、石井武彦、遠藤泰輔、内藤瑞、内田智士、長田健介、片岡一則、第 13 回未踏科学
サマー道場, P-02 (湘南国際村センター, 8 月 29 日~31 日, 2014 年)

7. 吉永直人、石井武彦、遠藤泰輔、内藤瑞、片岡一則、第 63 回高分子学会年次大会、P2f142 (名
古屋国際会議場, 5 月 28 日~30 日, 2014 年)

Patents

1. 片岡一則、石井武彦、吉永直人、内藤瑞、遠藤泰輔、「フェニルボロン酸／ポリオール結合を可逆的架橋剤として利用する核酸内包高分子ミセルと核酸キャリアとしての使用」、特表 2015-170757、東京大学、公開日 2015 年 11 月 12 日
2. 片岡一則、位高啓史、内田智士、吉永直人、「mRNA の機能化方法」、PCT/JP2017/046906、東京大学、2017 年 12 月 27 日
3. Satoshi Uchida, Naoto Yoshinaga, Eol Cho, “METHOD FOR STABILIZING MRNA”, 62/583691, 東京大学、2017 年 11 月 9 日
4. 安楽泰孝、片岡一則、中村直人、吉永直人、「高分子複合体」、特願 2017-39312、東京大学、2017 年 3 月 2 日

Awards

1. 第 34 回日本 DDS 学会学術集会 優秀発表賞(口頭) 2018 年
2. 第 66 回高分子学会年次大会 優秀ポスター賞 2017 年
3. 第 26 回バイオ高分子シンポジウム 優秀ポスター賞 2016 年
4. 第 16 回遺伝子・デリバリー研究会シンポジウム ポスター奨励賞 2016 年
5. 第 24 回インテリジェント材料・システムシンポジウム奨励賞 2015 年
6. 第 13 回未踏科学サマー道場 ポスター発表優秀賞 2014 年